GA-A13366
UC-77

THORIUM UTILIZATION PROGRAM

QUARTERLY PROGRESS REPORT FOR THE PERIOD ENDING FEBRUARY 28, 1975

Prepared under
Contract AT(04-3)-167
Project Agreement No. 53
for the
San Francisco Operations Office
U.S. Energy Research and Development Administration

DATE PUBLISHED - MAY 30, 1975

Printed in the United States of America
Available from
National Technical Information Service
U.S. Department of Commerce
5285 Port Royal Road
Springfield, Virginia 22161
Price: Printed Copy $7.60; Microfiche $2.25

DISCLAIMER

GENERAL ATOMIC

GA-A13366
UC-77

THORIUM UTILIZATION PROGRAM

QUARTERLY PROGRESS REPORT FOR THE PERIOD ENDING FEBRUARY 28, 1975

Prepared under
Contract AT(04-3)-167
Project Agreement No. 53
for the
San Francisco Operations Office
U.S. Energy Research and Development Administration

GENERAL ATOMIC PROJECT 3225
(FORMERLY 0852)

DATE PUBLISHED
MAY 30, 1975

QUARTERLY REPORT SERIES*

GA-A13178 - June 1974 through August 1974

GA-A13255 - September 1974 through November 1974

*Prior to GA-A13178, the Thorium Utilization Program was reported in the Base Program Quarterly Progress Report.

ABSTRACT

This publication is the third of a quarterly series presenting results of work performed under the National HTGR Fuel Recycle Program (also known as the Thorium Utilization Program) at General Atomic Company. Results of work on this program were previously included in a quarterly series on the HTGR Base Program.

The work reported includes the development of unit processes and equipment for reprocessing of High-Temperature Gas-Cooled Reactor (HTGR) fuel and the design and development of an integrated line to demonstrate the head end of HTGR reprocessing using unirradiated fuel materials. Work is also described on the evaluation of alternate techniques for fuel reprocessing to surmount possible operating problems with the reference flow sheet and the development of the conceptual design of a target recycle facility to identify the requirements of large-scale recycle of HTGR fuels.

INTRODUCTION

This report covers the work performed by General Atomic Company under U.S. Energy Research and Development Administration Contract AT(04-3)-167, Project Agreement No. 53. The work done under this project agreement is part of the program for development of recycle technology for High-Temperature Gas-Cooled Reactor (HTGR) fuels described in the "National HTGR Fuel Recycle Development Program" (ORNL 4702).

The objective of the program is to provide the necessary technology, development, engineering, and demonstration of the steps required in the economic recycle of HTGR fuels utilizing thorium as a fertile material. Work at General Atomic Company is concentrating on the development of reprocessing methods (subtask 110 of the National Program), engineering and economic studies (subtask 310), and the application of recycle technology to the conceptual design of a large-scale recycle facility (subtask 320).

The objectives of subtask 110, Reprocessing Development, are to develop the necessary technology for the construction and operation of a prototype reprocessing facility which will process irradiated fuel materials and to provide the capability for commercial recycle of HTGR fuels. The output of this subtask includes (1) definition of process flow sheets, (2) development of equipment components, and (3) definition of operating data.

The objectives of subtask 310 are to guide the development program from the viewpoint of overall recycle needs and to obtain an economical HTGR fuel recycle method for early recovery and use of bred U-233. Alternate methods and options for reprocessing and refabrication are evaluated, and recommendations are made for possible further experimental development.

The objectives of subtask 320 are to develop a conceptual design of a target-size recycle plant for the reprocessing and refabrication of HTGR fuels and to use the results developed in the preparation of this design to guide the development work. The output of this task is in the form of design criteria, reference process flow sheets, and equipment sizing for a target recycle facility.

CONTENTS

FIGURES

TABLES

1. SUMMARY

A comprehensive review of the UNIFRAME crushing system was completed and a design status report submitted to Allied Chemical Company (ACC) Idaho Operations and to ERDA. Agreement was reached to proceed on a longer term program for this system to include a broader scope and a demonstration of several additional design features.

Measurements have been performed to characterize the physical properties of crushed graphite for use in the design of pneumatic transport systems. The results of pneumatic classification of TRISO fissile - TRISO fertile particles typical of the Fort St. Vrain fuel design are reported.

Experimental runs on the 20-cm primary fluidized-bed burner indicated that the dilute-phase pneumatic recycle of unburned fines is not acceptable. During operation, fines transport is limited by the bed backpressure and the fines are cooled down by the large amount of transport gas required for dilute fines recycle. A dense-phase recycle system, which has been successfully operated by Allied Chemical Company Idaho Operations, is therefore being adopted into the burning system. The 20-cm primary burner has now been fitted with a perforated-cone distributor and initial runs indicate capability to handle larger-size feed than with the ball and cone design.

Design calculations for the prototype primary burner are continuing and are presented in this quarterly report. A finned-wall has been selected for the outside of the burner vessel for improved cooling characteristics.

The secondary burner program has concentrated on development of the automatic control loops and verification testing of the induction heating

design for both prototype burners. The 10-cm secondary burner includes all of the process steps of the prototype design, including the pneumatic feeder and product removal steps. Detailed design and analysis on the prototype are continuing.

Leaching runs have been conducted to investigate the dissolution of crushed burned-back TRISO fertile particles processed by a modified double-roll particle crusher which cracks and removes the SiC shell without pulverizing the particle. The larger size distribution resulting from this crushing system leads to longer dissolution times for the ThO_2 kernel.

Installation of the dryer for insoluble products from leaching, which was described in the previous Quarterly Progress Report, has been completed and shakedown testing has begun.

Solvent extraction experiments are continuing. Studies are being performed on uranium and thorium extraction, partitioning, and uranium stripping.

Initial feasibility tests have been performed with electrohydraulic equipment to evaluate the capability of a high-frequency electric discharge to achieve a controlled fracture of the graphite block.

2. FUEL ELEMENT CRUSHING

2.1. UNIFRAME PROTOTYPE FUEL ELEMENT SIZE REDUCTION SYSTEM

The UNIFRAME concept for head-end fuel element size reduction has been reviewed and the UNIFRAME Design Status Report was submitted to Allied Chemical Company (ACC), Idaho Operations, the lead contractor for reprocessing development in the Thorium Utilization Program. Following submittal of this report, a technical review meeting was held on January 16, 1975.

Relevant action has been initiated with respect to several of the agreements and commitments that resulted from this meeting.

It was agreed to proceed on a longer term UNIFRAME program, which will include performing a system reliability analysis and testing of a ventilation concept as well as several remote concepts. The adopted plan provides continuing documentation of design information for the Title I and Title II phases of the reprocessing demonstration facility and design of a "start-under-load" capability. The efforts during this quarter on the UNIFRAME system are discussed in the following sections.

The UNIFRAME system is designed to reduce spent HTGR fuel elements to -3/16-in. (ring size) particles suitable for subsequent recovery of the fissile materials. The system is comprised of five major equipment items stacked in an array to utilize gravity flow, to eliminate the need for intrasystem material transport devices, and to provide a continuous size reduction process.

The major equipment items include:

1. Primary crusher: an overhead eccentric jaw crusher, designed to reduce whole or partial fuel elements to less than 6-in. ring sized fragments.

2. Secondary crusher: an overhead eccentric jaw crusher designed to further reduce the fragments to less than 2-in. ring sized fragments.

3. Tertiary crusher: as double-roll crusher designed to reduce the fragments to -3/16-in. ring sized product.

4. Screener: a vibratory screener separator designed to separate the product from any potential oversized materials.

5. Oversized crusher: an eccentrically mounted single roll designed to reduce the oversized material to less than 3/16-in. product.

2.1.1. Structural Analysis of UNIFRAME

Structural analysis of the UNIFRAME system is 75% complete. The structure was analyzed using the SAP IV computer code (Ref. 2-1). Four analyses are being considered: (1) static, (2) mode shapes and frequencies, (3) response history, and (4) seismic. The seismic analysis is the only study not completed. This analysis has been deferred until receipt of further input from ACC on the type of structure under which the UNIFRAME is categorized and a more in-depth review of the seismic requirements described within ACC's System Design Description.

The structure has been idealized as 63 beam elements, 30 boundary elements, 2 plane stress beam elements (pitmans), and 2 tangent pipe elements (double-roll crusher). The beam elements were typical 8 by 8 WF and 6 by 6 WF structural steel beams boxed with 1/2-in. steel plate. The boundary elements were used to constrain the displacements of ten nodes in three directions, to compute support reactions, and to provide linear

elastic supports to nodes. The two plane stress elements were 5.16 in. thick and the two pipe elements had 2-in.-thick, 40-in.-diameter walls.

The response history analysis was performed by applying a vertical and a fore and aft sinusoidal load to the pushing block support beam of each pitman assembly. An operating frequency of 3.33 Hz (200 rpm) was used for the primary crusher and a frequency of 5.0 Hz (300 rpm) was used for the secondary crusher. The peak loads of these two conditions were combined to determine the maximum crusher loads. The structure was conservatively assumed to have no structural damping.

The results of the static analysis indicate a maximum stress of 4652 psi in the UNIFRAME support structure, which is more than adequate based on the yield stress for structural steel of 36,000 psi. In the analysis of mode shapes and frequencies, the first four main structure resonant frequencies were determined to be 11.6, 19.3, 21.3, and 31.5 Hz. These are relatively high resonance frequencies in comparison with the highest forcing frequency of 5.0 Hz for the secondary crusher. The results of the response history analysis demonstrate that maximum dynamic stresses of about 11,150 psi can be expected. The node displacement output for the dynamic response indicated the motion of the upper structure will be less than 0.1 in. peak-to-peak.

2.1.2. Toggle/Pitman Toe Pin-Joint Connection

Because the pin-joint connection between the toggle and pitman toe cannot maintain a squeeze film with liquid lubricants and bronze bushings will not take such high pressure-times-velocity (PV) values as those generated in this application, the decision was made to use a dry bushing, possibly using solid lubricants.

The initial assembly being considered consists of H-11 ultra-high-strength tool steel as the shaft material and M-2 molybdenum high-speed tool steel as the bushing material. The shaft will be grit blasted for maximum surface area and then coated with an air-cured polyimide resin

binder with a molybdenum disulfide (MoS_2) coating as the solid lubricant. This selection is not the final choice, but rather is one feasible way in which this problem could be resolved.

The assembly procedure consists of first heating the toggle and pitman toe. The outside diameter of the sleeve will be larger than the inside diameter of the mating components at room temperature, thus creating a pressure between the two interacting surfaces and complimentary stresses for the two components when contraction of the pitman toe and toggle occurs during the cooling process. The result is that the sleeve is subjected to an external compressive force. This is equivalent to press fitting the sleeve into the mating components so that it is permanently fixed at the lower temperature. The other alternative to this first step is to actually press fit the sleeve into the pitman toe, thus eliminating the thermal stresses generated during the heat expansion process. The other step is to press a chrome steel ball through the sleeve. The dimensions of the ball will be such that the stresses generated will be beyond the yield strength of the sleeve material, causing plastic deformation. This will put the sleeve in further compression, thus minimizing the effect of fatigue cracking caused by the failure mode of fretting and also increasing the operating life and reliability of the pin-joint connection.

The optimum design solution for this pin-joint connection has not yet been defined and studies of various options are continuing.

2.1.3. Double-Roll Crusher

The decision has been made to use a 40 by 26 in. double-roll crusher as the tertiary component of the UNIFRAME crushing train. Design and drafting effort is continuing on the support and remote maintenance mechanisms of this specific double-roll crusher. The effect of the crusher on the dimensions of the structure, the structure design, and the ventilation system is presently being defined.

2.1.4. Screener

The conceptual design for the screener has been completed. The basic dimensions were determined from considerations of the UNIFRAME system size limitations, the manufacturer's size restraints, and the necessary screening capacity. The axisymmetric design minimizes material residence time and material holdup and allows sufficient air flow necessary for the ventilation system. The concentric outer shell makes flexible couplings between the screener and the double roll crusher, the oversize pulverizer, and the pneumatic transport system unnecessary. Rigid joints will be simpler and less expensive and will have a longer life than flexible couplings. The screener motor must be designed to operate within a high-radiation environment from the irradiated fuel particles. Bearing lubricants and motor insulation materials that will withstand the high-temperature high-radiation environment are being sought. Discussions with screener manufacturer have eliminated foreseeable fabrication and operational problems, and the formal bid procedure has been initiated.

REFERENCE

2-1. Bathe, K., E. L. Wilson, and F. E. Peterson, "SAP IV - A Structural Analysis Program for Static and Dynamic Response of Linear Systems," University of California Report EERC 73-11, Earthquake Engineering Research Center, College of Engineering, University of California at Berkeley, June 1973.

3. SOLIDS HANDLING

3.1. SOLIDS PROPERTIES

Efforts this quarter using the flow factor tester and consolidating bench of Jenike (previously described in Ref. 3-1) have produced the design parameters listed below for the powder system described in Fig. 3-1. This powder system is considered to be typical particulate H-327 graphite elutriated during normal operation of the 20-cm primary burner. The design values associated with this system have been determined to be as follows:

Effective angle of friction, $\delta = 49.5°$
Kinematic angle of friction, $\phi' = 26.9°$
Hopper wall angle, $\theta' = 15°$
Bunker diameter (minimum), D = 6.4 in.

These values were determined at a relative humidity of 50% and an ambient temperature of 70°F. Additional constraints to the design data were (1) an effective minimum bunker volume of 2.3 ft^3 (note phantom lines characterizing powder system in Fig. 3-2), and (2) a 2-in.-diameter outlet.

A proposal is being prepared to enable GA and ORNL cooperative development of solids property data for use in the transport, storage, and flow of irradiated powder and/or granular materials of the head-end reprocessing flowsheet. Preparatory visits have been made to acquaint GA personnel with the ORNL hot cell facilities and ORNL with the GA experimental apparatus.

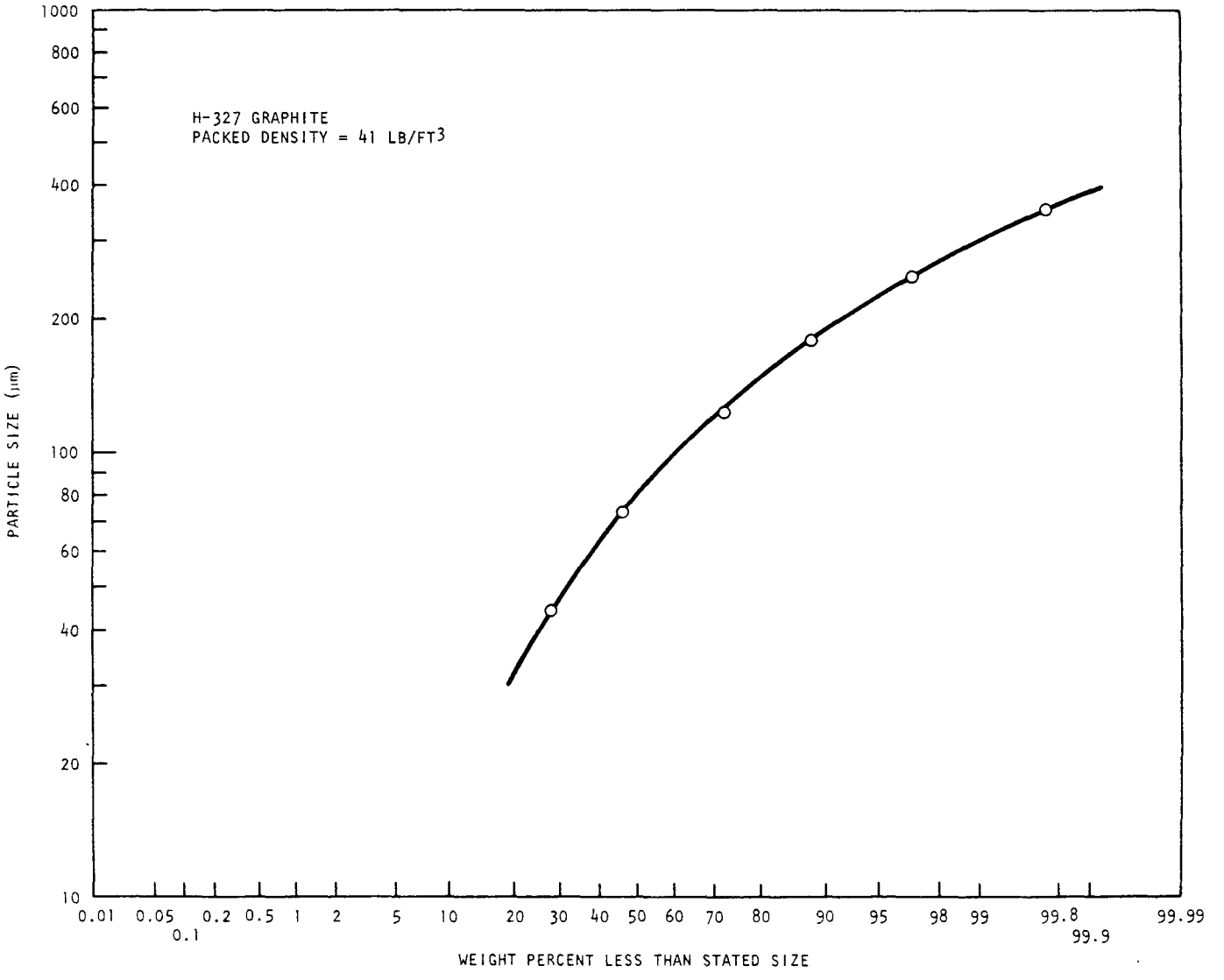

Fig. 3-1. Size-weight distribution of elutriated 20-cm primary burner fines

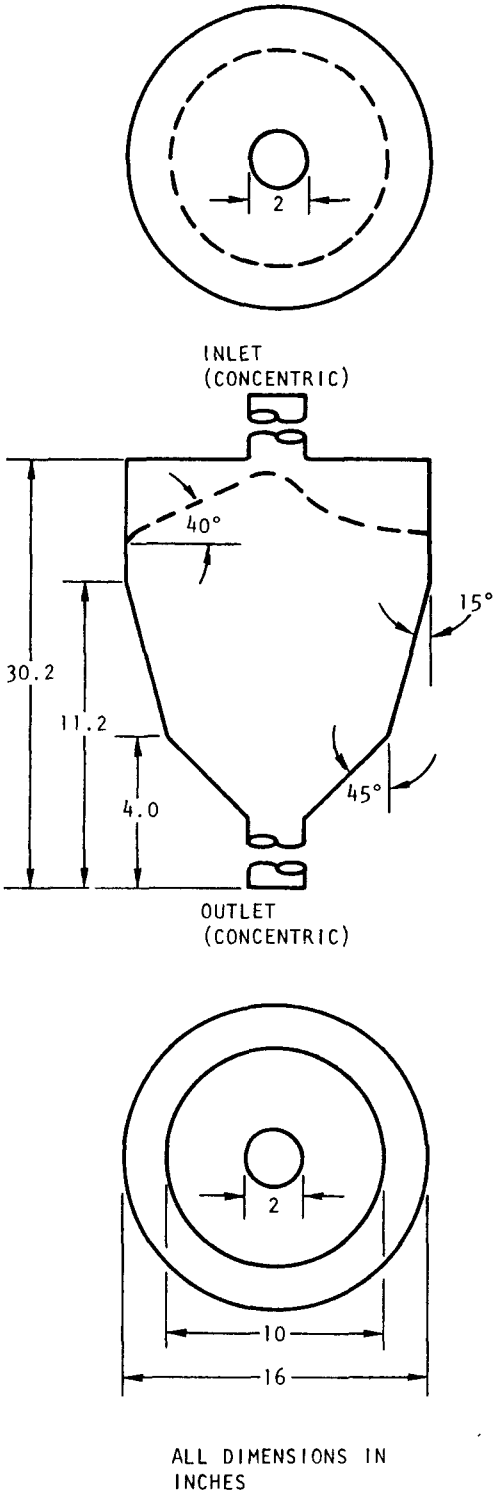

Fig. 3-2. Experimentally determined bunker dimensions, elutriated 20-cm primary burner fines

3.2. PNEUMATIC CLASSIFICATION

3.2.1. TRISO/TRISO Fuel System

3.2.1.1. Introduction

In the reference flowsheet for reprocessing of HTGR fuel, separation of the fissile and fertile fuel particles is required after the burning operation, and the material from these particles continues throughout the remaining process steps as separate streams. Separation of the bred U-233 in the fertile particles from the U-236-contaminated U-235 in the fissile particles avoids a significant fuel cycle penalty from buildup of U-236 in successive reactor reloads. The theory describing pneumatic classification of fuel particles is given in detail in Ref. 3-2.

3.2.1.2. Development of the Model

In most solid-solid separation processes, the accuracy of the separation is not as critical as it is in the separation of the fissile and fertile fuel particles used in HTGRs. The existing theory on separation was not adequate for the prediction of this separation because of both the tight separation limits imposed by the fuel cycle economics (Ref. 3-3) and the closeness of the particle size distributions. For these two reasons, the efficiency of separation of fissile from fertile fuel particles was determined experimentally on an Alpine multiplex zigzag air classifier (Fig. 3-3) and an empirical matrix model was found that could predict the behavior of this separation. The basic equations governing the model were established from experimental data on a simulated fuel distribution (Fig. 3-4) prior to actual tests with Fort St. Vrain fuel material.

A relationship was established between the separation efficiency (ϕ) and the feed rate of the solids (F) for each particle size increment and for several air velocities:

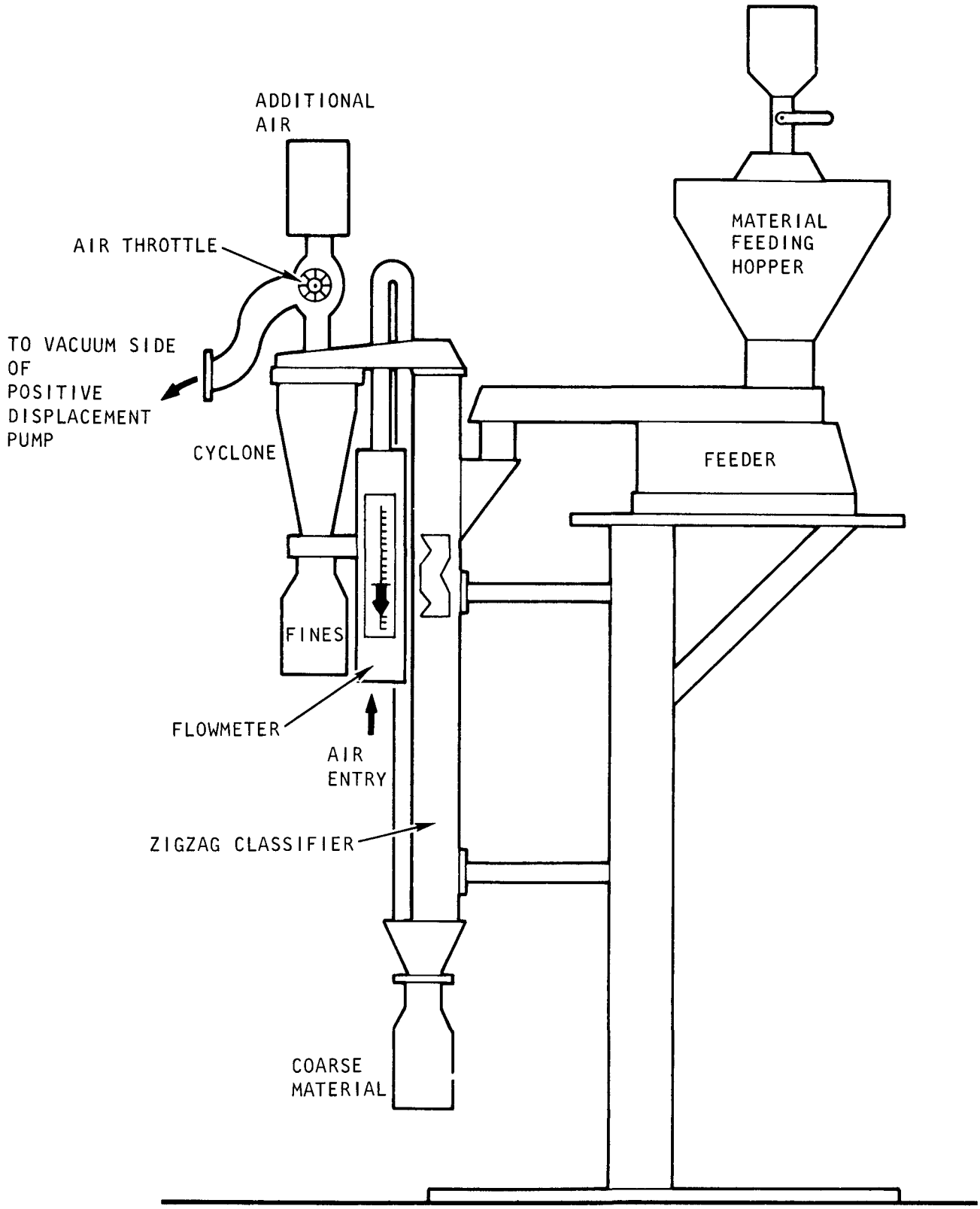

Fig. 3-3. Alpine air classifier

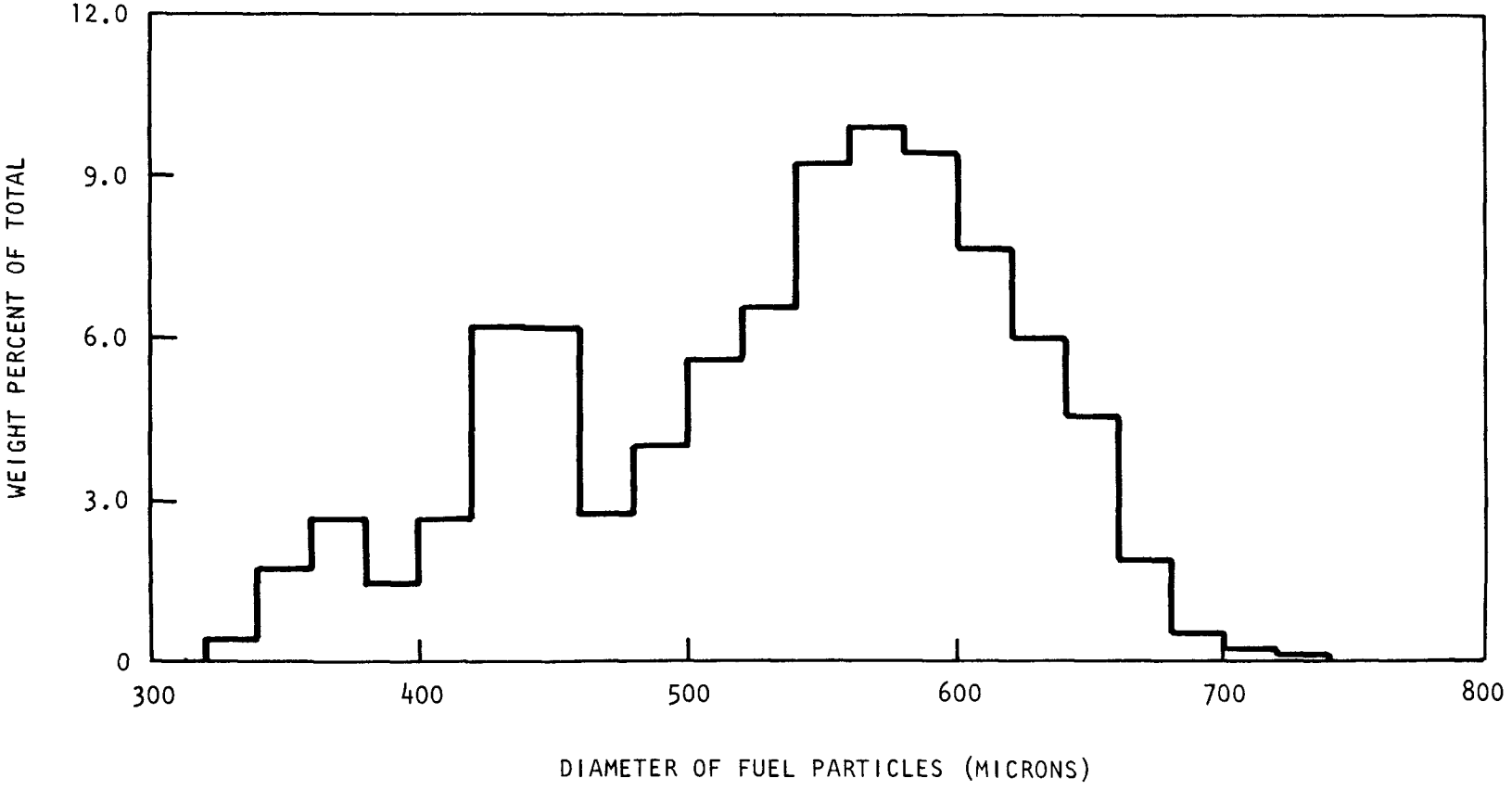

Fig. 3-4. Particle size distribution of simulated feed

$$\phi = \frac{F}{A' + B'F} \tag{3-1}$$

The relationship between separation efficiency and feed rate that occurs with simulated fuel and is described by Eq. 3-1 is as follows. Due to the increased concentration of particles in the classifier with increased feed rate, the separation efficiency worsens and the cut point shifts downward in size.

The constants A' and B' were then related to the particle diameter (d) at one air velocity (A). The change in air velocity was then incorporated as a diameter shift (d_a), giving the following relationships:

$$d_a = 676.4 - 124.24A \tag{3-2}$$

$$A' = \exp(28.52 - 0.03271d_a) \tag{3-3}$$

$$B' = 18 - \frac{4225}{d_a - 408} \tag{3-4}$$

$$d_a < 410,\ B' = -300 \text{ and } d_a > 656.5,\ B' = 1 \tag{3-5}$$

These four equations were the starting point for the model. Once these equations were formulated, the effect of graphite and the effect of the relative size of the distribution modes were incorporated. Preliminary tests indicated that the presence of graphite gave similar results to tests without graphite at higher feed rates.

Experiments with FSV-type fuel (see Figs. 3-5 and 3-6 for size distribution) were conducted to determine if there were any differences in the separation compared to preliminary tests with simulated fuel. A shift in the constant diameter lines was noted and also a change in their spacing. This shift was explained by the shift in the intersection of the size distributions and by the increased slope of the relationship between

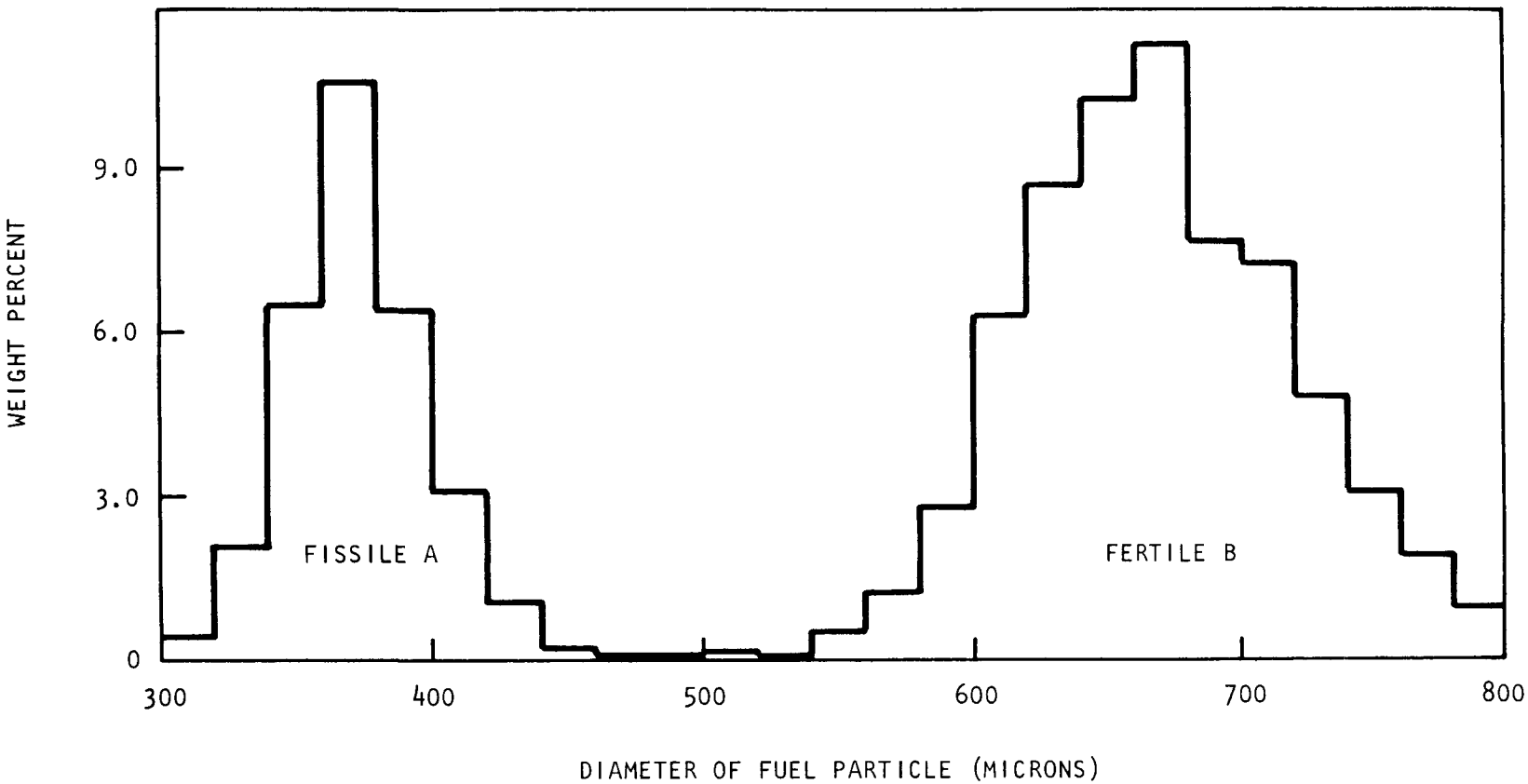

Fig. 3-5. Particle size distribution of FSV fuel, fissile A and fertile B

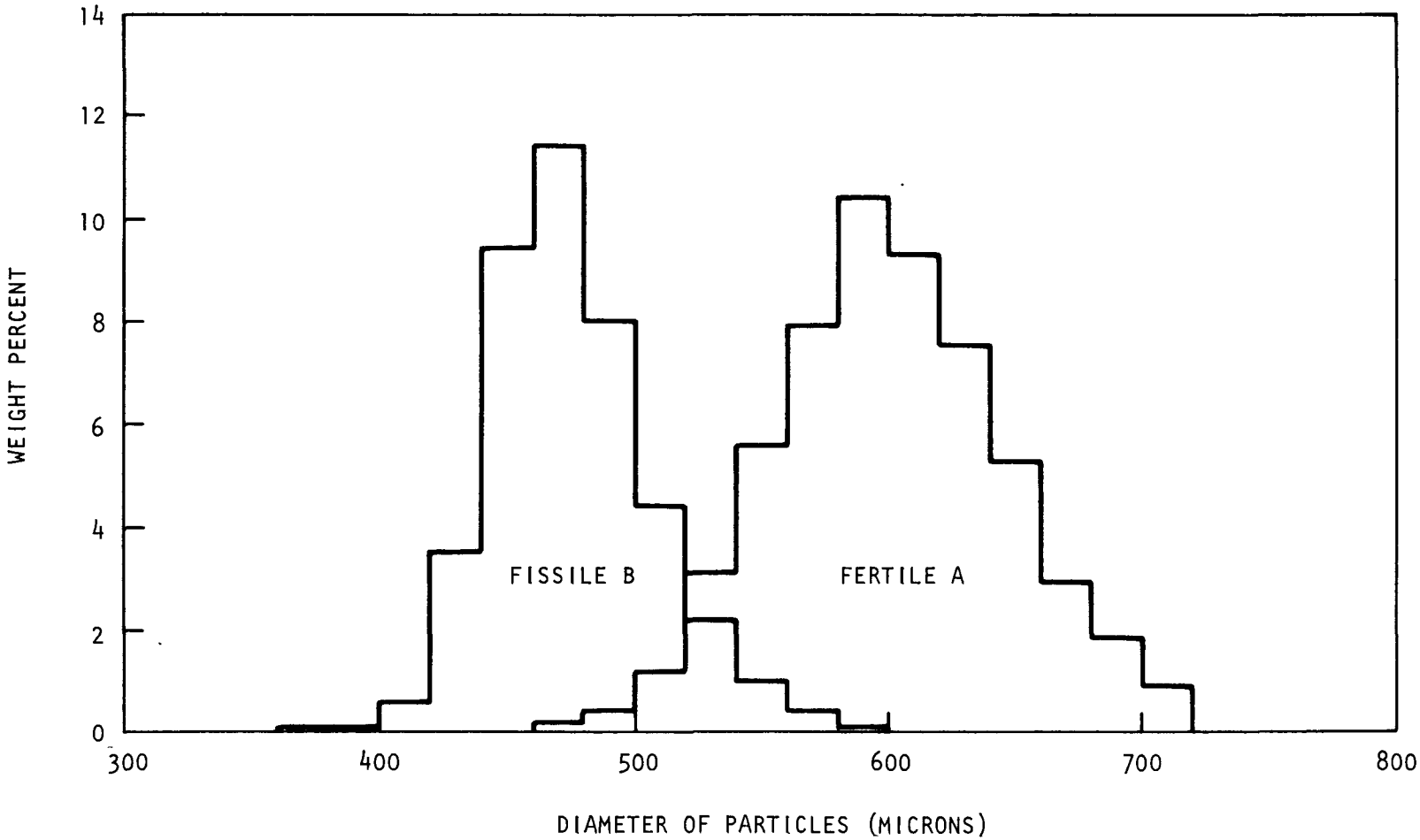

Fig. 3-6. Particle size distribution of FSV fuel, fissile B and fertile A

density and particle size. These tests also indicated a lack of dependence on feed rate, which stems from the increased slope of the density relation (Ref. 3-4), so that the feed rate term d defined in Eq. 3-1 was replaced by a constant.

The next step in refining the model was to predict the performance of the experimental classification system using material from FSV reject fuel rods (Ref. 3-5). Ten feed batches were used containing varying particle size distributions and varying amounts of carbon. When the runs using material with a size distribution similar to the earlier FSV fuel were analyzed, the prediction of the separation required an increase in the constant that replaced the variable feed rate. This increase was related to the addition of graphite in the feed. In earlier runs using simulated feed, similar results had occurred. The constant that replaced the feed rate in the simulated feed model correctly described the effect of graphite on the separation of FSV fuel, and a linear relationship between this constant and the percent graphite was added to the model.

Once the influence of graphite was established, the effect stemming from the relative breadth of the size distribution modes could be investigated. This investigation showed that the separation efficiency versus particle size shifted toward the smaller mode in an amount proportional to the net difference in the weight of the fissile B and fertile A particles in the feed. This result agrees with the observations made earlier in connection with the runs using simulated feed. With this last adjustment, the model can now predict the separation within the range of +3.3 to -6.4% error. The model has as inputs the air flow rate, weight percent carbon, and weight percent fissile A, fissile B, fertile A, and fertile B fuel. The following equations are used to describe the pneumatic classification of FSV fuel:

Modal Shift

$$S_m = -27.4 - 160(R_{ub} - R_{Ta})$$

For $R_{ub} = 0$ or $R_{Ta} = 0$, S_m [=] 0

Graphite Influence

$$G = 100 + 9.25P_g$$

Air Velocity Shift

$$S_a = 596.4 - 124.24A$$

Density Influence

$$d < 520 \qquad D = 15.2\left(\frac{d}{100}\right)2.15$$

$$520 < d < 560 \qquad D = d$$

$$d > 560 \qquad D = 22.7d^{0.507}$$

Separation Efficiency

$$\alpha = S_m + S_a + D$$

$$\beta = \exp(25.9032 - 0.03271\alpha)$$

$$\gamma = 18 - \frac{4225}{\alpha - 328} \qquad \left\{\begin{array}{l}\text{For } \alpha < 320,\ \gamma\ [=]\ -300\\ \text{For } \alpha > 576.5,\ \gamma\ [=]\ 1\end{array}\right\}$$

$$\phi = \frac{G}{\beta + \gamma G} \qquad \left\{\begin{array}{l}\text{For } \phi < 0,\ \phi\ [=]\ 0\\ \text{For } \phi > 1,\ \phi\ [=]\ 1\end{array}\right\}$$

where A = air flow rate (m/sec)
d = diameter (μm)
D = density influence
G = graphite influence
R = fraction of total fuel particles
P = percent of feed
S = diameter shift
α,β,γ = intermediate values
ϕ = separation efficiency

Subscripts are used as follows:

g denotes graphite
m denotes modal
a denotes air flow rate
ub denotes fissile B
$_{T}$a denotes fertile A

and [=] means set equal to

These equations are valid over the range of

Percent graphite - 0 to 45 wt %
Solids feed rate - 0 to 350 g/min
Gas flow rate - 3.15 to 4.8 m/sec

The final addition to the model converts separation parameters to percent crossover of the fissile and fertile streams. For this conversion, the percent fissile in a particular size increment in the fine and coarse products must be related to the ratio in the feed. Fortunately, the relationship is straightforward. First, the fissile ratio of the fines product for any size increment is equal to the ratio for a 20-μm larger size in the feed. The reverse is the case for the coarse product; i.e., the fissile ratio is equal to the ratio for a 20-μm smaller size in the feed. With this addition to the model, the percent crossover calculated was within ±14% error (e.g., if the predicted crossover is 10 wt %, the actual crossover will be between 8.6 and 11.4 wt %). The necessity for this shift supports the contention that, on the average, a fissile particle having the same size as a fertile particle is less dense.

The use of this model is its application to the reprocessing of FSV fuel. By knowing the particle size distribution of any batch, the optimum flow rate to give the least crossover can be determined. This crossover can then be related directly to the cost penalty. In this manner, the

economics of reprocessing can be estimated with greater accuracy, and optimum separation of the fuel can be assured. The only information required is the percent carbon in the feed and the amount of fissile A, fissile B, fertile A, and fertile B fuel in the feed. The amount of carbon in the feed is dependent on the operation of the primary burner and the particle size distributions can be obtained from Ouality Assurance data on FSV fuel for a particular fuel element being processed (Ref. 3-6).

3.2.1.3. Effect of Height and Feed Point

With the separation process characterized for a set height and feed point, tests were conducted using a modular classifier (Fig. 3-7) to determine the effect of height and feed point. First it was found that the increased height of the column resulted in no improvement for feed rates of approximately 100 g/min. However, as the rate increased toward 500 g/min, a marked improvement was noted. As the feed point was moved up, the efficiency of separation improved for both coarse and fine fractions.

3.2.1.4. Sieving

Extensive testing showed that although sieving leads to a better instantaneous separation efficiency, the overall separation efficiency of sieving is poorer than separation by pneumatic classification because the cut point decreases with time as the screen becomes plugged. Sieving also has the disadvantage of permanent plugging of the screen openings so that after a period of time the screen must be replaced. Further, the cut point of the screen cannot be changed except by replacement, and a 64-in. screen is required to give a 200 g/min throughput. Finally, the screener is harder to maintain because of the larger number of moving parts. Sieving has therefore been eliminated as a process option, and pneumatic classification has been adopted as the reference technique.

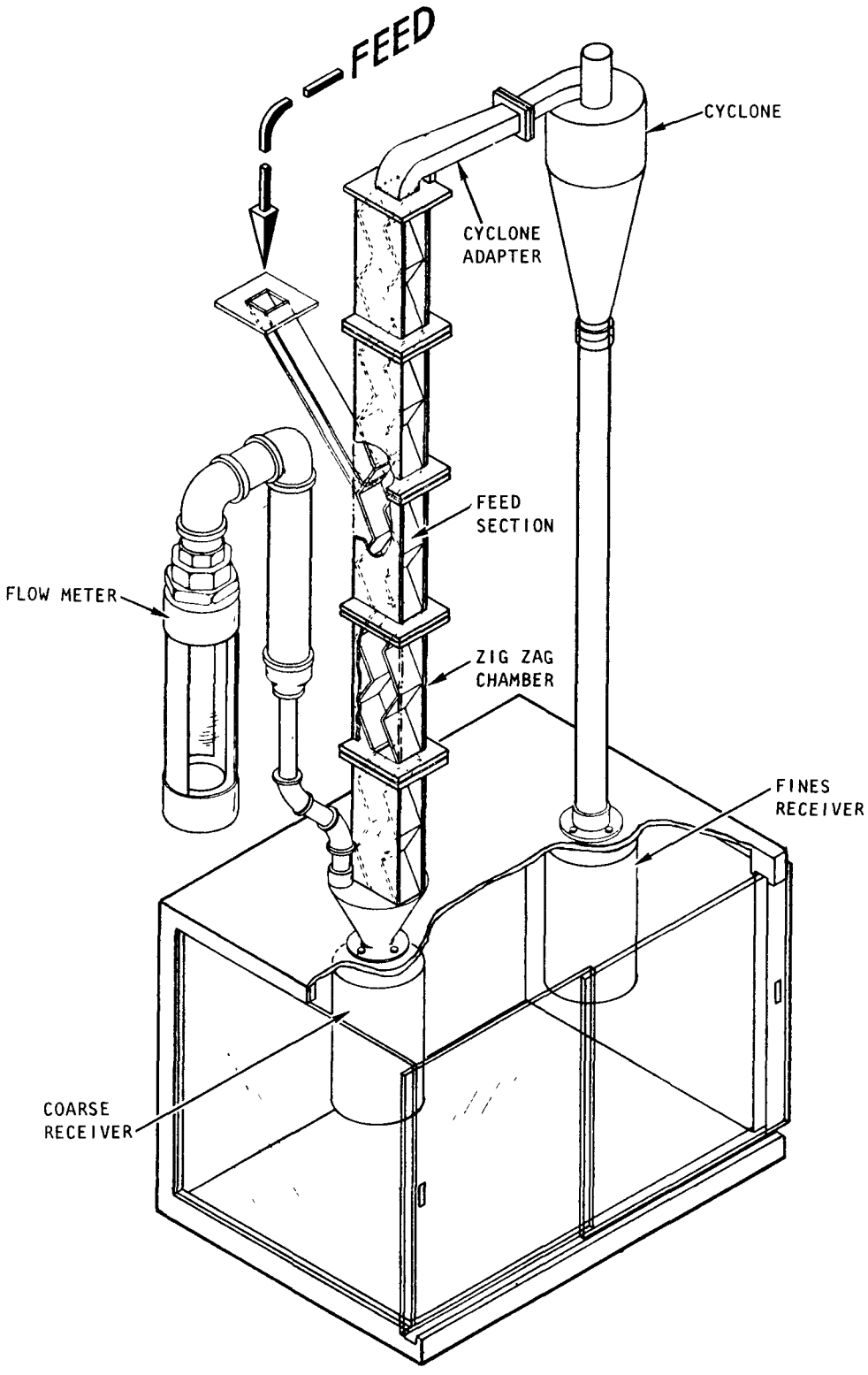

Fig. 3-7. Modular pneumatic classifier

3.2.1.5. Separation of the Particle Crusher Product

The preceding discussion concerns the separation of the fissile fuel from the fertile fuel after the fuel leaves the primary burner and before it enters the roll crushers. One other particulate system was investigated: crushed fertile particles. By classifying the fuel as it leaves the roll crushers, 84 wt % of the SiC hulls and 89 wt % of the carbon coatings can be removed from the kernels with only a loss of 0.5 wt % heavy metal. This has four advantages:

1. The load on the centrifuge would be reduced by a factor of six.

2. The carbon coatings, which are laden with fission product, could be diverted for disposal as solid waste.

3. The burning load on the secondary burner would be reduced.

4. The liquid waste from the aqueous separation would be reduced.

However, this method would require separation of heavy metal dust resulting from the breakage of particles in the fuel element crushing, primary burning, and classification operations. The dust would then be routed to the secondary burner. Typical broken particle weight percents, as given in Ref. 3-7, are:

Fissile A - 3.7 wt %
Fissile B - 3.2 wt %
Fertile A - 7.5 wt %
Fertile A and B - 17.1 wt %

An average of 0.7 wt % is broken in the classifier.

3.2.2. TRISO/BISO Fuel System

Pneumatic classification tests were carried out on the modular classifier (configuration as depicted in Fig. 3-7) using sol-gel thorium oxide kernels and weak-acid-resin fissile particles. The properties of the fissile particles are given in Table 3-1 and the ThO_2 particle size distribution is given in Fig. 3-8.

Preliminary results on these tests indicate that at a feed rate of 1500 g/min, the crossover loss of fissile particles to the fertile stream, and also fertile particles to the fissile stream, is less than 3 wt %. This value is for whole particles only; if broken particles are present it is assumed that ∿75% of both the fissile and the fertile particles (Ref. 3-7) would elutriate with the fissile particles.

3.2.3. Prototype Pneumatic Classifier

The design of the prototype unit has been finalized. The major design points are as follows:

1. The configuration will be of the zigzag design, 88 in. high with a cross section of 1.5 in. by 3 in. with the zigzag repeating every 2 in.

2. The feed will enter at the midpoint of the column.

3. A vibratory feeder will be used with a solids flow rate sensor coupled in a closed control loop with a feed rate of 600 to 1000 g/min.

4. The air flow rate will be monitored by a transmitting rotameter coupled in a control loop with a variable speed blower.

TABLE 3-1
PROPERTIES OF THE WEAK-ACID-RESIN PARTICLES

Substrate mean diameter	296 μm
Substrate density	2.91 g/cm^3
Buffer thickness	53.4 μm
Buffer density	0.942 g/cm^3
Inner LTI[(a)] thickness	34.4 μm
Inner LTI density	1.93 g/cm^3
SiC thickness	37.7 μm
SiC density	3.21 g/cm^3
Outer LTI thickness	39.3 μm
Outer LTI density	1.80 g/cm^3
Inner LTI OPTAF[(b)]	1.10
Outer LTI OPTAF	1.11

[(a)] LTI = low-temperature isotropic coating.

[(b)] OPTAF = optical anistropy factor.

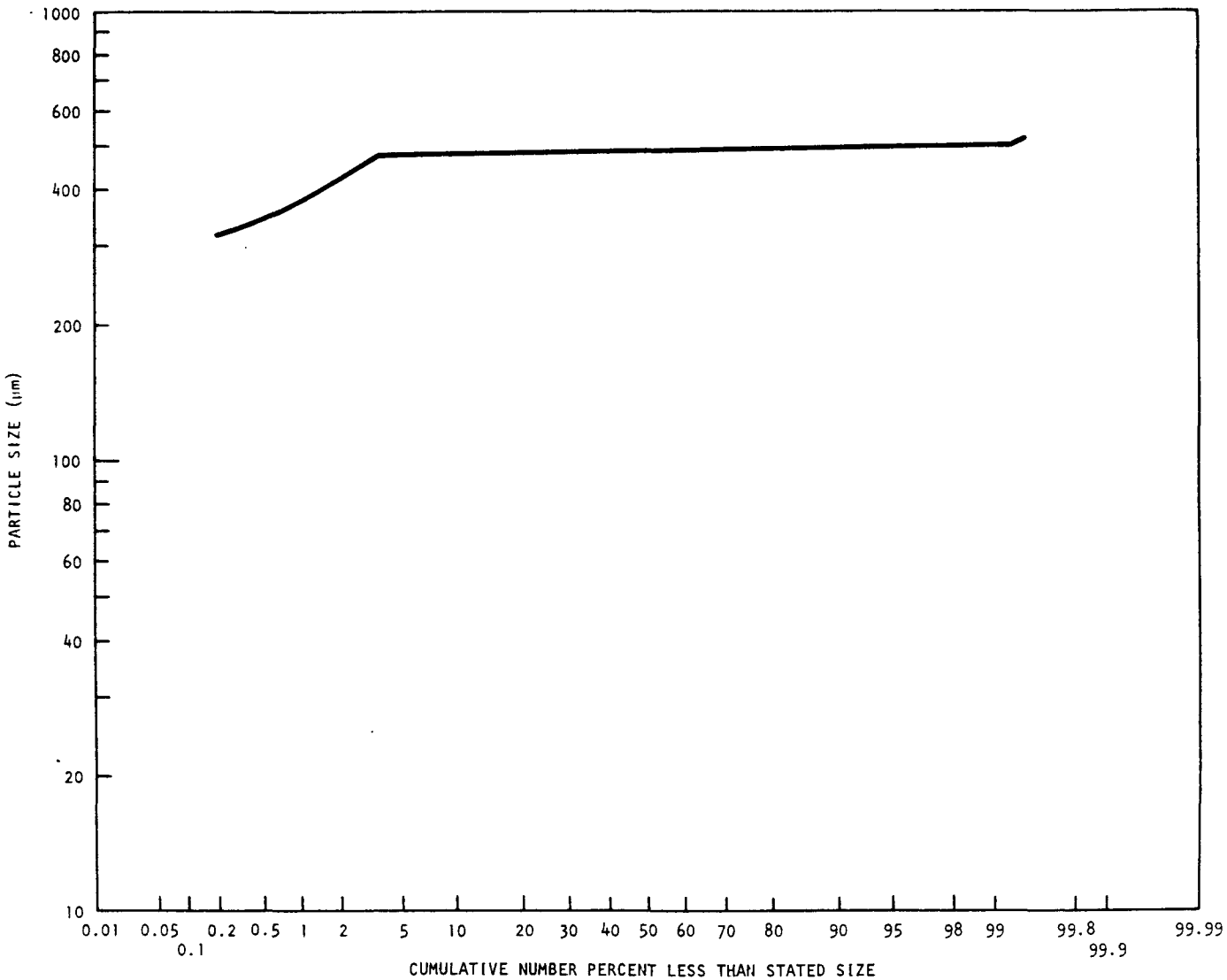

Fig. 3-8. Size distribution of ThO_2 particles

3.3. PNEUMATIC TRANSPORT

3.3.1. Experimental Pneumatic Transport System

Assembly of the experimental pneumatic transport system, as previously described in Ref. 3-8, for gathering information on the three major types of solids requiring transport in the proposed head-end process is nearing completion. Procurement of the necessary equipment, with the exception of the blow-back filters and the variable speed positive displacement blower, is complete. A long delivery time is anticipated for the blower; however, a spare blower is available.

3.3.2. Prototype Line

The prototype pneumatic transport system will link the four unit operations: crushing, burning, classification, and burning. For this connection, six forward transport systems will be required along with two recycle systems:

Forward Transport

1. Crusher to crusher product bunker.

2. Crusher product bunker to primary burner feed bunker.

3. Primary burner product removal to primary burner product bunker.

4. Primary burner product bunker to pneumatic classification feed bunker.

5. Pneumatic classification product bunker to particle crusher bunker feed.

6. Secondary burner product removal to secondary burner product bunker.

Recycle

1. Primary burner product bunker to primary burner feed bunker.

2. Pneumatic classification product bunker to pneumatic classification feed bunker.

A representation of these systems in relation to the various unit operations is shown in Fig. 3-9. Placement of the product bunkers and the size of all bunkers are inexact.

In these systems the major design considerations were as follows:

1. Transport capacities equal to or in excess of those required by the unit operations.

2. Tangential entry into receiving bunkers with an expansion tube prior to entry.

3. Flexible connections on bunkers with weigh systems.

4. In-bunker sintered metal filters with timed blow-back.

5. Flanged metal filters with integral eductors for remote maintainability.

6. Remote actuated blowers, valves, and feeders.

7. Time-delay interlocks on blower, valve, and feeder actuation.

8. Variable remote controlled feeders.

9. Interlocks between common transport systems.

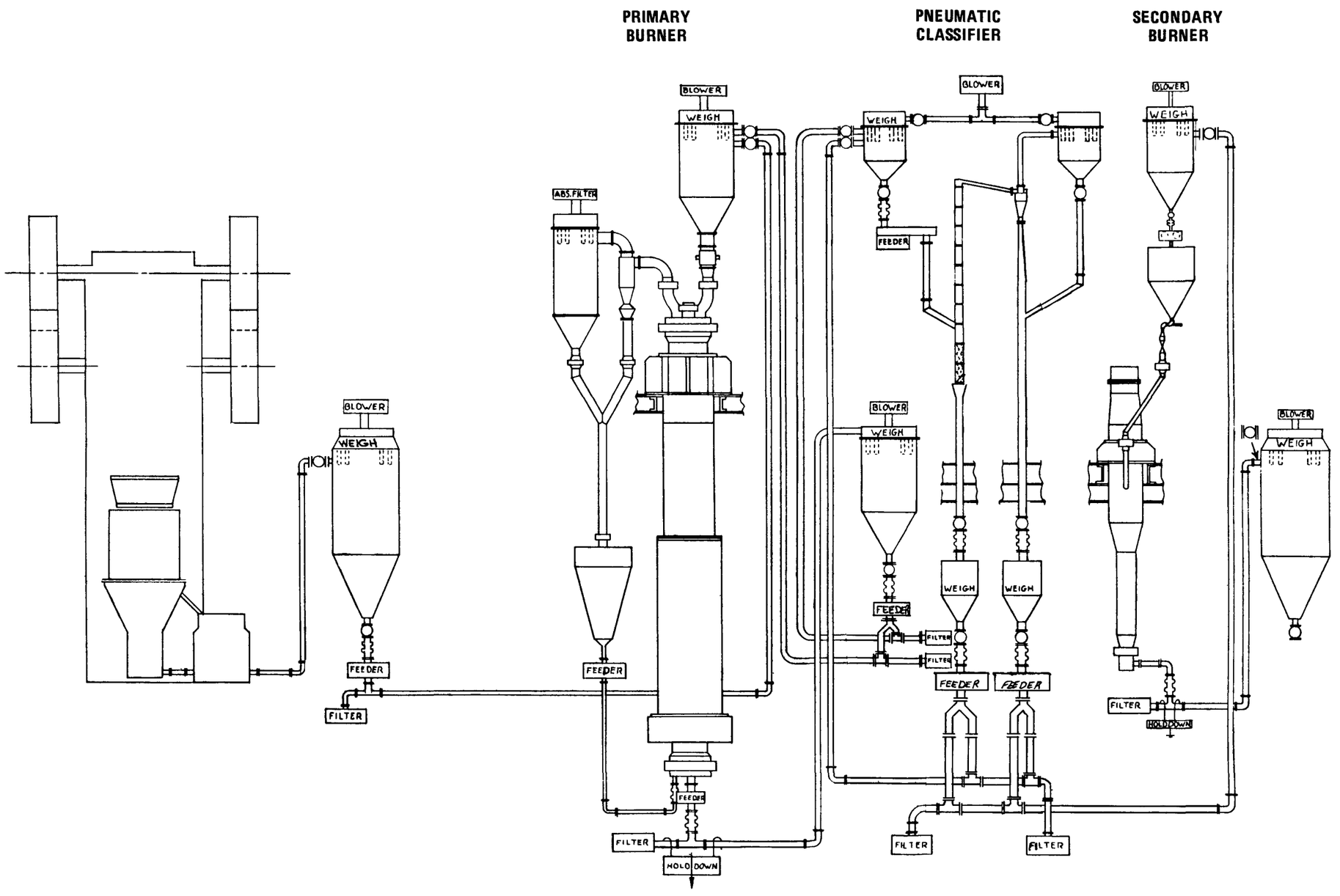

Fig. 3-9. Layout of prototype pneumatic transport system

From these criteria, the various components of the transport systems were identified and sized to ensure the required capacities. A parts list was then established and procurement was initiated.

3.4. FLOW RATE SENSOR

The in-line monitoring of solids flow rates is required at two points in the reprocessing head-end:

1. To determine the rate and cumulative amount of oversized material leaving the screener in the UNIFRAME size reduction system.

2. To determine the rate and to control the solids entering the particle air-classification system.

Since no commercially available device meets the required solids flow rate ranges (0 to 2000 g/min) for these applications, a device has been designed. Figure 3-10 is a schematic representation of the device where the impact force of the solids on the deflection plate is directly related to their distance of fall and mass flow rate.

Tests on a similar device using this principle (Ref. 3-9) gave a linear relationship (Fig. 3-11) between the output signal of the force transducer and the mass flow rate. However, two deficiencies were observed:

1. When the load on the system was removed, the points of contact in the mechanical linkage introduced a small drift and delay in the signal.

2. The point of impact on the deflection plate was critical.

Encouraged by results using strain gages (Ref. 3-10), the original design was changed to utilize strain gages to eliminate pivot points and the influence of the deflection plate. Figure 3-12 shows the new version

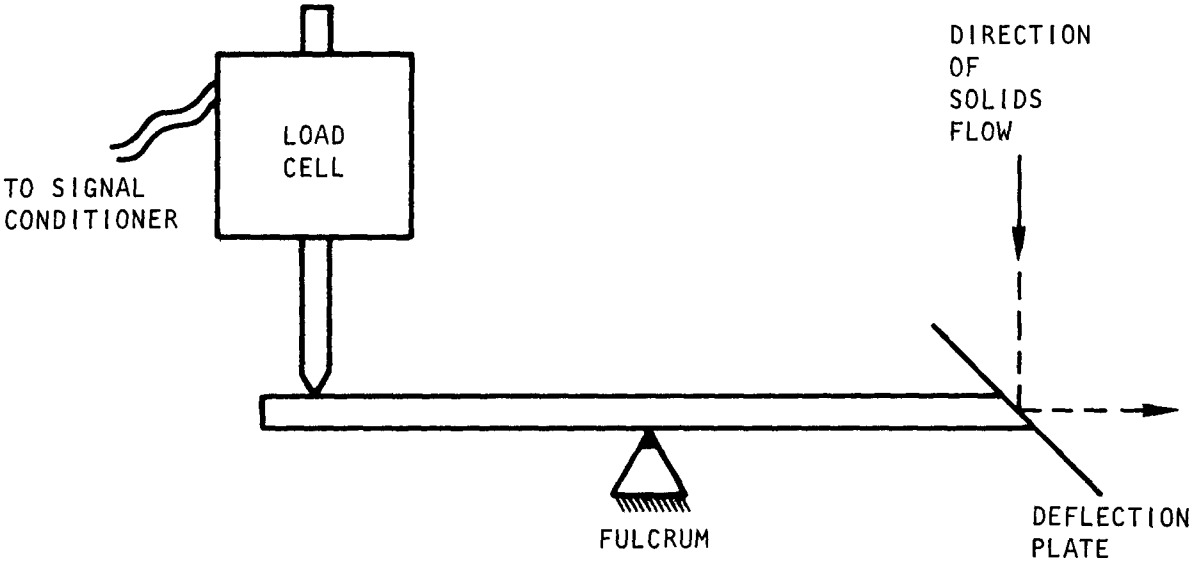

Fig. 3-10. Schematic of flow rate sensor

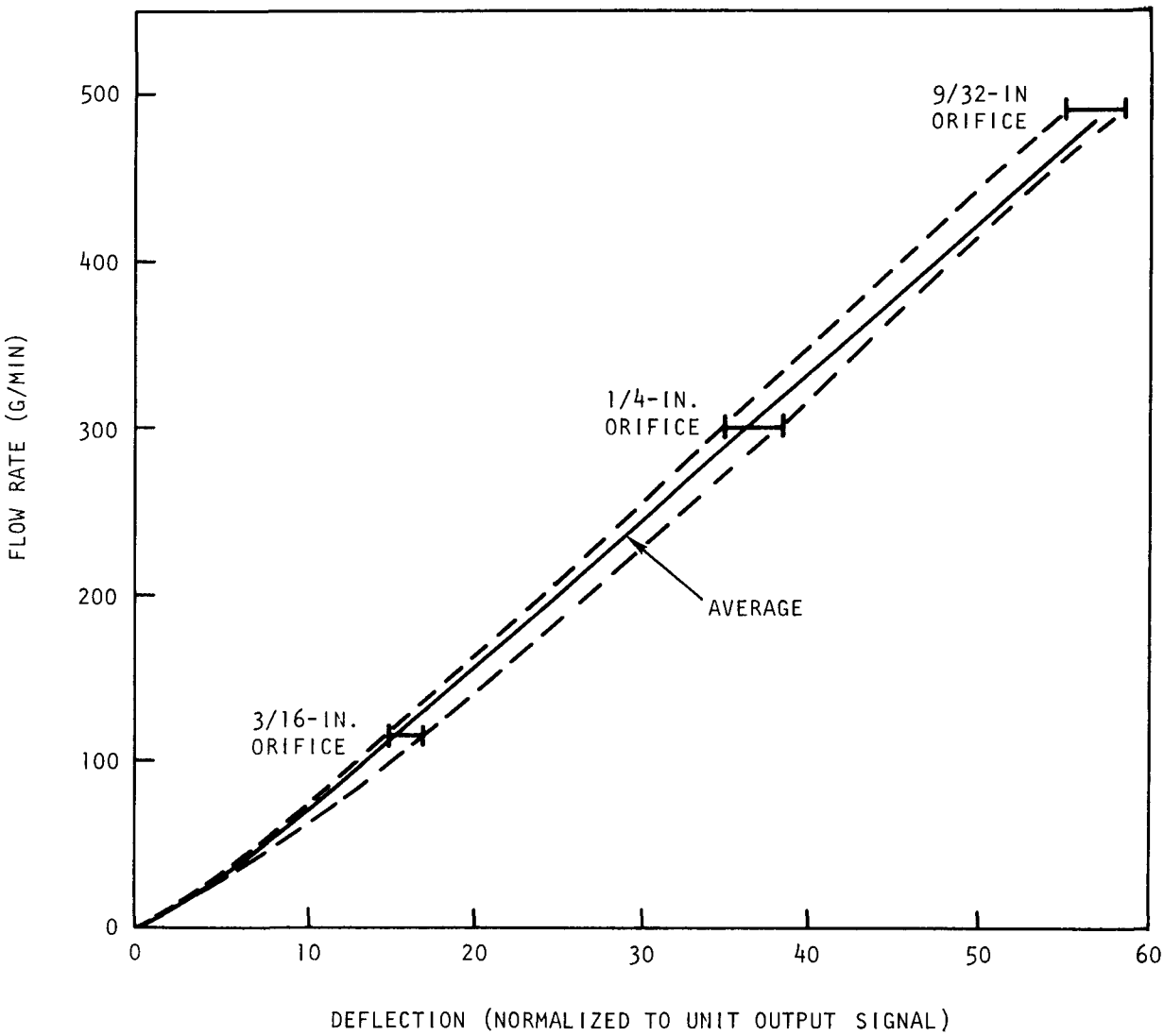

Fig. 3-11. Solids flow rate versus output signal deflection

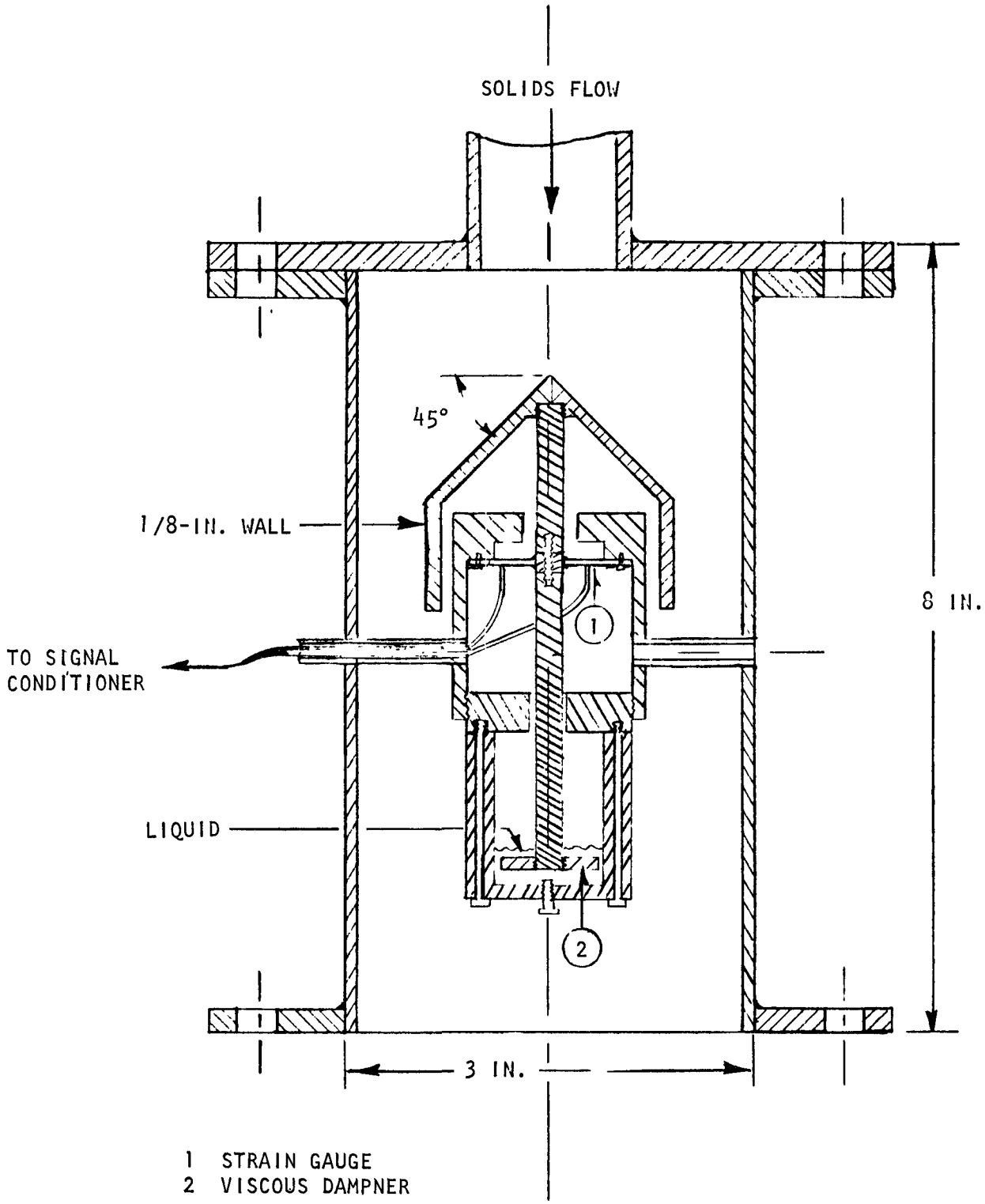

Fig. 3-12. Conceptual design of flow rate sensor

of the solids flow rate sensor. The design is complete and fabrication will commense in mid-March. An accuracy of ±25 g/min is expected (Ref. 3-10).

REFERENCES

3-1. "Thorium Utilization Program Quarterly Progress Report for the Period Ending November 30, 1974," USAEC Report GA-A13255, General Atomic Company, February 15, 1975.

3-2. DeLesdernier, D., and B. Baxter, "Pneumatic Classification of FSV Fuel Particles," USAEC Report GA-A13135, General Atomic Company, to be published.

3-3. "National HTGR Recycle Development Program Plan," USAEC Report ORNL-4702, Oak Ridge National Laboratory, August 1973.

3-4. Guha, S., A. Kumar, and P. Gupta, "Mechanism of Elutriation From Fluidized Beds," Can. J. Chem. Eng. 50, 602 (1972).

3-5. Cook, E., and D. deLesdernier to M. Spaeth, General Atomic Company, "Summary of the Scrap Rod Program, Crush-Burn-Classify," private communication, February 14, 1975.

3-6. DeLesdernier, D., to B. Baxter, General Atomic Company, "Computer Model Simulation of Pneumatic Classification of FSV Fuel," private communication, February 13, 1975.

3-7. deLesdernier, D., to B. Baxter, General Atomic Company, "Crossover and Particle Breakage Analysis of the Air Classification Step in the Scrap Rod Program," private communication, September 19, 1974.

3-8. "Thorium Utilization Program Quarterly Progress Report for the Period Ending August 31, 1974," USAEC Report GA-A13178, General Atomic Company, October 31, 1974.

3-9. True, M. D., to B. Baxter, General Atomic Company, "Flow Rate Sensor," private communication, February 8, 1975.

3-10. Papadates, K., and W. Surcek, "Low Range Flowmeter for Pulverized Solids," Instr. Tech. 21, 38, (1974).

4. FLUIDIZED-BED COMBUSTION

4.1. PRIMARY FLUIDIZED-BED COMBUSTION

During this reporting period the development program concentrated on the 20-cm primary fluidized-bed burner. This burner will be utilized to verify the prototype process design considerations and now incorporates the perforated conical distributor and pneumatic transport of feed and product. Testing of various pressurized pneumatic fines feeder systems is under way.

4.1.1. 20-cm Primary Fluidized-Bed Combustor

Nine runs were performed on the 20-cm primary burner during the last quarter. These runs are summarized in Table 4-1.

Runs 7 through 11 tested fines recycle to the ball/cone distributor using pneumatic fines recycle in dilute phase. This dilute, pneumatic recycle technique was found unacceptable in that more fines were generated than were burned. Major limitations to the fines recycle rate and fines burning were insufficient fines mass transport against the bed back-pressure and cooling of the fines in the fines recycle loop due to the high ratio of transport gas to fines required in dilute fines recycle. This conclusion would not be expected to change even if a different distributor, e.g., the perforated cone, were used.

Runs 12 through 15 were performed using a perforated conical distributor, the reference design for the prototype. Operation demonstrates satisfactory fluidization and product removal characteristics, with minor revisions to account for the distributor plenum temperature being higher than assumed in the design calculations. The fresh feed size used in these latter 20-cm burner runs was analogous to feed that caused operating problems in past primary burner runs using the ball/cone

TABLE 4-1
SUMMARY OF 20-CM PRIMARY BURNER RUNS

Run	Objectives	Fines Recycle[(a)]	Observations/Conclusions
7	Test fines recycle premixed with gas to cone bottom.	Yes, using Penberthy ejector on bottom of fines hopper. Fines introduced late in run to observe effects on equilibrium operation.	Limited fines transport was noted visually. Sampling of fines circulation was disrupted by cyclone bridging and fines salt-out in horizontal lines. Effects of fines injection were reduction of in-bed temperature and increases in above-bed temperatures.
	Test operation using startup that adds significant quantity of particles initially to maintain cone area material size average as low as possible.		No operating problems or agglomerates as seen in prior runs. The cone temperature was lower than temperatures higher on the bed, indicating high particle concentration in the cone, hence decreased spouting potential.
8	Longer duration of dilute phase fines recycle premixed with cone gas. Better fines circulation monitoring with N_2 purges to overhead lines to curtail bridging.	Yes: ejector on bottom of fines hopper, fines introduced during startup.	Material balance indicated about 50% of generated fines were burned at average bed back pressure of 38 in. H_2O. Partial blockage of ejector by pieces of the diverter valve plastic seal was thought to be the limiting factor in mass transport. Premixed fines injection again lowered in-bed temperature and increased above-bed temperatures.

TABLE 4-1 (Continued)

Run	Objectives	Fines Recycle[(a)]	Observations/Conclusions
9	Further study of dilute, pneumatic fines recycle. Fines sample diverter valve seat resurfaced with metal to improve fines circulator monitoring.	Yes, as in Run 8.	Negligible fines burning. Fines ejector was blocked by bed material backflow during initial fines transport gas introduction; called for reorientation of the ejector on the fines hopper to prevent material buildup and also a change in fines transport introduction. Fines ignited above the bed as bed carbon burned out.
10	Recycle fines with ejector on the side of the fines hopper and abrupt fines introduction to preclude bed material backing up and blocking ejector.	Yes: ejector body reoriented and method of introduction changed.	Fines lowered bed temperature and hence oxygen consumption and ignited above the bed. The run was shut down to prevent thermowell burn-through. Abrupt fines introduction not desirable. Need to bring in fines during startup with a continuous ejector bypass gas purge to prevent bed material backflow and to stabilize fines introduction.

TABLE 4-1 (Continued)

Run	Objectives	Fines Recycle[(a)]	Observations/Conclusions
11	Recycle fines tangentially to cone with ejector bypass purge.	Yes: introduced during startup by increasing fines transport gas while decreasing purge gas. Tangential injection versus vertical, premixed injection in prior runs.	Fines flow initially high but decreased as bed level was increased. About 15% fines burning at average bed back pressure of 52 in. H_2O. No material in ejector which represented optimum; hence, this method is unacceptable. Tangential injection yielded smoother in-bed temperature effects with less significant temperature decreases.
12	Initial operation with perforated cone distributor. Startup with full-sized fresh feed.	No	Cone area temperature excursions during startup with the full-sized fresh feed thought to be due to defluidized burning of the large graphite under limited startup gas flow rate conditions. Cone area temperature excursions as bed carbon burned out thought to be due to decreased heat transfer of large graphite remaining in the cone at bed burnout. Small (<4000 μm) agglomerates were found in the final bed, amounting to 0.5% of the total final bed weight. These fused particles were thought to be formed during the temperature excursions.

TABLE 4-1 (Continued)

Run	Objectives	Fines Recycle[a]	Observations/Conclusions
13	Further testing of the perforated cone with full-sized fresh feed for startup. Initial O_2 introduction made through cone perforations instead of vertex inlet as in Run 12.	No	Temperature excursions occurred as in Run 12. Excursions as bed burned out were less significant. This was thought to be due to a larger quantity of final bed particles in Run 13 than in Run 12 and resultant better heat transfer. Agglomerates (<4000 μm) constituted 0.45% of the final bed.
14	Avoid startup temperature excursion using an initial feed of -1400 μm graphite mixed with particles prior to full-sized fresh feed addition.	No	No startup cone area temperature excursions seen. Smooth operation with large fresh feed. Cone area temperatures again increased as bed carbon burned out. Agglomerates were found but in less than half the quantity seen in Runs 12 and 13 (0.2% of final bed).
15	Longer run with product take-off during operation to pinpoint time of any agglomerate formation. Increased diluent flow at bed burnout to improve large graphite circulation in the cone area and to dampen temperature effects of immobile large graphite burning. Test full batch dump at end of the run.	No	No significant cone area temperature excursions during startup or shutdown. No agglomerates found in mid-run products or in the final bed. Twenty-five kilograms of final bed material were dumped in approximately 2 minutes with no problems.

[a] Runs 7 through 11 with ball/cone distributor testing dilute phase pneumatic fines recycle. Runs 12 through 15 with perforated cone and no fines recycle.

distributor. The ball/cone distributor difficulties with "oversized" fresh feed were evidenced by the bed ΔP cycling up to 15 to 20% of the total ΔP, accompanied by cycling of both the bed temperatures and the off-gas compositions and the agglomeration of particles. It is believed that these operating problems were due to cyclic gas spouting caused by "oversized" graphite feed that accumulated in the single gas inlet ball/cone distributor (Ref. 4-1). This spouting phenomenon accompanying feeding large sized material to the single gas inlet cone may be eliminated by the perforated cone distributor and the acceptable feed size range can possibly be extended. Runs with larger sized fresh feed are planned to test this possibility.

Testing of dilute, pneumatic fines recycle in 20-cm burner runs 7 through 11 indicated the dilute transport mode excessively cooled recycling fines. This cooling prevented complete fines ignition during their short residence time in the bed. The effect of injecting the cooled fines was to decrease in-bed temperatures, as the recycled fines absorbed bed heat, and to increase the above-bed temperature as the elutriating fines carried the heat into the disengaging space. This phenomenon was especially significant in Run 10 when recycling fines cooled bed temperatures and decreased bed oxygen consumption to a degree that allowed oxygen to reach and ignite the hot above-bed fines.

Mass transport of the fines in dilute phase flow decreased as the bed size and bed back-pressure increased. The effect of bed back-pressure on fines flow was confirmed qualitatively in Run 11 by visual observation of fines flow reduction as the bed level increased. Comparing fines burning in Run 8 to that in Run 11 showed 50% fines burning when dilute fines transport was against a bed back-pressure of 38 in. H_2O, and 15% fines burning with transport against a bed back-pressure of 52 in. H_2O. The erratic recycle flow behavior and the low, back-pressure-sensitive, fines burning efficiency of dilute, pneumatic fines recycle proved that this mode is unacceptable. The area of difficulty was in the mechanism of fines transport; hence, changes in the burner distributor design or in burner

operation would not be expected to improve recycled fines burning using dilute phase transport.

Future work with dense, pressurized pneumatic fines recycle on the 20-cm burner will be used to evaluate the system capabilities under conditions of prototype operation. Such a system has worked well on a smaller 10-cm burner operated at ACC-ICPP (Ref. 4-1a) with an atypical, high particle concentration bed. An alternative system to be bench tested is high-flow recycle of fines to an upper burner section designed for velocities and fines mass flow in the "fast fluidization" range. This technique offers potential in avoiding the bed back-pressure problems and bed upset phenomena seen with recycle of fines to the lower section of the burner.

Runs 12 through 15 tested the reference distributor design, a perforated cone. Operation in Runs 12 and 13 was smooth except for cone area temperature excursions in starting up with -3/16-in. fresh feed and also as the bed carbon burned out at the end of the runs. Particle agglomerates were noted in both Runs 12 and 13 and amounted to 0.5% and 0.45% of the respective final bed weights. Run 14 used an initial feed period of -1400-μm graphite mixed with particles prior to feeding the -3/16-in. material. The initial temperature excursion did not occur, but a cone area excursion was again seen as the bed burned out. Agglomerates were again found but in much less quantity (0.2% of the final bed weight). Run 15 combined the startup technique used in Run 14 with N_2 gas diluent increases at the end of the run. The startup excursion was again nonexistent, and the bed burnout excursion was much less significant than in prior runs. No agglomerates were found in the final bed.

The initial cone area excursions were thought to be due to defluidized burning of large -3/16-in. graphite. Gas velocities are low in the startup period relative to later operation. These low gas velocities are imposed by a requirement to minimize heat losses when using a CO torch heatup and by insufficient diluent gas capacity to fluidize a "cold" burner bed. A revised high-capacity diluent gas system will be available for runs in the next quarter. The availability of higher diluent flow will allow testing of CO torch startup with -3/16-in. fresh feed material.

The cone area temperature excursions accompanying bed burnout were thought to result from decreased bed-to-wall heat transfer in the local cone area. The primarily large-sized graphite that remains for burning during the final stages of combustion is less mobile than the bed graphite in equilibrium operation; as a result, solids convection and the resultant heat transfer in the local cone area decreases. The dampening of the burnout cone temperature excursion by increasing the diluent gas flow was probably due to a combination of increased solids circulation and increased heat absorption.

4.1.2. Prototype Primary Fluidized-Bed Combustor

The design of the prototype primary burner is proceeding. Two modifications have been made to the conceptual design based upon development work on the 20-cm primary burner. A pressurized pneumatic transfer system was chosen for the fines recycle loop and the cooling jacket incorporates a finned burner outer wall and an increased cooling annulus.

4.1.2.1. Operating Cycle - Design Basis

Table 4-2 indicates the operating cycle that will serve as the design basis for the prototype primary burner. This cycle is based on the reference cycle for the commercial facility. Figure 4-1 shows the approximate bed conditions during the cycle. Startup will be accomplished by induction heating an initial charge of 0.7 fuel element, bringing the bed temperature up to ignition (800°C), adding oxygen to ignite the bed, and then adjusting the oxygen and cooling air flows to maintain a 900° ± 50°C bed temperature. This startup method is discussed in more detail in Sections 4.1.2.2 and 4.1.2.3.

After ignition, feed is added at the rate of 0.5 fuel element (containing 800 g carbon) per hour. After the expanded bed height reaches

TABLE 4-2
PRIMARY BURNER OPERATING CYCLE, 24-HOUR TOTAL

Feed system (crushed fuel) (15 min)	
Feed rate to hopper	0.7 FE
Hopper capacity	0.7 FE
Hopper discharge rate	0.5 FE/hr
Ignition (2 hr)	
Preheat, initial bed, ignite	0.7 FE
Continuous feed (21 hr)	
Average burn rate	0.43 FE/hr
Design burn rate, 35 kg/hr-ft^2	0.5 FE/hr
Fines burnout and dump (1 hr)	184 kg particles (TRISO/TRISO)
Total cycle, avg (24 hr)	9.1 FE

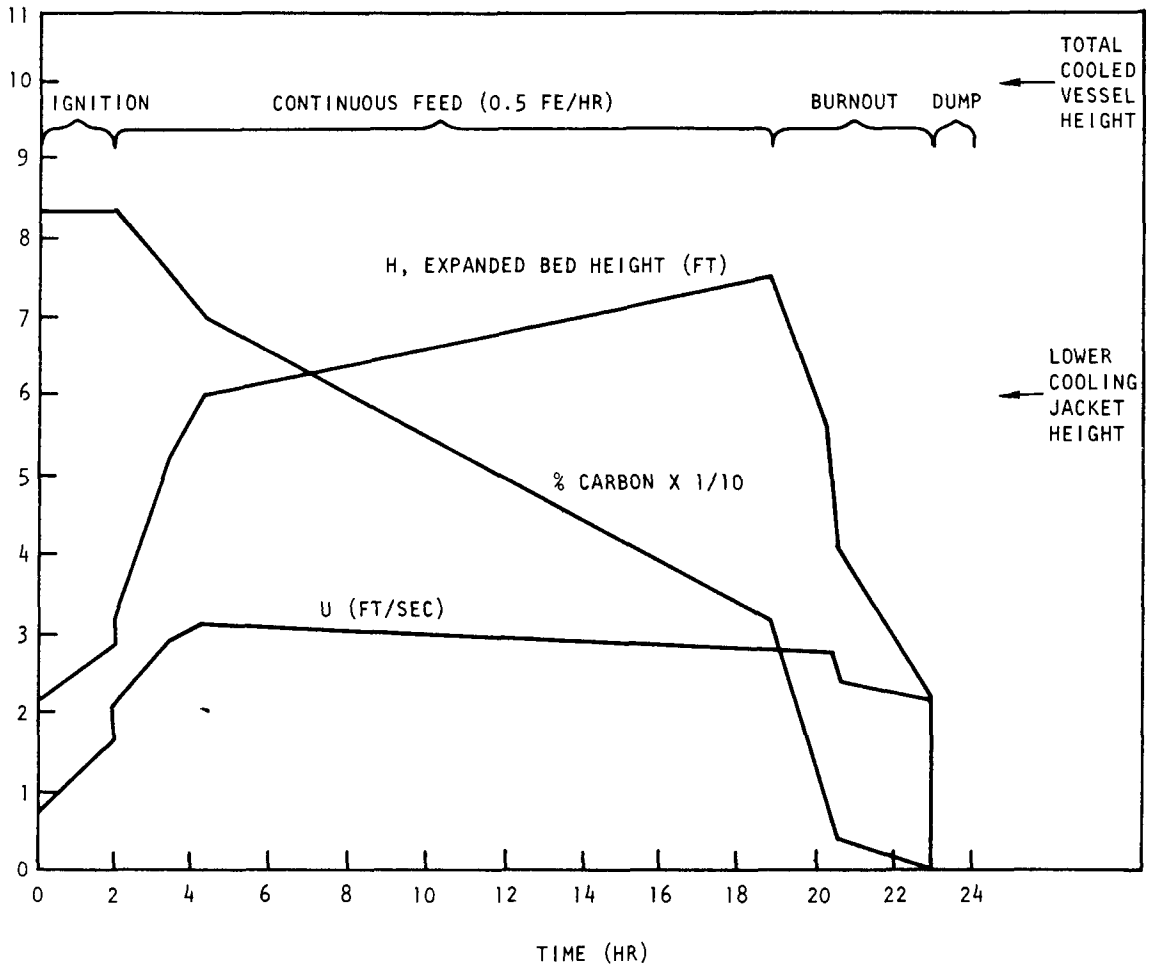

Fig. 4-1. Estimate of bed conditions for commercial cycle

6 ft, sufficient heat transfer area is available to achieve the design burn rate of 800 g C/min. The total cooled vessel height is 10 ft, which is more than adequate to contain the maximum expanded bed height of approximately 8 ft. After a batch of fuel (9.1 fuel elements on the average) is processed, the bed is burned out of carbon. Toward the end of the run, external heat is added to the bed to maintain combustion of fines during the "burnout" phase; this is necessary to balance heat losses. When burning fines in beds of low carbon concentration, the oxygen flow must be kept low to prevent concentration of oxygen in the off-gas; this lowers the heat produced by combustion, requiring additional heat to maintain the bed temperature in the range required to maintain fines burning (900° ± 50°C). At the end of the cycle, the bed of particles is batch dumped.

4.1.2.2. Burner Vessel

The design of the burner vessel (Fig. 4-2) has been modified to allow for cooling the burner with a 6-ft bed height by utilizing a 0.75-in. cooling jacket gap, pin fins, and a 0.25-in. vessel wall. This modification has several advantages:

1. A lower bed back-pressure; experimental work indicated that reducing the bed back-pressure was an important consideration for successful fines recycle.

2. Reduced fatigue caused by cyclic wall thermal stresses.

3. The bed is large enough to achieve the design capacity during most of the operating cycle (Fig. 4-1). This raises the average burn rate compared to the previous design which relied on a 10-ft expanded bed.

The design of the burner support is currently being reviewed. An alternate support, which would further minimize thermal stresses, is being considered.

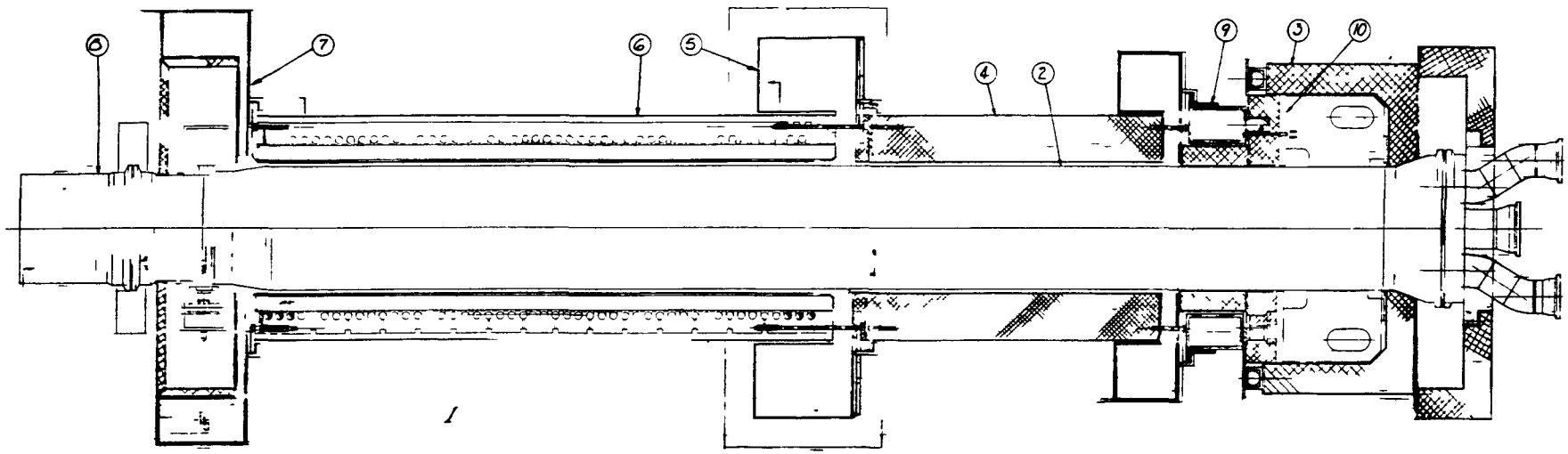

1. BURNER ASSEMBLY
2. BURNER VESSEL
3. INSULATION BONNET ASSEMBLY
4. UPPER INTAKE SHROUD ASSEMBLY
5. EXHAUST PLENUM ASSEMBLY
6. HEATER ASSEMBLY
7. LOWER INTAKE PLENUM ASSEMBLY
8. SPOOL ASSEMBLY
9. MOUNTING ASSEMBLY
10. SADDLE ASSEMBLY

Fig. 4-2. Prototype primary burner assembly

4.1.2.3. Heating System

The present startup method is induction heating. The expected modes of startup operations are:

1. Normal startup ignition with an 0.8 fuel element bed.

2. Re-ignition of a whole bed (∿3 fuel elements) after a process upset.

Figure 4-3 shows the transients for a normal startup with 0.8 fuel element. In this "rapid dump" startup technique, the tube wall is preheated to 900°C before fresh feed is introduced. Whole bed startups have been documented in Ref. 4-2.

Preliminary evaluation of direct hot gas ignition as an alternate heating method is under way. In this method carbon dioxide gas at 900°C is introduced through the distributor, and heatup of the bed material is by direct contact with the hot gas. The hot gas will also serve as the fluidizing gas for the process.

An alternate to fluidizing directly with hot gas is to utilize a CO-O_2 torch for direct heating while fluidizing with sufficient inert gas flow to provide a bed average temperature of 900°C at the entrance. The average bed temperature must be kept at 900°C because of temperature limitations on the material of construction and to help prevent sintering of SiC coated particles. The CO-O_2 flame temperature is high enough to cause problems with SiC sintering (Ref. 4-3). Local temperatures will be higher than the bed temperature with this system.

The thermal analysis model for either hot gas system is the same. The model shown in Fig. 4-4 was used for this evaluation. This model may be overly optimistic; however the purpose of the analysis is to establish the feasibility of a hot gas startup technique.

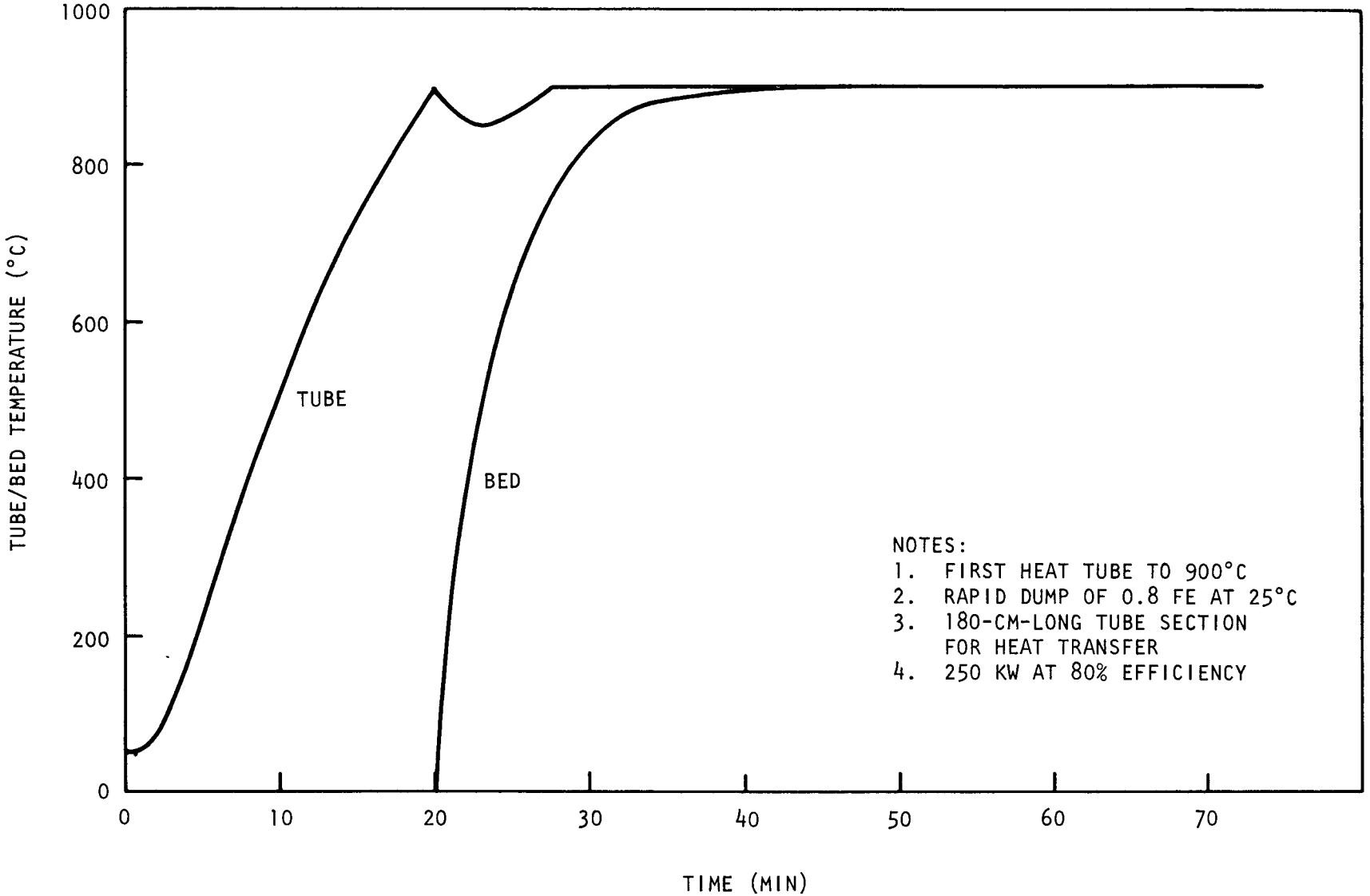

Fig. 4-3. Normal startup with 0.8 fuel element (with susceptor)

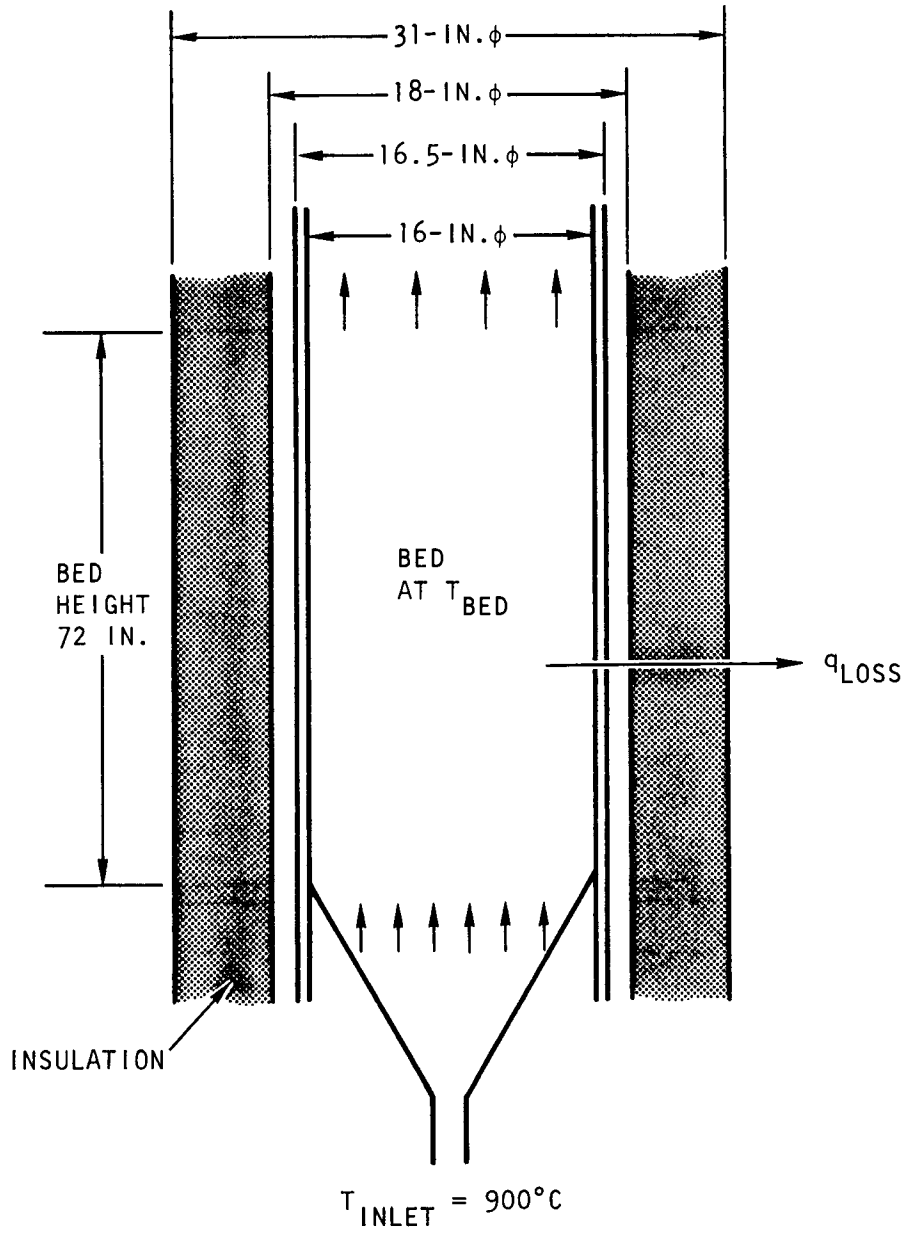

Fig. 4-4. Model for hot gas startup

Hot gas transients for a whole bed startup and a normal 0.8 fuel element normal startup are shown in Figs. 4-5 and 4-6, respectively. A 0.8 fuel element normal startup takes slightly over 1 hr to reach 800°C, which is well within the allowable time in the operating cycle. However, further evaluations are warranted to include the effect of axial losses, the effect of fluidization control, and fines elutriation. It is too early to determine the feasibility of the hot gas startup technique for larger size burners.

Heating the wall by induction heating is favored over hot wall heating because it provides the capability for burning out fines at the end of the run by maintaining at least 800°C bed temperature. Torches ($CO-O_2$) have the undesirable feature of creating local high temperatures and side penetrations that can fill with material, creating the potential for sintering the fuel particles.

4.1.2.4. Cooling System

The reference design of the cooling system has been changed to accommodate the more severe cooling requirements of removing heat from the burner wall over a 6-ft heat transfer surface area instead of the previous 10-ft surface area. The reasons for changing the reference design are:

1. It was observed that back-pressure buildup in the bed during fines recycling affects proper operation of the fines injection device. Lowering the bed from a 10-ft expanded height to 6 ft will decrease the back-pressure from 4.5 psi to 3 psi.

2. Lowering the bed level will induce better particle mixing and thereby enhance the bed-to-wall heat transfer coefficient.

3. A 10-ft expanded bed exists only for a portion of the operating cycle. As carbon is being slowly depleted, the bed height also decreases, reducing the heat transfer surface area especially

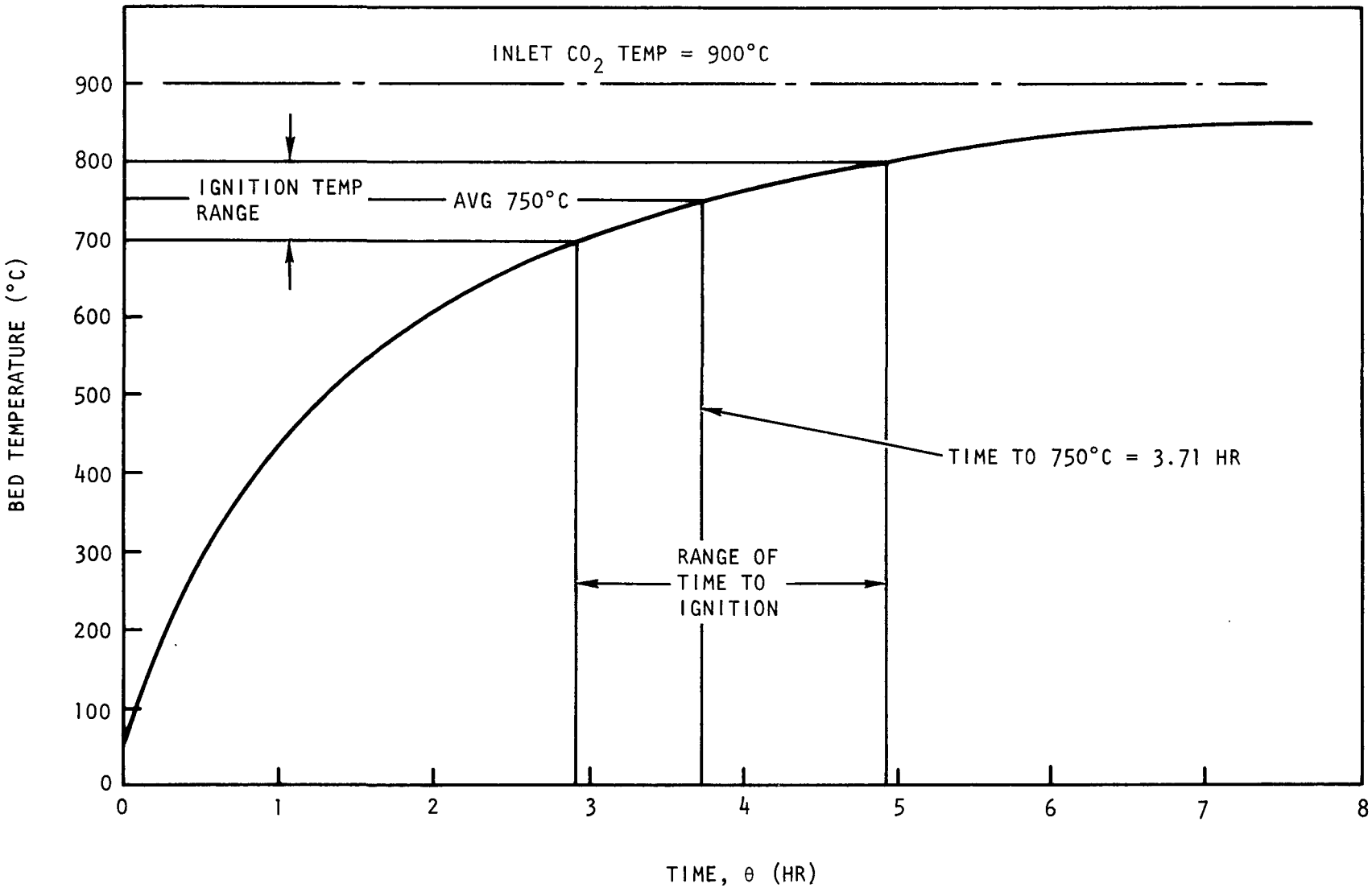

Fig. 4-5. Bed temperature versus time for hot gas startup (whole bed, 3 fuel elements)

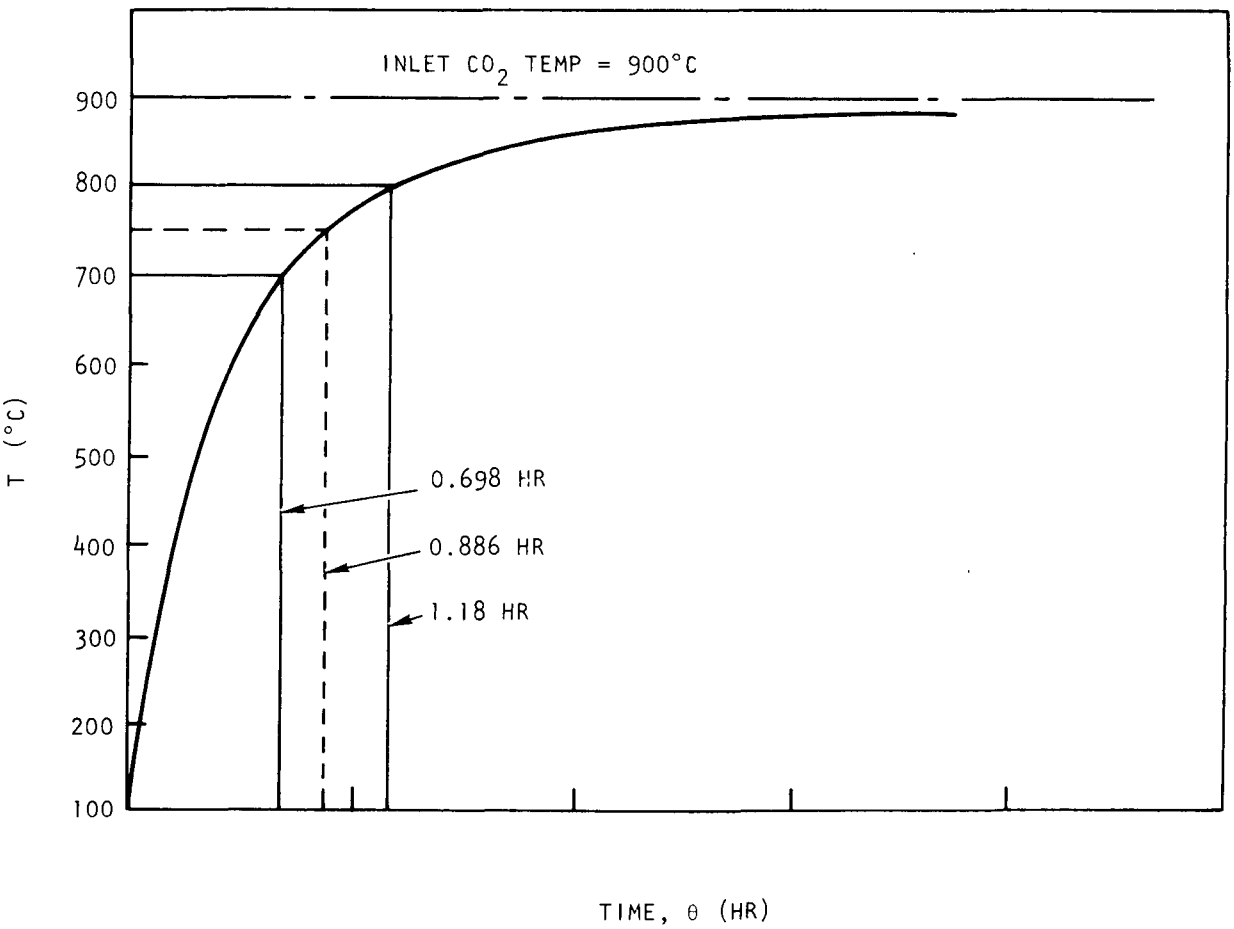

Fig. 4-6. Bed temperature versus time for hot gas startup (0.8 fuel element)

during the tail-burning period. The reduction of the bed is due to the fact that particles represent less than 20% of the fresh feed.

A new heat balance in which the heat generated that is not removed by the off-gas is removed through the vessel wall with a 6-ft heat transfer surface area is shown in Fig. 4-7. To accomplish this heat transfer, pin fins will be added to the 6-ft burner section. A total of 216 rows of pins will be arranged over the burner section. Each circumferential layer will have 100 1/2-in. by 3/16-in.-o.d. pins. The layers will be staggered to break up boundary layer buildup in an effort to maximize heat transfer. The annular gap for passage of cooling air will be 3/4 in. and the vessel wall thickness will be 1/4 in. A fin pattern for the prototype primary burner is shown in Fig. 4-8.

In the cooling analysis both continuous and discontinuous fins were considered. Tapered-type continuous or discontinuous fins (e.g., spines and tapered strip fins) were disregarded on the basis of complex geometry in fabrication and less suitable structural strength. Longitudinal, strip, and pin fins were evaluated and their performance has been compared with the 1/2-in. bare annular cooling design.

Figure 4-9 is a model for the cooling calculation. The heat removed from the bed through the vessel wall (Q) is transferred to the cooling air by forced convection (Q_c) and by radiation (Q_r) to the susceptor surface, which acts as an extended surface for convective heat transfer (Q_s). The following major assumptions were included in the cooling model:

1. The bed is homogeneous with a uniform bed temperature due to vigorous mixing motion of the particles.

2. Heat flux through the vessel wall is uniform throughout the heat transfer surface.

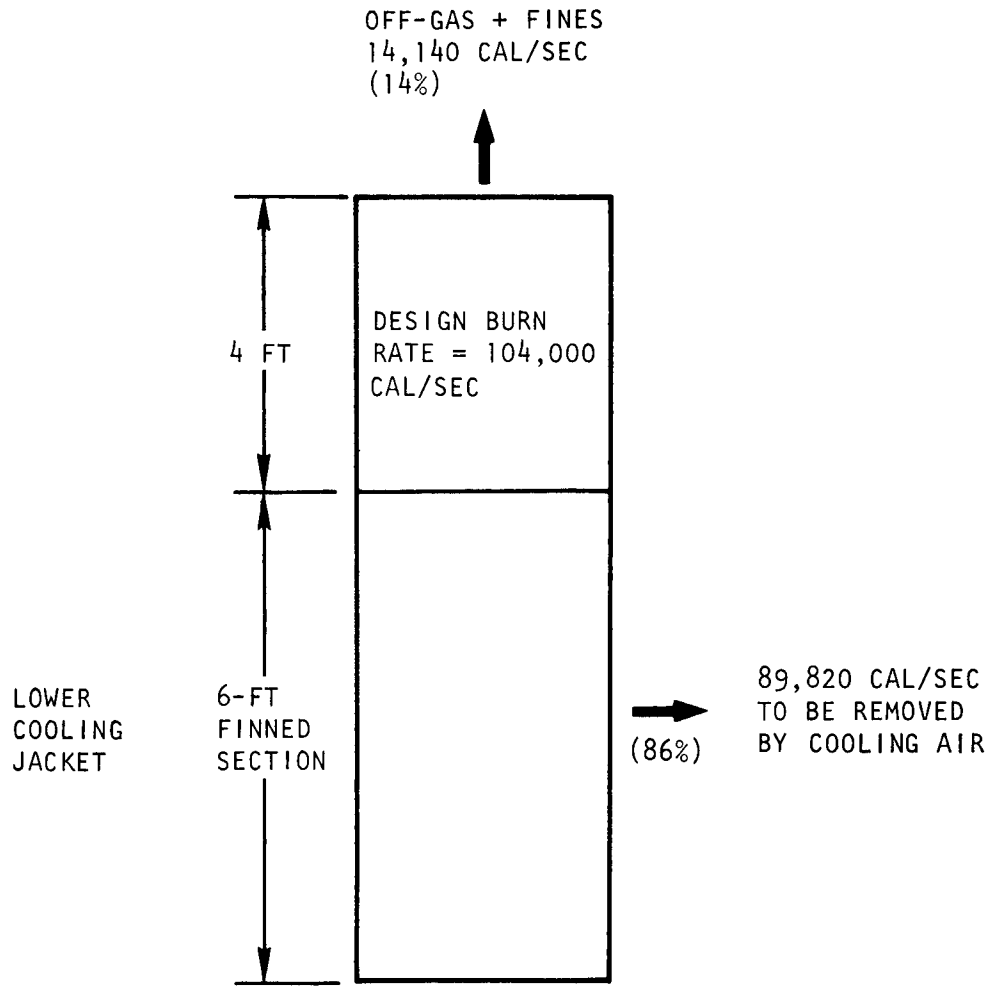

Fig. 4-7. Heat balance for 40-cm prototype primary burner with fins

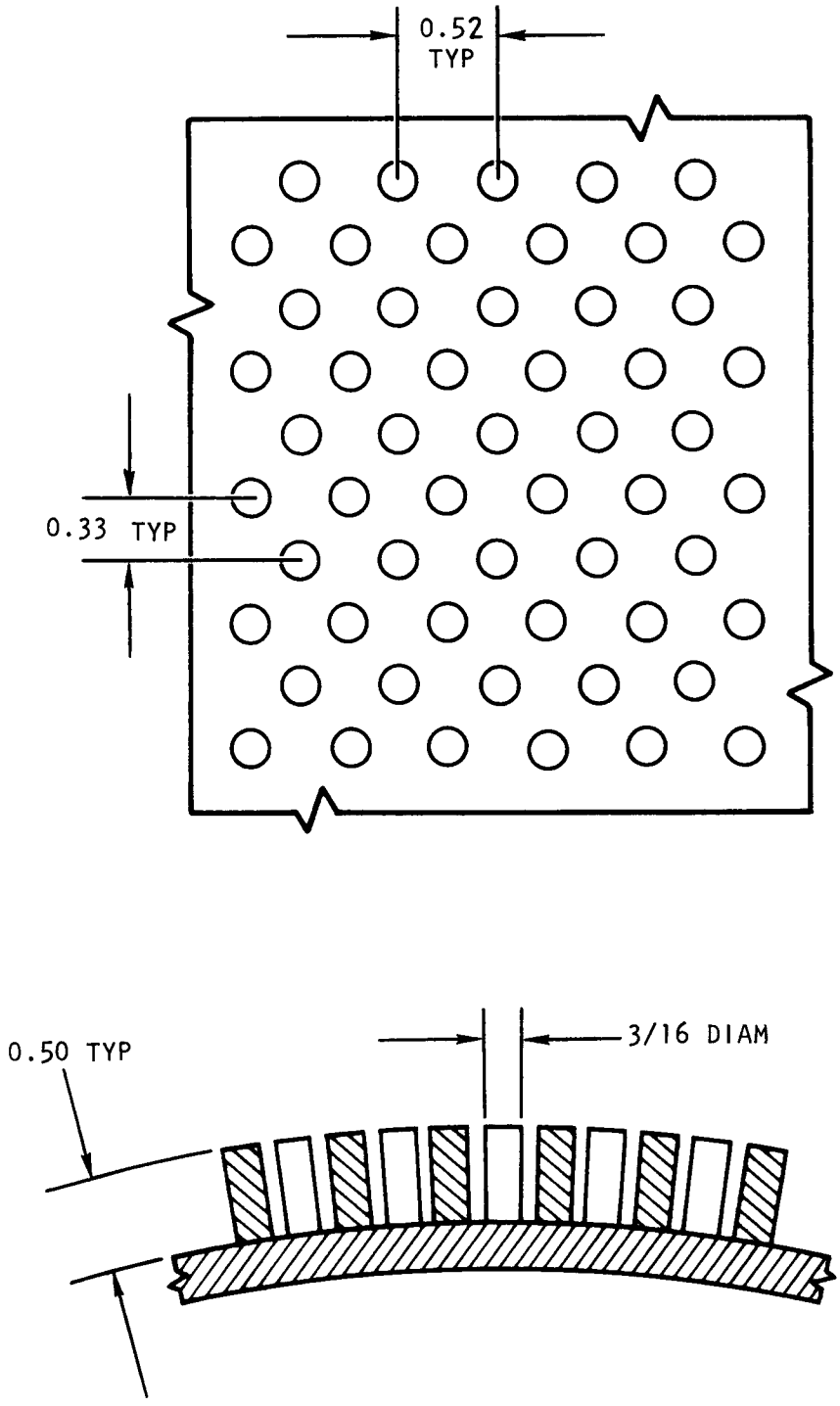

Fig. 4-8. Fin pattern for 40-cm primary burner

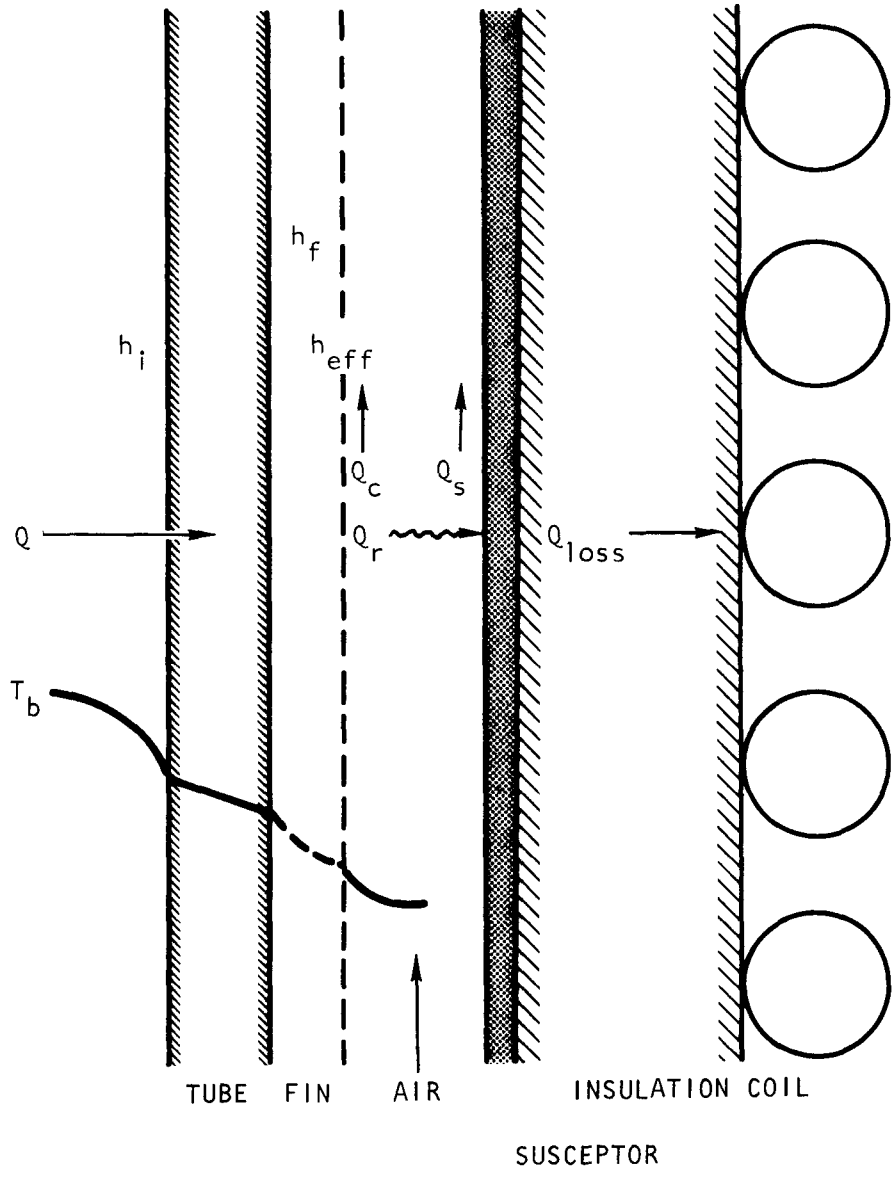

Fig. 4-9. Model for cooling calculations

3. The bed-to-wall internal coefficient, h_i, is uniform throughout the length of the heat transfer surface.

4. There is no axial variation in inner and outer wall temperatures throughout the length of the heat transfer surface.

5. Axial heat losses (i.e., end losses through top and bottom plenum and flanges) by conduction and radiation are neglected.

6. Off-gases leave at the bed temperature.

The bed-to-wall coefficient, h_i, used in the model is 106 Btu/hr-ft^2-°F based on the conductive fluidized-bed heat transfer correlation (Ref. 4-4) and radiation heat transfer (Ref. 4-5). The values of h_i obtained from experimental runs vary from 90 to 100 Btu/hr-ft^2-°F depending on the fluidizing velocity and bed height. At a fluid bed superficial velocity of 2.5 ft/sec, an h_i of 114 Btu/hr-ft^2-°F has been measured (Ref. 4-6).

The external film coefficient [bare surface (h_o), finned surface (h_f)] varies with the air flow. The correlations for calculating h_o or h_f for the different types of fins evaluated here are:

1. Bare annular cooling (Ref. 4-7)

$$\frac{h_o D_e}{k} = 0.020\left(\frac{GD_e}{\mu}\right)^{0.8} (Pr)^{1/3} \left(\frac{D_2}{D_1}\right)^{0.53} , \qquad (4\text{-}1)$$

where $D_e = D_2 - D_1$

D_2 = annulus outside diameter

D_1 = annulus inside diameter

Pr = Prandtl number, $C_p\mu/k$

G = mass flux

k = thermal conductivity of cooling medium

μ = viscosity of cooling medium

2. Longitudinal fin (Ref. 4-8)

$$\frac{h_f D_{e_h}}{k_b} (Pr)_b^{-1/3} \left(\frac{\mu_b}{\mu_w}\right)^{-0.14} = 0.0152 \left(\frac{D_{e_h} G}{u_b}\right)^{0.85} \qquad (4\text{-}2)$$

$$(\text{for } Re_h > 10^4)$$

where D_{eh} = equivalent diameter based on wetted heat transfer surfaces

Re_h = Reynolds number, GD_{e_h}/μ

subscript b = bulk temperature

subscript w = wall temperature

μ = viscosity

3. Pin and strip fins (Refs. 4-9, 4-10)

$$\frac{h_f}{C_{p_b} G_{max}} \left(\frac{C_p u}{k}\right)^{2/3} = \left[\frac{Z_p G_{max}}{\mu_f}\right]^{-1/2} , \qquad (4\text{-}3)$$

where Z_p = 2(fin thickness + fin width) or pin fin diameter

G_{max} = maximum mass flux based on minimum cross section for flow

C_p = specific heat of cooling medium

The pressure drops for the various cooling designs are evaluated on the basis of the heat exchanger pressure drop equation in Ref. 4-10. The total pressure drop includes the effect of friction (Refs. 4-6, 4-11) and flow acceleration, entrance contraction, and exit expansion effects.

The selection of the fin type is based primarily on considerations of: (1) heat removal effectiveness, (2) pressure drop, (3) velocity of air in the annulus, (4) thermal stress, and (5) ease of fabrication.

Heat removal effectiveness. Figure 4-10 shows the heat removal rate as a function of cooling air flow for various fin geometries. The solid lines are the operating curves for the various fin types, and the dotted lines are the exit air temperature isotherms. It can be seen that pin fin is roughly 50% more effective in heat removal than the bare annulus at the same air flow rate.

Table 4-3 is a comparison of the heat removal effectiveness of the various types of fins at a fixed cooling rate of 1470 standard ft^3/min (SCFM), based on the data in Fig. 4-10. The increase in removal rate is the percentage increase of each type of fin as compared to the bare annulus. The last column presents the data from another angle; e.g., the bare annulus can take care of only 2/3 (66.5%) of the design heat removal rate.

TABLE 4-3
COMPARISON OF HEAT REMOVAL EFFECTIVENESS

Fin Type	Heat Removal Rate at 1470 SCFM, 800 g C/min (cal/sec)	Increase in Removal Rate (%)	Relative Percent of Removal Rate
Pin	89,820	50.5	100 (basis)
Strip	86,500	45	96
Longitudinal	75,700	26.8	84
Bare annulus	59,700	0 (basis)	66.5

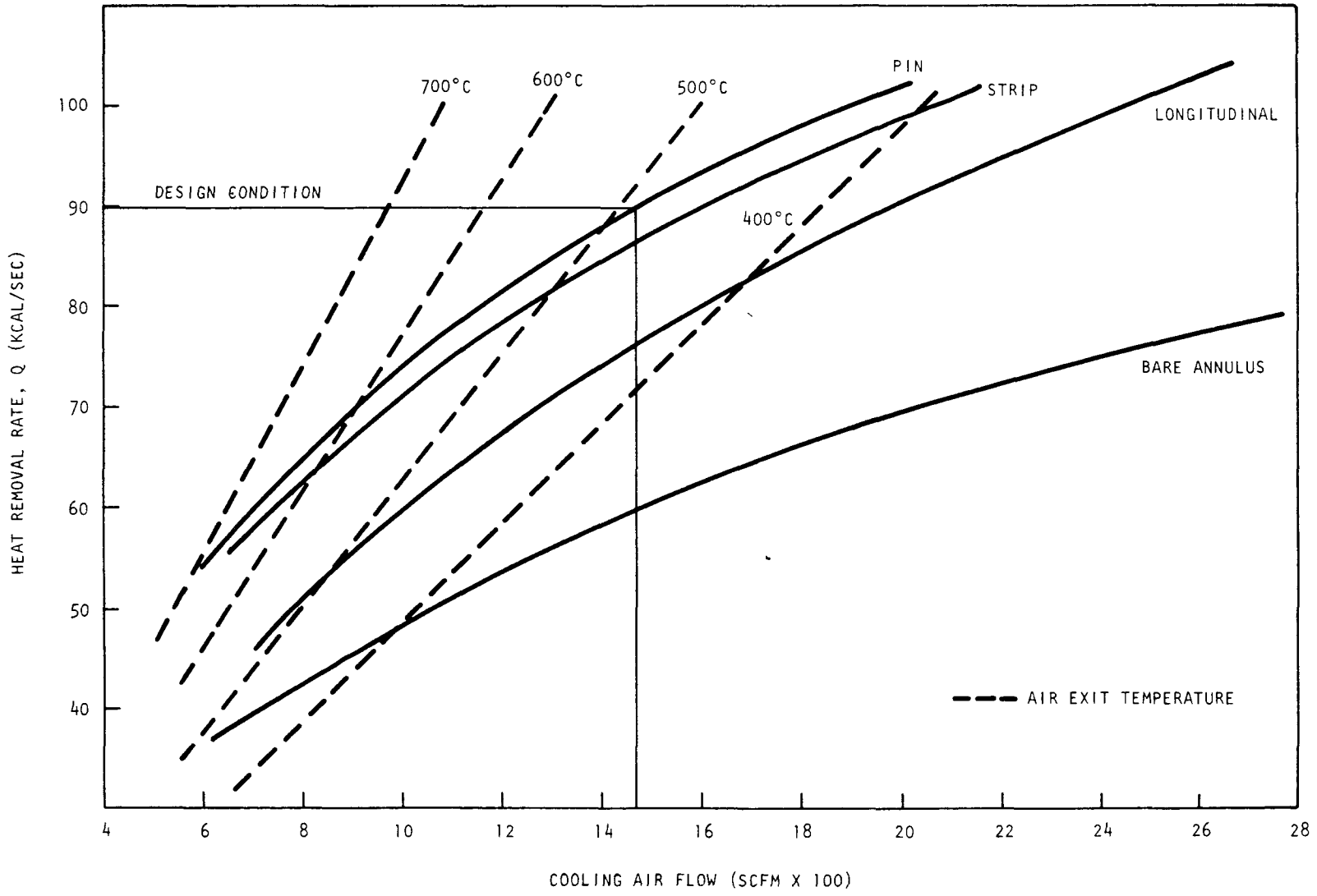

Fig. 4-10. Heat removal rate versus cooling air flow

By holding the heat removal requirement at the design condition (89,820 cal/sec), the cooling air requirement for the various types of fins can also be compared. From Table 4-4 it can be seen that bare annulus cooling requires 2-1/2 times as much cooling air as pin fin cooling.

TABLE 4-4
COMPARISON OF COOLING AIR REQUIREMENTS AT A REMOVAL RATE OF 89,820 CAL/SEC (800 g C/MIN)

Fin Type	Cooling air Required (SCFM)	Cooling Required, Pin Fin as Unity
Pin	1470	1 (basis)
Strip	1587	1.08
Longitudinal	1977	1.35
Bare annulus	3660	2.50

From the above analysis, it can be concluded that fins will be required to keep the cooling air capacity of the blower within reason.

Pressure drop. Figure 4-11 shows the pressure drop in the cooling shroud at various cooling rates. Although the pin fin has the highest pressure drop at a fixed heat removal rate, its magnitude of 4.2 psi at the design rate is within reason and poses no problem on the blower.

Velocity consideration. Tables 4-5 through 4-8 summarize the process parameters, heat transfer parameters, and physical characteristics for each fin type considered as a function of heat removal rate. Under process parameters it can be noted that the exit air velocity is highest for the bare annulus and lowest for the strip fin. It is desirable to keep the exit velocity below 300 ft/sec to limit vibration, noise, and surges in the cooling shroud. In addition, above 300 ft/sec compressible flow gradually occurs, resulting in a much higher blower horse power requirement for a

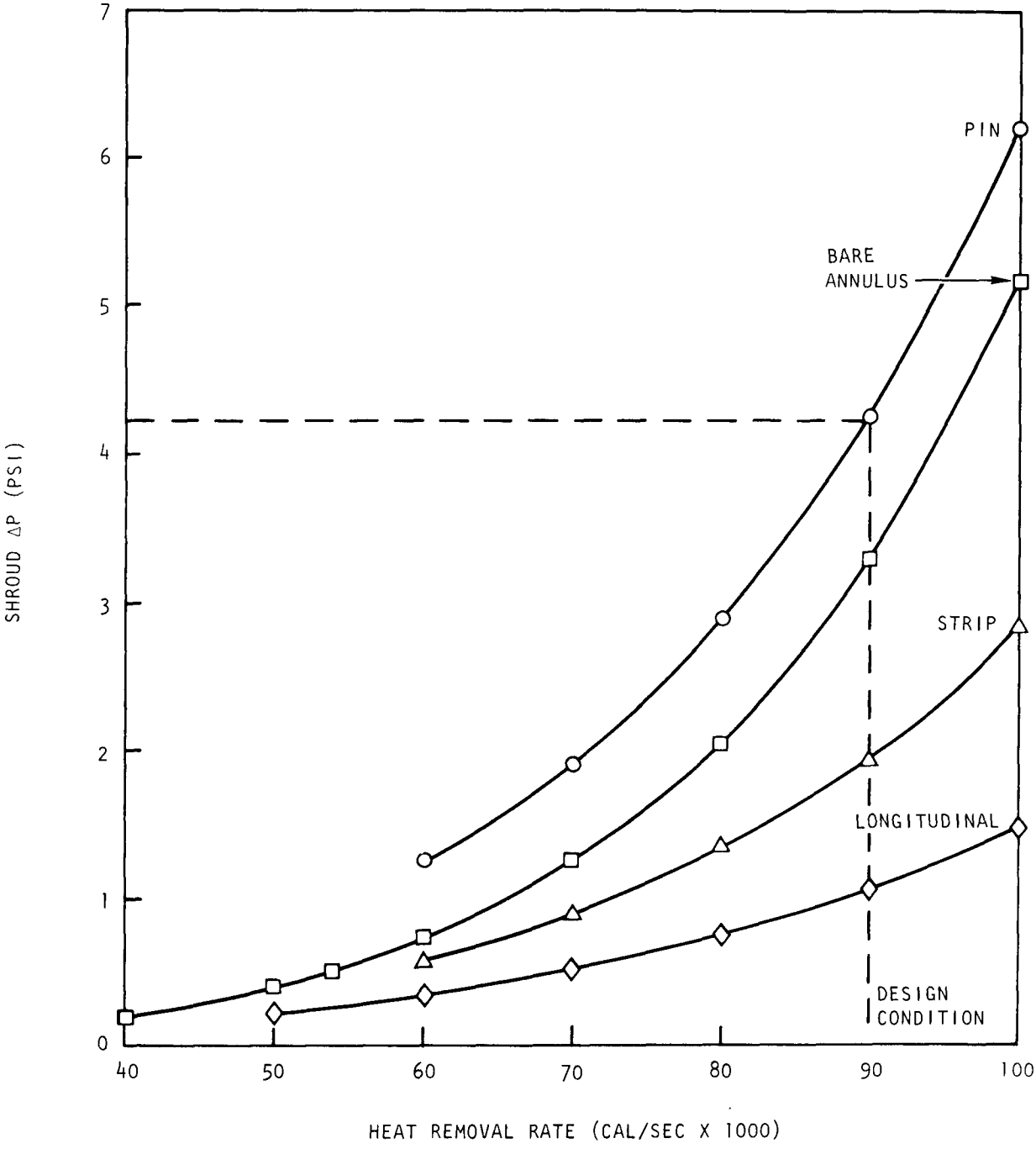

Fig. 4-11. Cooling shroud pressure drop as a function of heat removal rate

TABLE 4-5
PIN FIN COOLING DESIGN
(1/2-in. by 3/16-in.-o.d. fins)

	Heat Removal Rate, Q				
	100,000 cal/sec, 1.429×10^6 Btu/hr	89,820[a] cal/sec, 1.283×10^6 Btu/hr	80,000 cal/sec, 1.143×10^6 Btu/hr	70,000 cal/sec, 1.0×10^6 Btu/hr	60,000 cal/sec, 0.8571×10^6 Btu/hr
Process parameters					
Inlet velocity, ft/sec	114.0	98.2	83	68.3	54.9
Inlet flow, ft^3/min	1485	1278	1080	889	715
Outlet velocity, ft/sec	354.8	298.8	252	210.7	173.5
Outlet flow, ft^3/min	4620	3890	3282	2743	2259
Cooling air flow, SCFM	1889	1470	1152	897	690
Shroud ΔP, psi	6.22	4.23	2.87	1.9	1.22
Reynolds number for ΔP	2.89×10^4	2.2×10^4	1.69×10^4	1.28×10^4	0.972×10^4
Reynolds number for heat transfer	2.89×10^4	2.2×10^4	1.69×10^4	1.28×10^4	0.972×10^4
Mass flux, lb/ft^2-hr	3.92×10^4	3.05×10^4	2.39×10^4	1.86×10^4	1.43×10^4
Mass flow rate, lb/min	141.7	110.3	86.4	67.3	51.8
Heat transfer parameters					
Cooling air temperatures, °C					
Exit	432	490	549	609	671
Inlet	50	50	50	50	50
ΔT (rise)	382	440	499	559	621
Log mean bulk	177	193	208	223	239
Film	257	275	293	310	328
Burner wall temperatures, °C					
Bed	900	900	900	900	900
Bed wall ΔT	298	268	238	209	179
Inner wall	602	632	662	691	721
Burner wall ΔT	41	37	33	29	25
Bare wall	561	595	629	662	696
Mean fin	418	454	490	527	566
Mean outer wall	465	500	536	572	609
Fin efficiency	0.63	0.65	0.67	0.69	0.72
Heat transfer coefficients, Btu/ft^2-hr-°F					
Fin	72.5	65	58.3	52.2	46.4
Bare tube	28.8	23.8	19.8	16.3	13.4
Effective outer wall	104.7	94.7	85.9	77.7	69.9
Bed wall	106	106	106	106	106
Overall	49.4	47	44.7	42.4	40

PHYSICAL DESCRIPTION

Fin	Areas	Dimensions
Length = 1/2 in. Outside diameter = 3/16 in. Effective length = 72 in. Layers = 216 Fins/layer = 100 Total fins = 21,600	Bare surface = 21.78 ft^2 Fin surfaces = 44.17 ft^2 Frontal flow cross section = 0.217 ft^2 Inner heat transfer = 25.13 ft^2	Inner tube diam. = 16 in. Annulus o.d. = 18 in. Tube thickness = 1/4 in. Equiv. diam. for ΔP = 0.0549 ft Equiv. diam. for heat transfer = 0.0491 ft

[a] Design condition.

TABLE 4-6
STRIP FIN COOLING DESIGN

	Heat Removal Rate, Q				
	100,000 cal/sec, 1.429×10^6 Btu/hr	89,820[a] cal/sec, 1.283×10^6 Btu/hr	80,000 cal/sec, 1.143×10^6 Btu/hr	70,000 cal/sec, 1.0×10^6 Btu/hr	60,000 cal/sec, 0.8571×10^6 Btu/hr
Process parameters					
Inlet velocity, ft/sec	136	109.7	89.8	71	55
Inlet flow, ft^3/min	1949	1572	1287	1019	793
Outlet velocity, ft/sec	337	280	237	197	161
Outlet flow, ft^3/min	4832	4023	3398	2824	2314
Cooling air flow, SCFM	2076	1587	1252	966	737
Shroud ΔP, psi	2.84	1.91	1.33	0.89	0.59
Reynolds number for ΔP	5.82×10^4	4.16×10^4	3.35×10^4	2.53×10^4	1.89×10^4
Reynolds number for heat transfer	5.82×10^4	4.16×10^4	3.35×10^4	2.53×10^4	1.89×10^4
Mass flux, lb/ft^2-hr	3.91×10^4	2.99×10^4	2.36×10^4	1.82×10^4	1.39×10^4
Mass flow rate, lb/min	155.7	119	93.9	72.5	55.3
Heat transfer parameters					
Cooling air temperatures, °C					
Exit	399	459	510	570	633
Inlet	50	50	50	50	50
ΔT (rise)	349	409	460	520	583
Log mean bulk	168	184	198	214	230
Film	300	360	341	362	383
Burner wall temperatures, °C					
Bed	900	900	900	900	900
Bed wall ΔT	298	268	239	209	179
Inner wall	602	632	661	691	721
Burner wall ΔT	41	37	32	28	25
Bare wall	561	595	629	663	696
Mean fin	463	499.9	537	575	614
Mean outer wall	491	526	563	600	637
Fin efficiency	0.75	0.77	0.79	0.81	0.82
Heat transfer coefficients, Btu/ft^2-hr-°F					
Fin	50.9	46.2	40.8	36.4	32.2
Bare tube	28.6	23.3	19.5	16.0	13.0
Effective outer wall	98.5	88.8	79.2	70.8	62.9
Bed wall	106	106	106	106	106
Overall	47.9	45.5	42.8	40.2	37.6

PHYSICAL DESCRIPTION

Fin	Areas	Dimensions
Length = 1/2 in. Width = 1/2 in. Thickness = 1/8 in. Effective length for heat transfer = 72 in. Layers = 144 Fins/layer = 100 Total fins = 14,400	Bare surface = 19.7 ft^2 Fin surface = 49.98 ft^2 Frontal flow cross section = 0.239 ft^2 Inner heat transfer area = 25.13 ft^2	Tube i.d. = 16 in. Annulus o.d. = 18 in. Tube thickness = 1/4 in. Equiv. diam. for ΔP = 0.0585 ft Equiv. diam. for heat transfer = 0.104 ft

[a] Design condition.

TABLE 4-7
LONGITUDINAL FIN COOLING DESIGN
(1/2-in. by 1/8-in. by 72-in. fins)

	Heat Removal Rate, Q					
	100,000 cal/sec, 1.429×10^6 Btu/hr	89,820[a] cal/sec, 1.283×10^6 Btu/hr	80,000 cal/sec, 1.143×10^6 Btu/hr	70,000 cal/sec, 1.0×10^6 Btu/hr	60,000 cal/sec, 0.857×10^6 Btu/hr	50,000 cal/sec, 0.714×10^6 Btu/hr
Process parameters						
Inlet velocity, ft/sec	173	144	119	97	77	59.5
Inlet flow, ft^3/min	2483	2067	1708	1390	1102	853
Outlet velocity, ft/sec	366	311	265	223	183	147
Outlet flow, ft^3/min	5245	4468	3799	3190	2626	2113
Cooling air flow, SCFM	2440	1977	1602	1285	1006	773
Shroud ΔP, psi	1.47	1.04	0.74	0.51	0.34	0.22
Reynolds number for ΔP	3.6×10^4	2.86×10^4	2.26×10^4	1.78×10^4	1.37×10^4	1.03×10^4
Reynolds number for heat transfer	6.6×10^4	5.27×10^4	4.21×10^4	3.33×10^4	2.57×10^4	1.95×10^4
Mass flux, lb/ft^2-hr	4.6×10^4	3.73×10^4	3.02×10^4	2.42×10^4	1.9×10^4	1.45×10^4
Mass flow rate, lb/min	183	148.3	120.2	96.38	75.5	58
Heat transfer parameters						
Cooling air temperatures, °C						
Exit	347	379	411	443	480	515
Inlet	50	50	50	50	50	50
ΔT (rise)	297	329	361	393	430	465
Log mean bulk	153	162	171	180	190	199
Film	301	319	337	355	373	392
Burner wall temperatures, °C						
Bed	900	900	900	900	900	900
Bed wall ΔT	298	268	238	209	179	149
Inner wall	602	632	662	691	721	751
Burner wall ΔT	41	37	34	28	24	21
Bare wall	561	595	628	663	697	730
Mean fin	479	520	559	599	640	682
Mean outer wall	502	541	578	617	657	696
Fin efficiency	0.8	0.82	0.85	0.87	0.89	0.91
Heat transfer coefficients, Btu/ft^2-hr-°F						
Fin	37.8	31.7	26.7	22.2	18.1	14.6
Bare tube	37.8	31.7	26.7	22.2	18.1	14.6
Effective outer wall	89.8	77	65.9	55.9	46.4	37.8
Bed wall	106	106	106	106	106	106
Overall	45.8	42.2	38.6	34.9	30.98	26.9

PHYSICAL DESCRIPTION

Fin	Areas	Dimensions
Length = 1/2 in. Width = 72 in. Thickness = 1/8 in. Effective length for heat transfer = 72 in. Fins/layer = 100 Total fins = 100	Bare surface = 19.7 ft^2 Fin surface = 50.0 ft^2 Frontal flow cross section = 0.239 ft^2 Inner heat transfer area = 25.13 ft^2	Tube i.d. = 16 in. Annulus o.d. = 18 in. Tube thickness = 1/4 in. Equiv. diam. for ΔP = 0.059 ft Equiv. diam for heat transfer = 0.082 ft

[a] Design condition.

TABLE 4-8
BARE ANNULAR COOLING DESIGN

	Heat Removal Rate, Q							
	100,000 cal/sec, 1.429×10^6 Btu/hr	89,820[a] cal/sec, 1.283×10^6 Btu/hr	80,000 cal/sec, 1.143×10^6 Btu/hr	70,000 cal/sec, 1.0×10^6 Btu/hr	60,000 cal/sec, 0.857×10^6 Btu/hr	53,892[b] cal/sec, 0.7699×10^6 Btu/hr	50,000 cal/sec, 0.714×10^6 Btu/hr	40,000 cal/sec, 0.571×10^6 Btu/hr
Process parameters								
Inlet velocity, ft/sec	345	292	238.5	185	138	113	99	68
Inlet flow, ft^3/min	3958	3349	2733	2125	1582	1299	1134	782
Outlet velocity, ft/sec	688	556	447	354	276	235	211	157
Outlet flow, ft^3/min	7885	6366	5121	4060	3165	2695	2418	1800
Cooling air flow, SCFM	4787	3660	2773	2053	1481	1200	1041	708
Shroud ΔP, psi	5.18	3.28	2	1.23	0.71	0.5	0.4	0.2
Reynolds number for ΔP	1.32×10^5	9.90×10^4	7.26×10^4	5.31×10^4	3.68×10^4	2.95×10^4	2.52×10^4	1.67×10^4
Reynolds number for heat transfer	1.32×10^5	9.9×10^4	7.26×10^4	5.31×10^4	3.68×10^4	2.95×10^4	2.52×10^4	1.67×10^4
Mass flux, lb/ft^2-hr	1.13×10^5	8.63×10^4	6.54×10^4	4.84×10^4	3.49×10^4	2.83×10^4	2.45×10^4	1.67×10^4
Mass flow rate, lb/min	359	274.5	208	154	111.1	90	78.05	53.05
Heat transfer parameters								
Cooling air temperatures, °C								
Exit	202	229	260	298	344	375	397	458
Inlet	50	50	50	50	50	50	50	50
ΔT (rise)	152	179	210	248	294	325	347	408
Log_b mean bulk	109	117	127	139	152	161	167.5	184
Film	314.5	337.5	361.5	386	412	428	439	466
Burner wall temperatures, °C								
Bed	900	900	900	900	900	900	900	900
Bed wall ΔT	298	268	238	209	179	161	149	120
Inner wall	602	632	662	691	721	739	751	780
Burner wall ΔT	82	74	66	58	49	44	41	32
Bare wall	520	558	596	633	672	695	710	748
Susceptor	205	236	276	329	399	448	483	574
Mean outer wall	--	--	--	--	--	--	--	--
Fin efficiency	--	--	--	--	--	--	--	--
Heat transfer coefficients, Btu/ft^2-hr-°F								
Fin	--	--	--	--	--	--	--	--
Bare tube	63.9	51.9	41.9	33.2	25.8	22	19.69	14.6
Effective outer wall	--	--	--	--	--	--	--	--
Bed wall	106	106	106	106	106	106	106	106
Overall	37.47	33.2	29.04	24.82	20.66	18.25	16.73	13.1

PHYSICAL DESCRIPTION

Areas	Dimensions
Bare surface = 26.7 ft^2 Inner heat transfer surface = 25.13 ft^2 Susceptor surface = 28.27 ft^2 Annular cross section = 0.191 ft^2	Tube i.d. = 16 in. Tube o.d. = 17 in. Annulus o.d. = 18 in. Tube thickness = 1/2 in. Equiv. annular diam. = 0.083 ft Effective heat transfer length = 72 in.

[a] Design condition.

[b] Design case with 10-ft bed height.

given flow. Based on this consideration, the bare annulus is rejected because its exit velocity is in excess of 500 ft/sec. The longitudinal fin is slightly above 300 ft/sec and is considered on the border line.

Thermal stress. From a thermal stress standpoint, the longitudinal fin is especially undesirable for thermal cycling during an operating cycle. Pin or strip fins, being discontinuous, have little thermal stress buildup.

Ease of fabrication. The pin fin is easier to fabricate and weld than the strip fin using the capacitor discharge fastening technique. Vendor testing is under way to determine the weldability of Hastelloy-X studs to the vessel wall.

The pin fin satisfies all the criteria discussed above and was therefore selected over the other designs.

Figure 4-12 is a sensitivity check of the cooling requirement as the bed temperature varies at a fixed heat removal rate. A change of bed temperature from 900° to 950°C (a 5-1/2% change) will produce a 12% change in the cooling air requirement. The difference is due to the increase in temperature driving force. This indicates that the use of cooling air to control bed temperature does not provide a quick response and should only be considered as a secondary means of bed temperature control.

The internal heat transfer coefficient, h_i, is generally very sensitive to the fluidizing conditions and the effect of design features, such as the form of the distributor and bed internals (Ref. 4-12). Therefore, we cannot be overly dependent on applying correlations to obtain h_i, unless the design conditions are very close to the original experimental conditions on which the correlation was based. This uncertainty in h_i in the present analysis can result in an error of 10 to 20% in the cooling air requirement. If h_i is 90 Btu/hr-ft^2-°F instead of

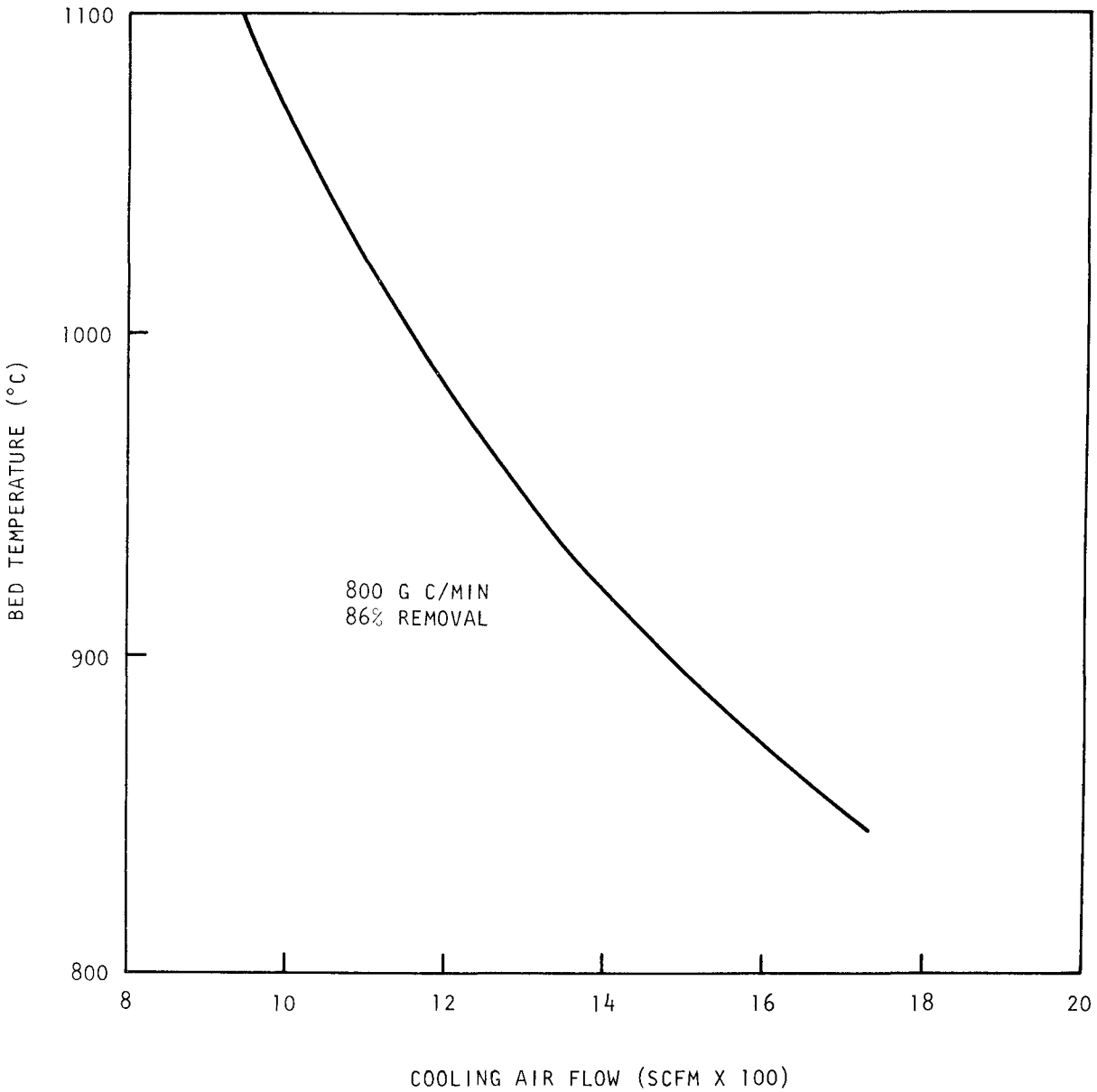

Fig. 4-12. Bed temperature versus cooling air requirement

106 Btu/hr-ft^2-°F, the cooling air will have to increase by ∿14%. Experimental data are needed to establish a representative average h_i over a 6-ft bed height at ∿2-1.2 ft-sec fluidizing gas velocity and with a perforated cone distributor. The cooling blower has enough capacity margin to allow for this slight uncertainty in h_i.

4.1.2.5. Transport System

The transport system is shown conceptually in Fig. 4-13; the current plan is to utilize pneumatic transport between the unit operations. A provision for the recycle of unacceptable product has been included. The line size and gas flow requirements for the pneumatic transport system are dependent on the physical properties of the material, especially the particle size. The transport system will include weigh hoppers to provide an accountability system as follows:

1. Feed hopper (item 2, Fig. 4-13) weight.

2. Feed rate to the burner.

3. A material balance on the batch cycle.

4. Calculated product carbon content.

The design basis feed rates and required hopper capacities are shown on Table 4-2.

The current plan is to utilize rotary air locks between the feed hopper and the burner and at the burner vessel product removal penetration. The top rotary will meter the feed rate to the burner and also prevent fission products from entering the pneumatic transport gas line. The bottom rotary may be necessary to control the loadings in the product removal line. The product removal system is currently being tested on the 20-cm primary burner.

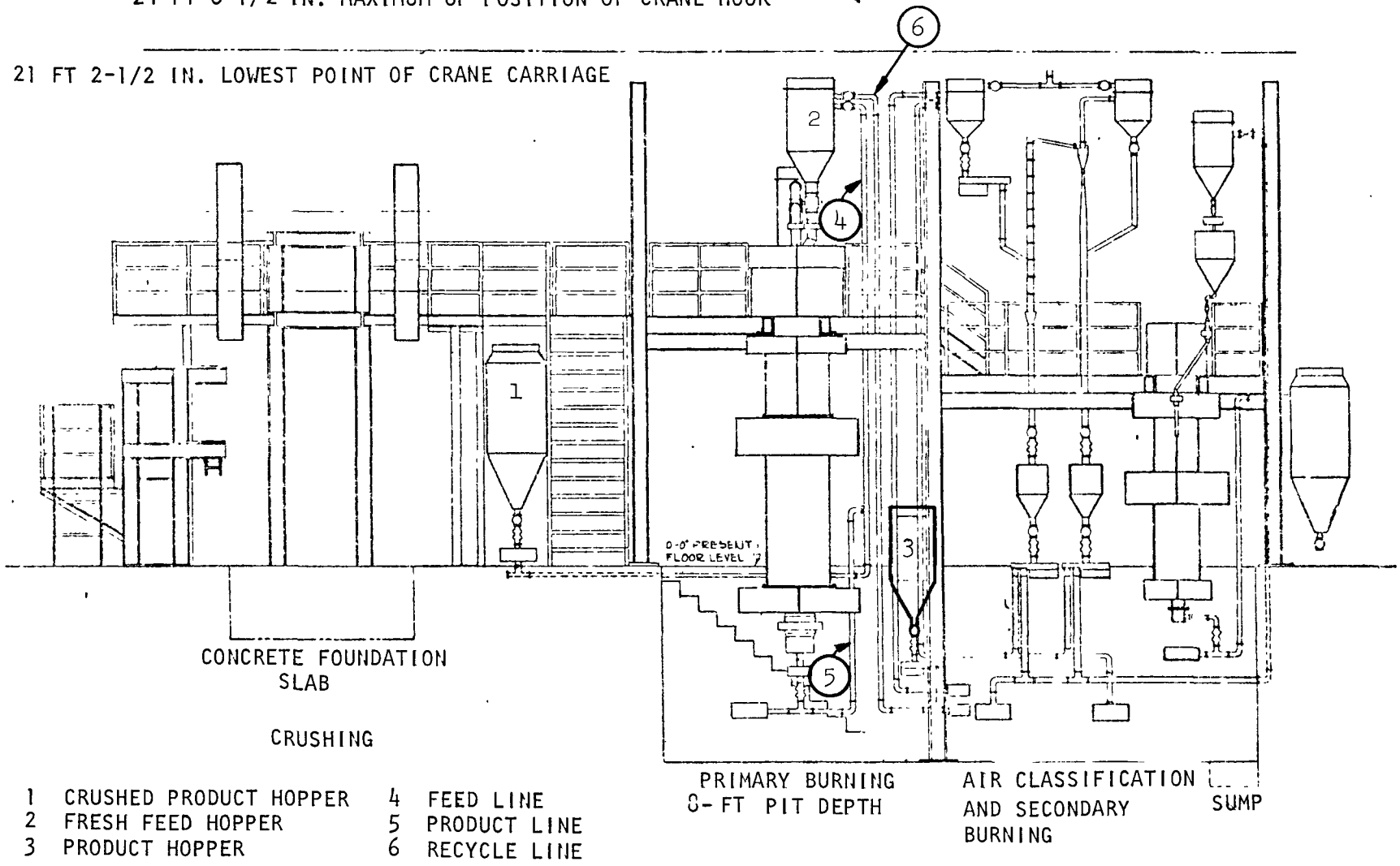

Fig. 4-13. Prototype plant arrangement, burning and crushing

4.1.2.6. Feed Size Requirements

The feed size requirement for the burner was reestablished by investigating different feed size distributions and their effect on operation. Previous work had established the -3/16-in. ring size (Refs. 4-13, 4-14). That work utilized a ball and cone distributor; the size requirements are being further investigated on the 20-cm primary burner utilizing a perforated conical distributor (see Fig. 4-14). The criterion for an acceptable feed size is smooth operation, primarily even temperature profiles, during normal operation throughout the operating cycle (see Table 4-9).

Figure 4-15 shows size distributions that define the areas of good and poor fluidization. The curve for good fluidization was drawn as an envelope encompassing the maximum fraction of material of any screen size for runs which had stable temperatures during operation. The area between the good and poor fluidization encompasses data where the profiles exhibited rapid oscillations but operation could be maintained by having high superficial velocities (approximately twice the normal value). Figure 4-15 also shows the only data available, in the larger size fractions, on a 16-in.-diameter fluidized bed burner utilizing a perforated conical distributor (Ref. 4-15). These data should give an indication of the size that would be expected on the prototype burner with the perforated cone. The results are similar to those obtained with the ball and cone distributor on the 10-cm primary burner.

Figure 4-15 shows feed size distributions for material crushed in the existing three-stage crusher system, the tertiary double-roll product, and similar product after the "oversize" (+3/16 in.) material has been screen separated and crushed to less than 1/8 in. in an eccentric single-roll crusher. Based on current data (10-cm primary burner, ball and cone distributor), unstable temperatures are anticipated during operation and

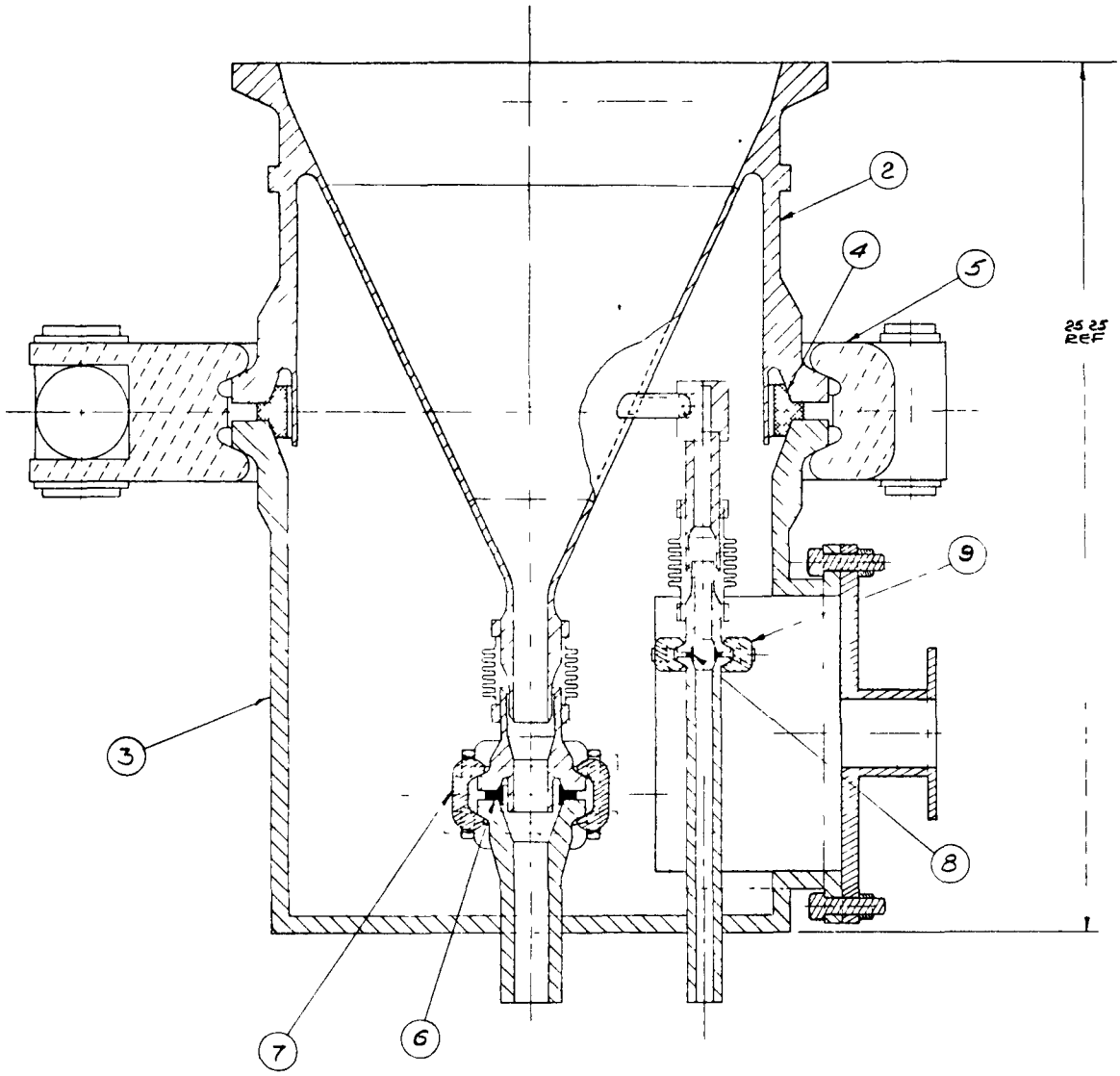

2. HUB AND CONE ASSEMBLY
3. LOWER CAP ASSEMBLY
4. SIZE 140 GRAYLOC SEAL RING
5. 14-IN. GRAYLOC SWING BOLT CLAMP
6. SIZE 14 GRAYLOC SEAL RING
7. 1-1/2-IN. GRAYLOC CLAMP
8. SIZE 4 GRAYLOC SEAL RING
9. 1/2-IN. GRAYLOC CLAMP

Fig. 4-14. Spool assembly, fluid bed, 40-cm primary burner

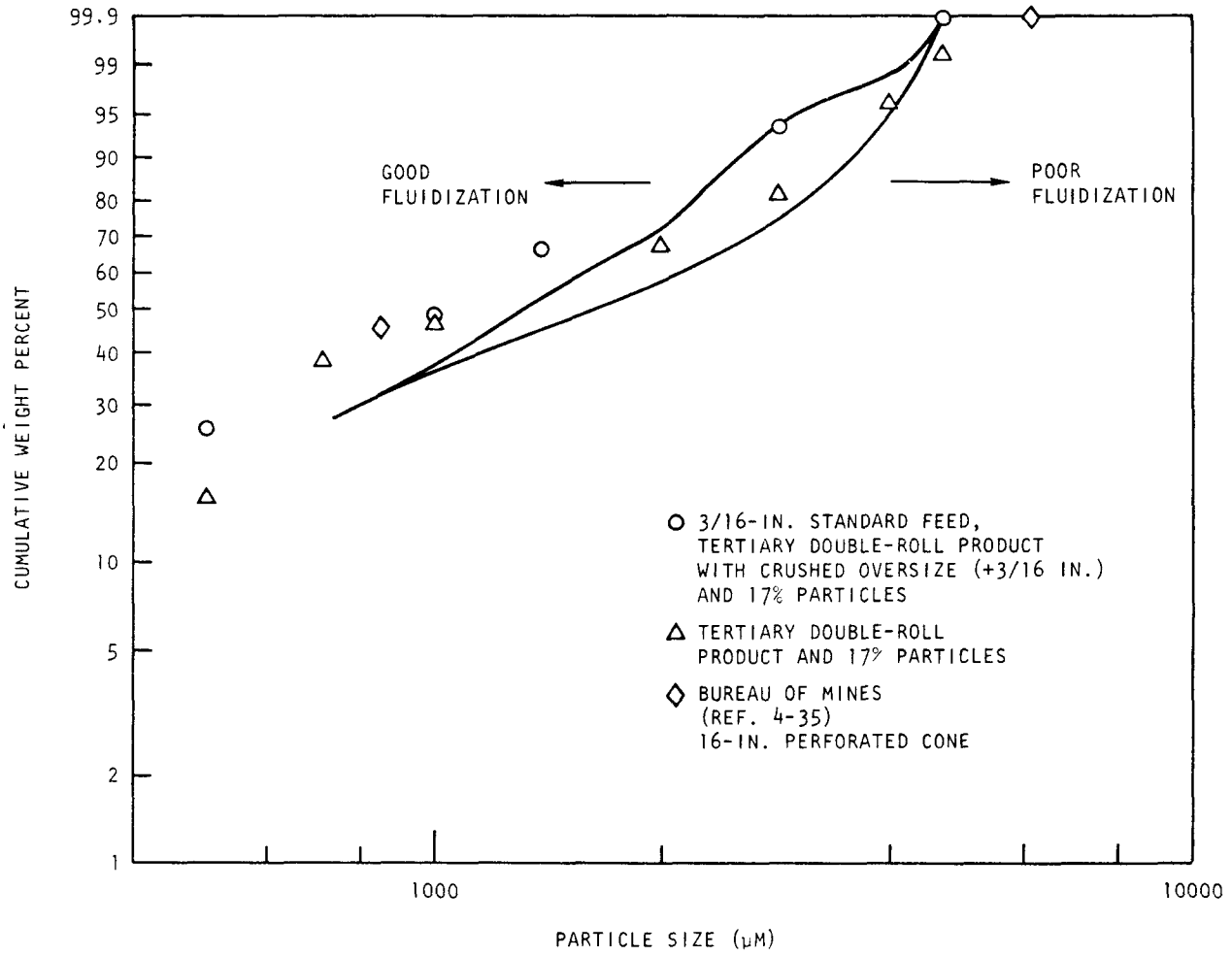

Fig. 4-15. Feed requirements, 10-cm primary burner

high superficial velocities will be required with three-stage crusher product from which oversize material has not been separated. It is anticipated that with the perforated conical distributor and a larger diameter burner, three-stage crusher product will be acceptable (see Section 4.1.1). Testing of this material on the 20-cm primary burner with the perforated cone is planned during the next quarter. The feed size required for the burner will be re-evaluated at that time.

At this time -3/16 in. remains the criterion for crusher product. Before a change is made in this criterion, several additional requirements must be evaluated:

1. The existing data (Fig. 4-15) were obtained primarily for beds with ≤50% carbon, which is not representative of conditions during startup (Fig. 4-1). Startup with the perforated conical distributor and -3/16 in. fresh feed requires careful operator attention and exhibits temperature instabilities. It is desirable to use the same feed material for startup as the normal feed to simplify material preparation, handling, and accountability. Currently special startup beds (either smaller sized graphite or particle beds) are required for a smooth startup. Tests will be performed on the 20-cm burner following the design basis operating cycle (Table 4-9) and utilizing actual burner feed, the perforated conical distributor, and sufficient inert gas flows to provide good fluidization (see Section 4.1.1).

2. Increasing the particle size of crusher product will increase the gas flows necessary in the pneumatic transfer lines.

3. The screener and oversize pulverizer are presently utilized to bring the tertiary product within the -3/16 in. requirement. This product falls within the range of size distributions having good fluidization. Decreasing the roll gap adjustment to produce feed that is within the good fluidization range would increase particle breakage.

TABLE 4-9
ESTIMATED FLUIDIZED-BED CONDITIONS, COMMERCIAL CYCLE[a]

	Temp (°C)	FE Feed	Gas Flow		U (cm/sec)	H_{max} (cm)	Bed		Burn Rate (g C/min)
			SLPM	% O_2			(kg)	(% C)	
Startup									
0	250	0.7	1000	0	23.2	64.3	81.4	83	
0	500	0.7	1000	0	34.3	73.7	81.4	83	
0	700	0.7	1000	0	43.2	81.6	81.4	83	
2	900	0.7	1000	0	52.0	88.4	81.4	83	
Continuous Feed									
2	900	0.7	1213	68	63.1	96.8	81.4	83	∿477
3.4	900	1.4	1714	77	87.4	159.3	112.8	75	∿711
4.3	900	1.85	1880	79	94.8	183.8	124.4	70	800
18.8	900	9.1	1880	79	86.2	227.6	270.9	32	800
Burnout									
20.2	900		1880	79	86.5	171.4	202.0	9	757
20.5	900		1516	75	73.2	126.0	187.9	2	605
23.0	900		386	0	3.6	63.0	184.2	0	0

[a] 1. Feed rate 0.5 FE/hr.
2. Fines holdup in hopper negligible until burnout.
3. CO_2 inert flow sufficient for minimum fluidization of final bed.
4. Heat transfer area (L = 183 cm) accounts for 86% of heat loss at 800 g C/min. The design burn rate, 800 g C/min, requires 183 cm of bed height to remove 86% of the heat of combustion. The balance is removed by the off-gas.

4. The size distribution data (Fig. 4-15) for the crusher product do not necessarily represent the product for the UNIFRAME system. Use of unscreened tertiary crusher product from the UNIFRAME system will not be possible for some time.

4.1.2.7. Fines Recycle

The reference fines recycle loop is a pressurized, "dense phase," pneumatic transport system. The design utilizes aerated hoppers, which are pressurized by means of an air-lock system. The aeration gas fluidizes the fines to prevent bridging and to maintain flow. The same gas pressurizes the hopper and pushes the fines into the burner through the distributor plate (Fig. 4-14). The design of the pressurized hopper will be determined from testing on the 20-cm primary burner with different hopper configurations.

The decision to adopt a pressurized pneumatic transport system was based on development work on augers, dilute phase pneumatic transport, and pressurized systems. Table 4-10 summarizes the results of this work. At present most work with fines recycle has been with low carbon content beds and is not representative of the current operating cycle (see Section 4.1.2.1). It has been shown that the fines can be successfully burned in low carbon content beds. Augers and pressurized pneumatic transport result in similar feeding and fines burning characteristics (Table 4-10) for low carbon content beds.

With augers the physical size of the equipment creates design problems. With high carbon content beds (>50% carbon) a 5-cm (2-in.) barrel auger on the 10-cm (4-in.) burner was not sufficient for the elutriation rates. With the pressurized system the physical size of the penetration in the burner vessel is much smaller for the same throughput.

TABLE 4-10
COMPARISON OF FINES RECYCLE TESTING

System	Capacity	Delivery Characteristics
Dense Phase		Adequate fines burning and transport; the inlet fines temperature is above the ignition point.
Auger, aerated hopper	280 g/min at 25 rpm 2-in. barrel 1.75-in. auger diameter 0.5-in. core diameter	0.5 to 0.7 g/cm^3 of swept volume. Steady-state fines elutriation rate approximately three times the burn rate with up to 25% carbon beds.
Pressurized pneumatic	500 g/min 14 SLPM 3/8-in. tubing	∿36 g/SLPM of gas.
Dilute Phase		High gas flows required, resulting in poor fines burning; the fines are cooled below the ignition temperature.
Eductor	500 g/min with 750 SLPM CO_2	0.7 g/SLPM CO_2, feed rate inversely proportional to back pressure, erratic flow.

At the end of the run the oxygen flow must be lowered to maintain a low (<1%) oxygen content in the off-gas. This is necessary as a safety precaution because of the potential for uncontrolled combustion of the fine carbon in an oxygen-rich vapor space. The fines residence time in the bed is low at high fluidizing velocity; toward the end of the run when the only available carbon is fine particles, the oxygen utilization is not complete unless the fluidizing velocity is lowered. The decrease in gas flow rate improves the carbon-oxygen contact and subsequent oxygen utilization by increasing the fines residence time in the bed and also by decreasing the bypass of excess oxygen. As the burn rate decreases, external heat from the induction heater will be supplied to balance heat losses, maintaining the bed temperature at 900° ± 50°C and sustaining fines combustion.

4.1.2.8. Plenum

Figure 4-14 shows the revised plenum configuration for the on-going prototype. The status of the 20-cm primary burner test program is discussed in Section 4.1.1.

4.2. SECONDARY FLUIDIZED-BED COMBUSTION

The secondary burner program has concentrated on development of the automatic control loops and verification testing of the induction heating design for both prototype burners. The 10-cm secondary burner includes all of the process steps of the prototype design, including the pneumatic feeder and product removal steps. Detailed design and analysis on the prototype are continuing.

4.2.1. 10-cm Secondary Fluidized-Bed Combustor

Four experimental burner runs were performed in the 10-cm secondary burner. The first two runs were to evaluate an inlet O_2 ramping technique that allows automated burner startup. The automatic ramping operation used for these two runs provided a smooth and controllable startup and has, therefore, been recommended for future use.

The last two runs were for shakedown and operational testing of an induction-heated susceptor plate assembly for providing process heat during the startup and final bed burnout portions of the runs. This assembly, which closely simulates the prototype reference design, improved the burner heating capabilities and simplified both the induction coil construction and the cooling gas manifolding technique. Determination of electrical efficiencies, heat transfer coefficients, and areas of high heat loss will be possible using data gathered in these two runs.

After modifications to burner insulation to reduce heat losses, carbon content in the product from the latest run was reduced to 0.19%.

Product removal rates were determined during all four runs using the pneumatic transport system coupled to the high-temperature bed removal system. This information will be used in the design calculations for prototype burner transport systems.

4.2.1.1. Summary of Operations

Run 45. An automatic O_2 ramping sequence was used to start the 10-cm secondary burner for Run 45. Process parameters concerning product removal, heating and cooling, and off-gas filters were actively collected during the run.

Fourteen kilograms of crushed TRISO fertile particles were used as feed for this run. The particles were prepared through the double-roll crushing system with a roll gap of 0.016 in.; the resultant size distribution is shown in Fig. 4-16. The feed contained 60.8% ThC_2, 17.4% C, and 21.8% SiC.

This run used the operating procedures outlined for Run 43 in the previous Quarterly Progress Report (Ref. 4-5). The burner tube was preheated to 950°C. The entire feed batch was then added and fluidized with 40 standard liters/min (SLPM) of N_2. When the bed had heated to 700°C, O_2 flow was automatically ramped, starting at 40 SLPM and increasing

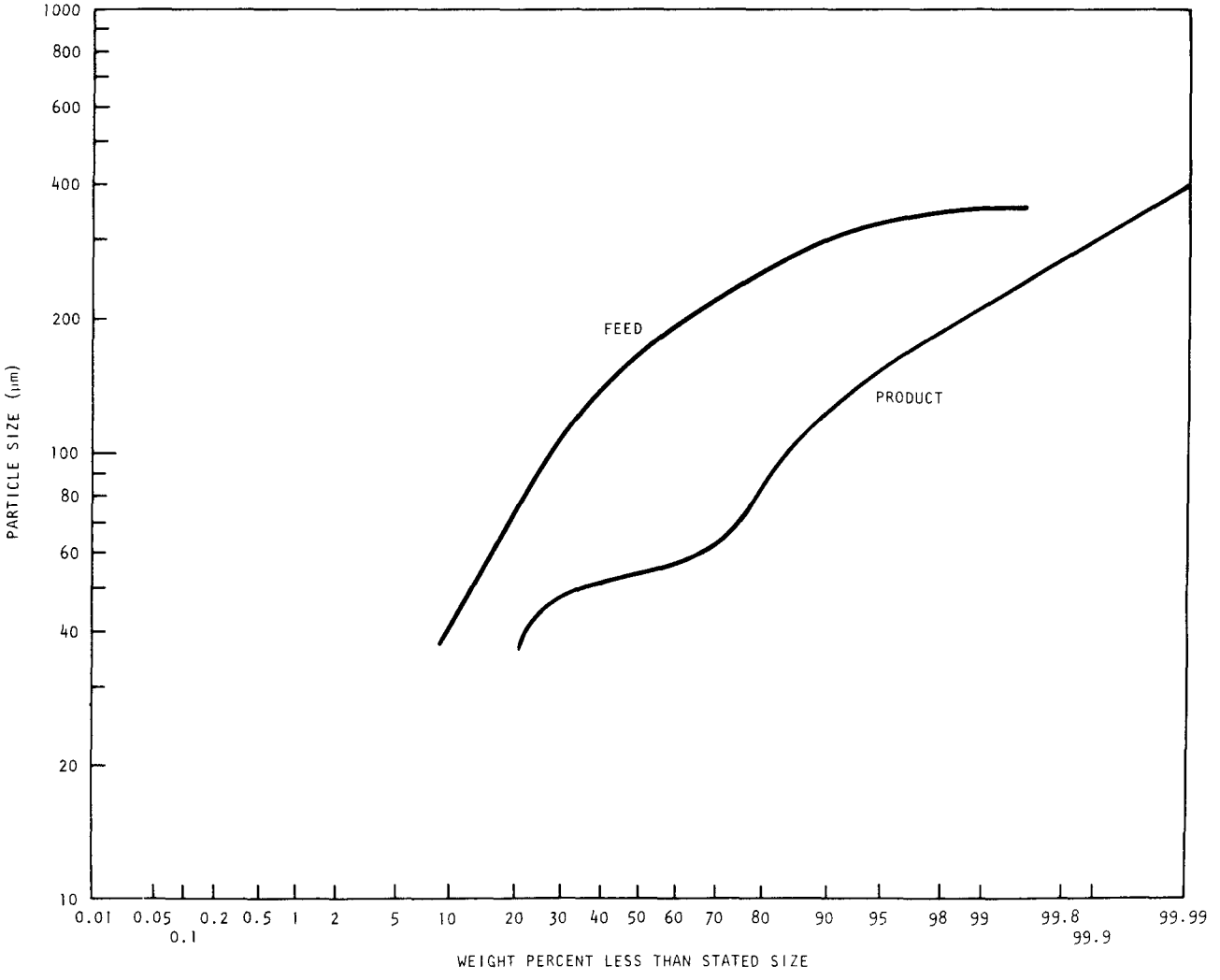

Fig. 4-16. Feed and product size distribution, Run 45

to 100 SLPM over a 6-minute period. Burner cooling to yield a 900°C bed temperature was provided by: (1) induction water coils surrounding the tube, and (2) air jacket cooling in the filter chamber. Forced air cooling of the burner tube was not required.

When the off-gas CO concentration decreased to 2%, the O_2 inlet flow was dropped to 60 SLPM to reduce the superficial velocity. This had the effect of: (1) allowing fines to re-enter the bed from the filter chamber where they could be burned, and (2) reducing the heat load on the filter chamber by decreasing both the hot gas and particulate influx to the filter region.

The maximum filter ΔP was 20 in. H_2O during the main burn portion, decreasing to 5 in. H_2O during the final burnout stages. The filters reached a peak temperature of 800°C during the middle of the run, but were cooled to 650°C before the O_2 front penetrated the bed.

When the O_2 inlet flow was dropped, the bed temperature rapidly fell to below 750°C because the induction heater was not actuated. Combustion was severely hampered due to the low temperature in this burnout stage and was thus terminated.

The product was fluidized with 100 SLPM of N_2 and removed through the product port just above the distributor plate. In the first 5 minutes, 84% of the product was removed from the burner and pneumatically transported to an upper deck hopper; the remainder was removed in the next 5 minutes. Subsequent disassembly and inspection of the burner showed that the product removal was successful in cleaning all the material off the distributor plate.

The product size distribution is shown in Fig. 4-16. The product contained 2.8% carbon and had a bulk density of 2.5 g/cm^3 and a tap density of 3.3 g/cm^3. The product angle of repose was 39°.

Run 46. The automatic O_2 ramping operation was again used to successfully start the 10-cm secondary burner in Run 46. This sequence will be used in the overall control system presently being evaluated. A more definitive estimate of product removal rates was made.

In this run, 14 kg of TRISO fertile particles were crushed through a double-roll crusher system to yield crushed feed suitable for burning. The roll gap was measured at 0.018 in. before the crushing began. The feed contained 60.8% ThC_2, 17.4% C, and 21.8% SiC.

This run was carried out using the modified operating procedures used in Run 43 (Ref. 4-5). The burner tube was preheated to 975°C before adding the bed and fluidizing it at 40 SLPM of N_2 flow. After the bed had heated to 650°C, the O_2 ramping system was actuated, bringing the O_2 flow to 100 SLPM over a 6-minute period.

The maximum filter temperature during the main burning portion of the run was 825°C, with a peak pressure drop of 16 in. H_2O. Blow-back of the filters was a 1-sec pulse every 20 sec at a nozzle pressure of 45 psig.

When the off-gas CO concentration dropped below 2%, the O_2 flow was decreased to 60 SLPM and the induction heater was actuated, holding the bed above 800°C for the remainder of the run. This decrease in O_2 flow dropped the filter temperature to 650°C, precluding oxidation of fines in the filter chamber when the O_2 front entered the filter area. The filter pressure drop was reduced to 5 in. H_2O in this final burning stage.

When the off-gas CO_2 concentration dropped below 4%, the run was terminated by fluidizing with 100 SLPM N_2, actuating the pneumatic transport system, and opening the product removal valve. In the first 2 minutes, 90% of the product was transported out of the burner, with the remainder removed in 5 minutes.

The initial product contained 0.1% burnable carbon, while the final product (comprising 10% of the total) contained 4.1% burnable carbon. The overall product contained 0.5% carbon. The size distributions are shown in Fig. 4-17.

These data indicate that the last product removed contained much more carbon than the average, probably because it included a singificant amount of material from the filter chamber that had not yet had a chance to re-enter the bed and be oxidized.

Runs 47 and 48. Runs 47 and 48 were made on the 10-cm secondary burner to shake down the new susceptor plate heating system. Heat losses were identified and reduced, yielding improved heating capabilities and a lower carbon content in the product.

In both runs, the feed was prepared by crushing 14 kg of TRISO fertile particles through a double-roll crusher system (two identical crushers in parallel). Prior to these runs, the crusher rolls had been replaced, with a resultant roll gap of 0.0183 in. After processing 28 kg from both runs, the roll gap had increased to 0.0193 in. The size distribution of the crushed feed is shown in Fig. 4-18.

The heating method used in these runs is an induction-heated susceptor plate made of RA-333 (comparable to Hastelloy-X). In principle, it simulates the prototype burner heating systems designed by U. Park and H. Yip of General Atomic.

As shown in Fig. 4-19, the susceptor is a 33-in.-long, 7-in.-I.D. cylinder made from 1/8-in.-thick RA-333, with removable end plates to seal cooling air flow as well as to allow removal of the susceptor over the 6-1/2-in. burner flanges. The susceptor outer surface is insulated with 1-1/2 in. of WRP-X-AQ moldable insulation; a 26-in.-long, ten-turn helical induction heating coil made from 3/4-in. copper tubing surrounds the

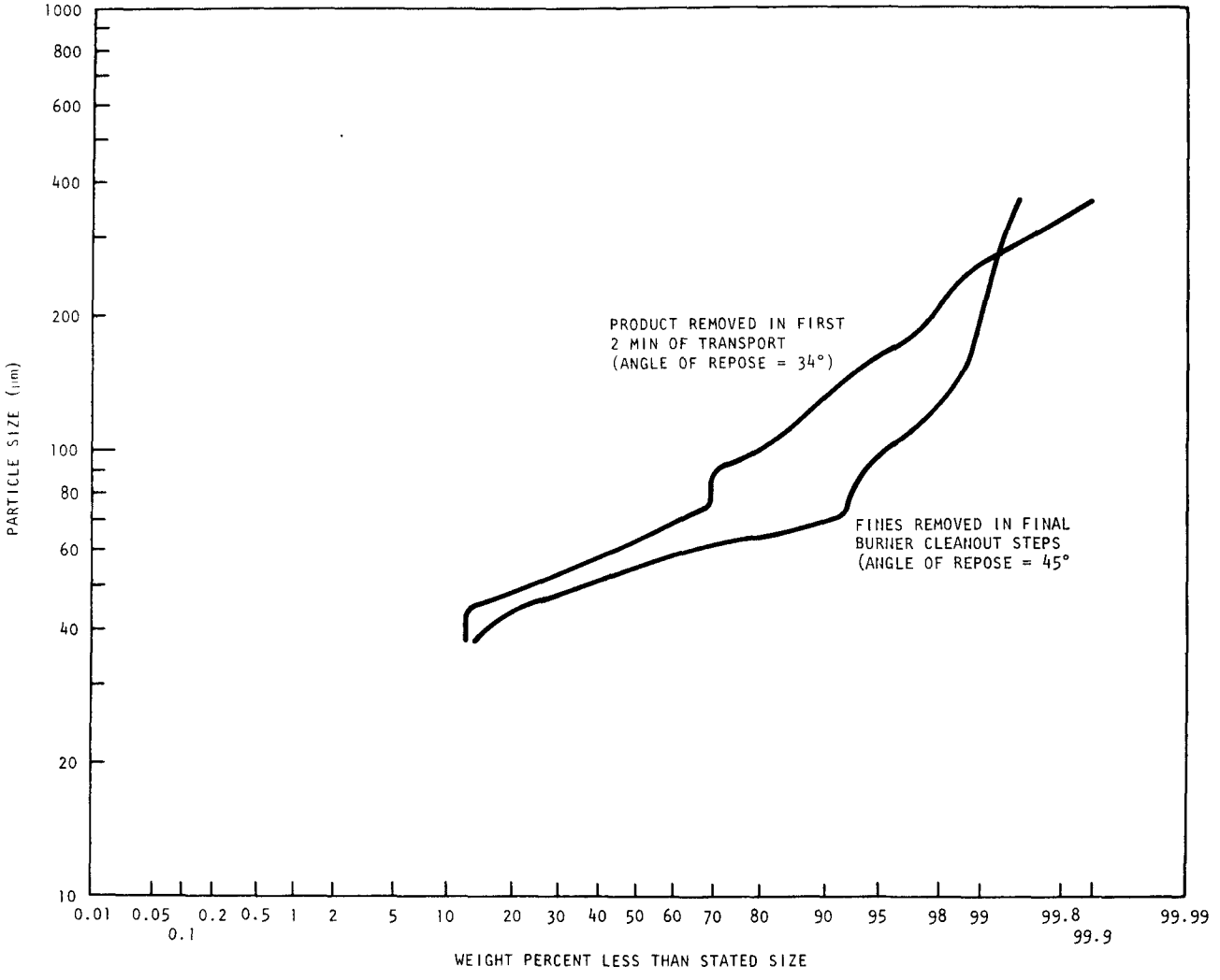

Fig. 4-17. Product size distribution, Run 46

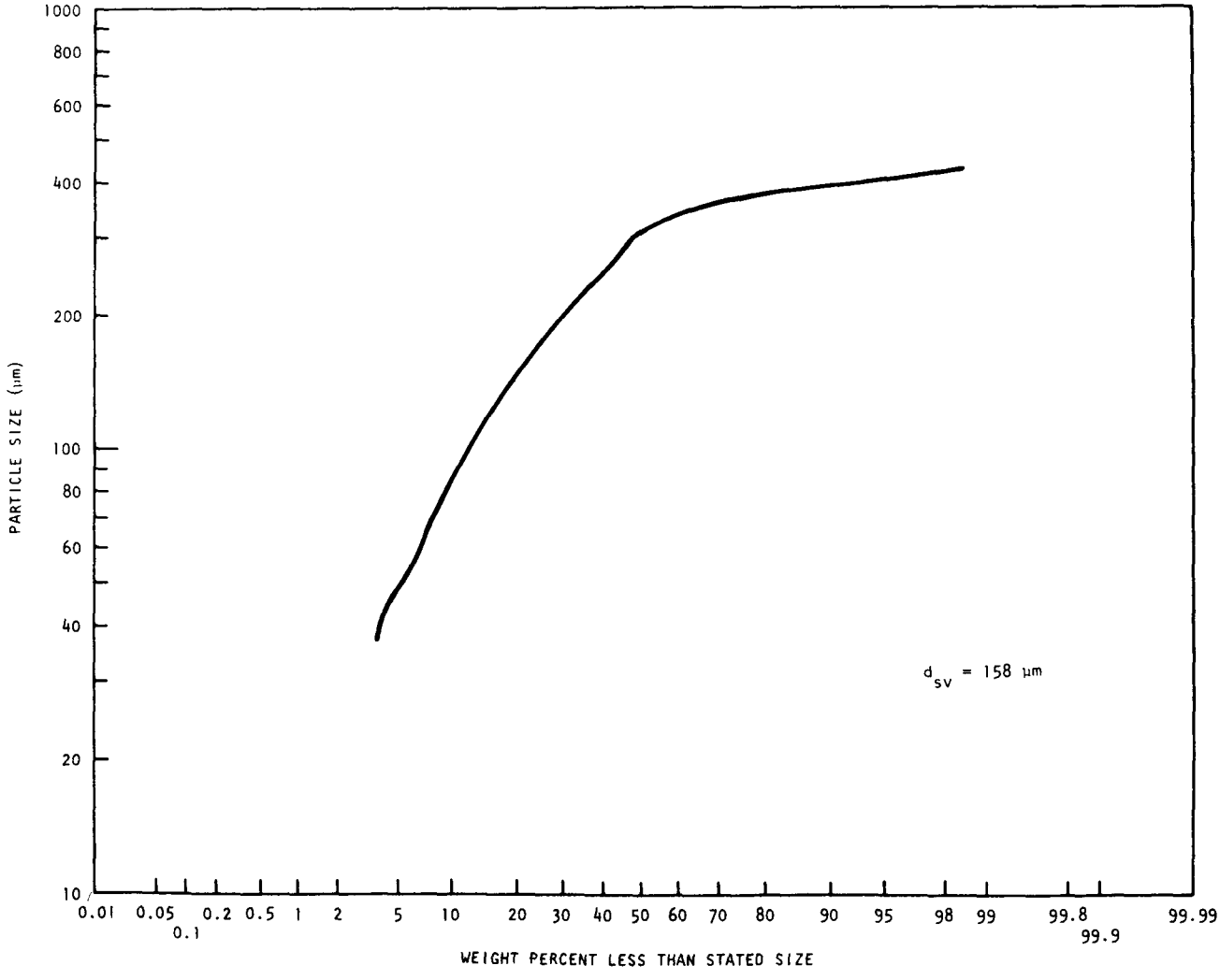

Fig. 4-18. Crushed feed size distribution, Runs 47 and 48

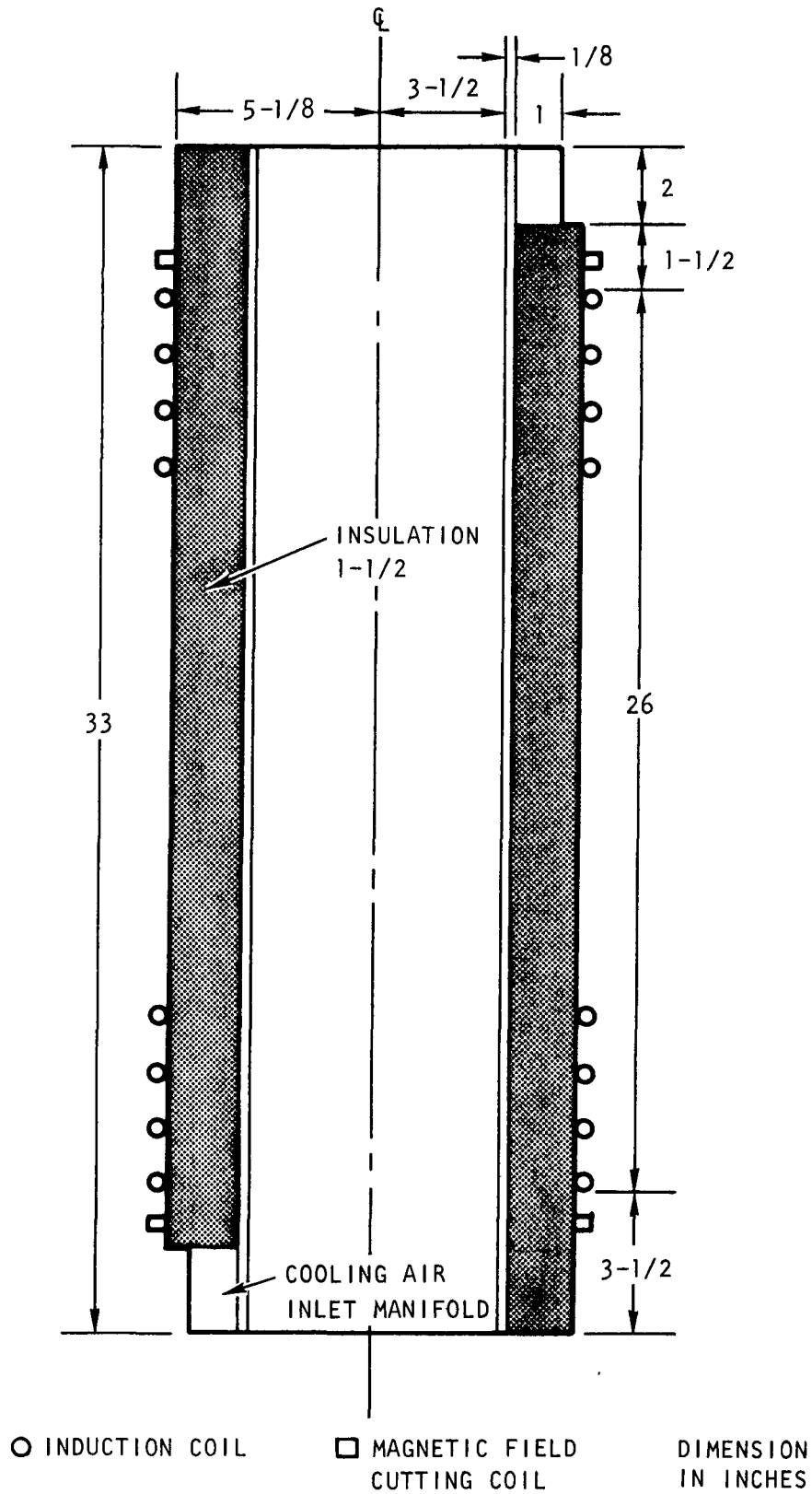

Fig. 4-19. Susceptor coil assembly

insulation. One single-turn field cutting copper coil is located at each end of the induction coil, adjacent to the end plate. These cutting coils serve to block the induction field from coupling to the end plates and dissipating heat therein.

Heating tests were made prior to the burner runs using the empty burner tube. Figure 4-20 shows the time-temperature plot of the susceptor and the tube. The heating rate corresponds closely (within 10%) to the measured input power.

In Run 47, the product removal spool piece and the susceptor end plates were uninsulated. Insulation of these components in Run 48 resulted in improved heating characteristics.

In Run 47 the bed was added after preheating the tube to 950°C. After 30 minutes, the bed had heated to 700°C and was ignited and burned using the O_2 inlet flow ramping technique developed in previous runs. Cooling air was utilized in the main burning portion for 20 minutes to keep bed temperatures below 900°C. During the final burning portion of Run 47, the bed was held at 750°C, with combustion terminated after the off-gas CO_2 concentration dropped to 4%.

In Run 48, the tube was preheated to 900°C followed by adding the bed, heating to 750°C, and ignition. This higher preheat temperature was made possible by the insulation mentioned above. Cooling air was used intermittently during the run whenever the bed temperature increased above 900°C. The bed temperature during final burnout was held above 800°C, with burner shutdown occurring after the off-gas CO_2 level dropped below 1%.

During the main burning portion of Run 47, the filter ΔP rose to a maximum of 18 in. H_2O with the filters at 825°C. By the time shutdown occurred, the filter ΔP had decreased to 5 in. H_2O and the filter temperature was 410°C.

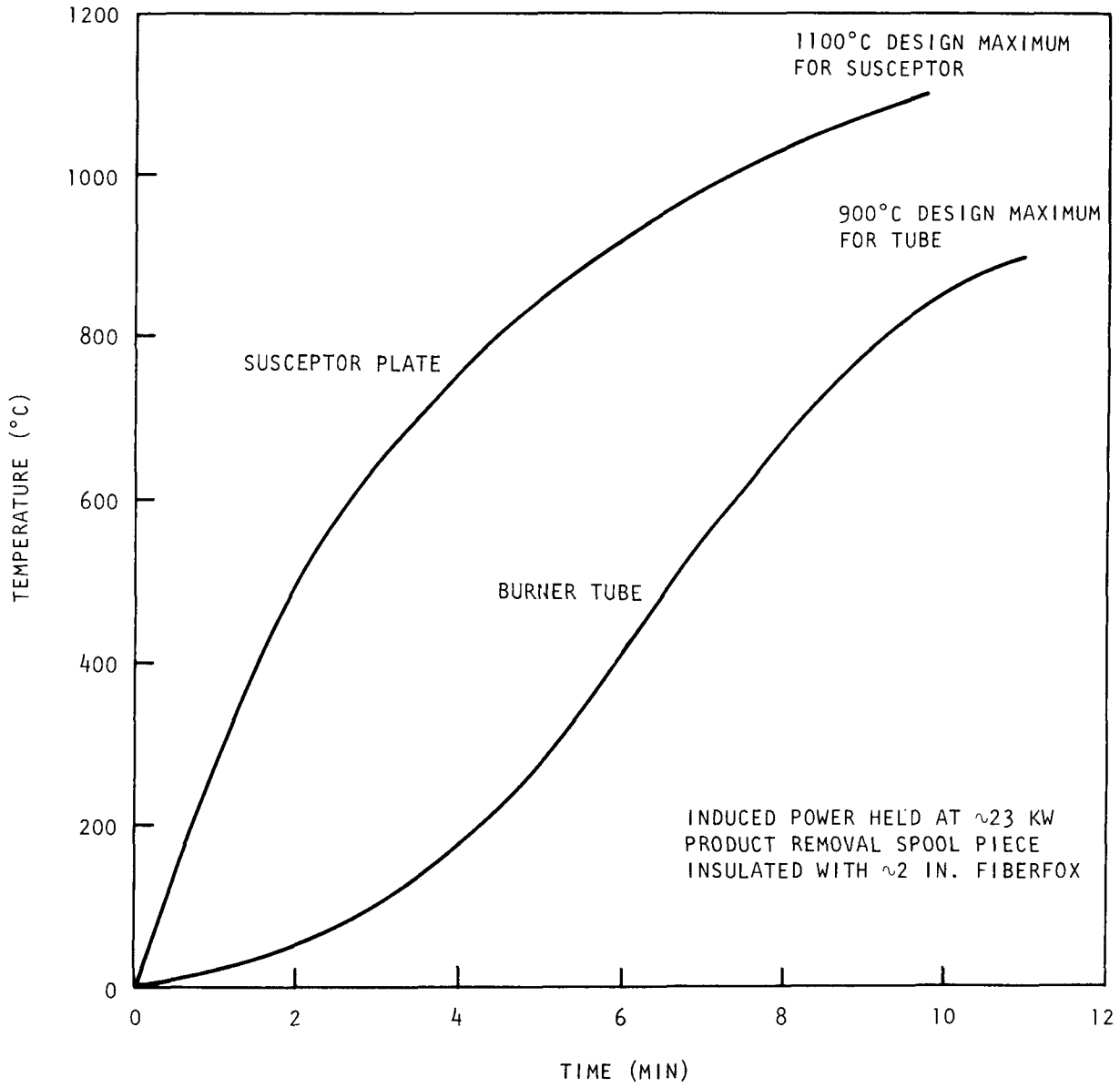

Fig. 4-20. Temperature versus time for susceptor and empty burner tube

In Run 48, the maximum filter ΔP was 17 in. H_2O during the main burning portion, with the filter temperature at 820°C. Just before shutdown, the filter ΔP had decreased to 5 in. H_2O with a filter temperature of 450°C.

Hastelloy-X off-gas filters should be received in the near future. These filters will be installed and operated under the conditions described above, which are considered to be the most severe operating conditions possible for the prototype secondary burner. The transport disengaging section of the prototype burner has an enlarged diameter, which should yield significant decreases in filter operating temperature over the 10-cm layout (which has no such transport disengaging section).

In both runs, the product was fluidized with 100 SLPM of N_2, cooled to a predetermined temperature, and pneumatically transported through the product removal valve to an upper deck hopper.

The bed was cooled to 500°C before transport in Run 47. A plastic vacuum hose between the filter-receiver and the transport pump collapsed due to the high heat. Because of this obstruction, the bed transported slowly, taking 10 minutes to be completely transferred to the hopper. This hose was replaced before Run 48 and the bed was cooled to 325°C prior to transport, with no problems due to overheating the hose.

In the Run 48 product transport, 74% of the bed was lifted to the upper deck hopper in the first minute, with the remainder being removed from the burner and transported in 5 minutes.

Temperature and pressure measurements of the transport gas were obscured in Run 47 due to the tube collapse and were of minor importance in Run 48 due to the low temperature at which the product was transported. To allow more representative data to be taken, the transport system is being converted to all metal piping such that the bed can be removed at high temperatures (>500°C).

The product from Run 47 contained 0.95 wt % burnable carbon and the Run 48 product contained 0.19 wt % carbon. This reduction in carbon content is due to the improved bed heating capabilities made possible by the addition of insulation to the lower burner sections. Product size distributions are shown in Figs. 4-21 and 4-22.

4.2.1.2. Evaluation of Gravity-Pneumatic Feeder System for Secondary Burners

Reprocessing HTGR TRISO/TRISO fuel requires a secondary burning step to oxidize crushed fuel particles. The method chosen is a batch fluid bed burner with in-vessel filters. Loading the burner batchwise requires a feeder of high throughput to perform the job quickly while maintaining a reasonably constant solids flow rate. The feeder must be as simple as possible with a minimum possibility of blockages and a capability for virtually complete cleanout for accountability purposes.

In February 1972 a feeding system meeting these requirements was developed for use on a 20-cm primary burner. Although the system was never used for this original purpose, it found immediate use on the 10-cm secondary burner, where it has since been used in making 44 separate burner runs over a 2-1/2-year period.

The gravity-pneumatic feeder was first developed for the addition of fresh feed to the upper portion of the primary fluidized-bed burner. The augers being used at that time were resulting in frequent problems due to their tendency to bind and/or lock-up. A feeder without mechanically moving parts was viewed as a solution to these types of problems.

In the gravity-pneumatic feeder shown in Fig. 4-23, the bottom of the feed hopper cone empties into a double-elbow arrangement, which leads to the burner. The distance between the elbows is sufficiently long so as to

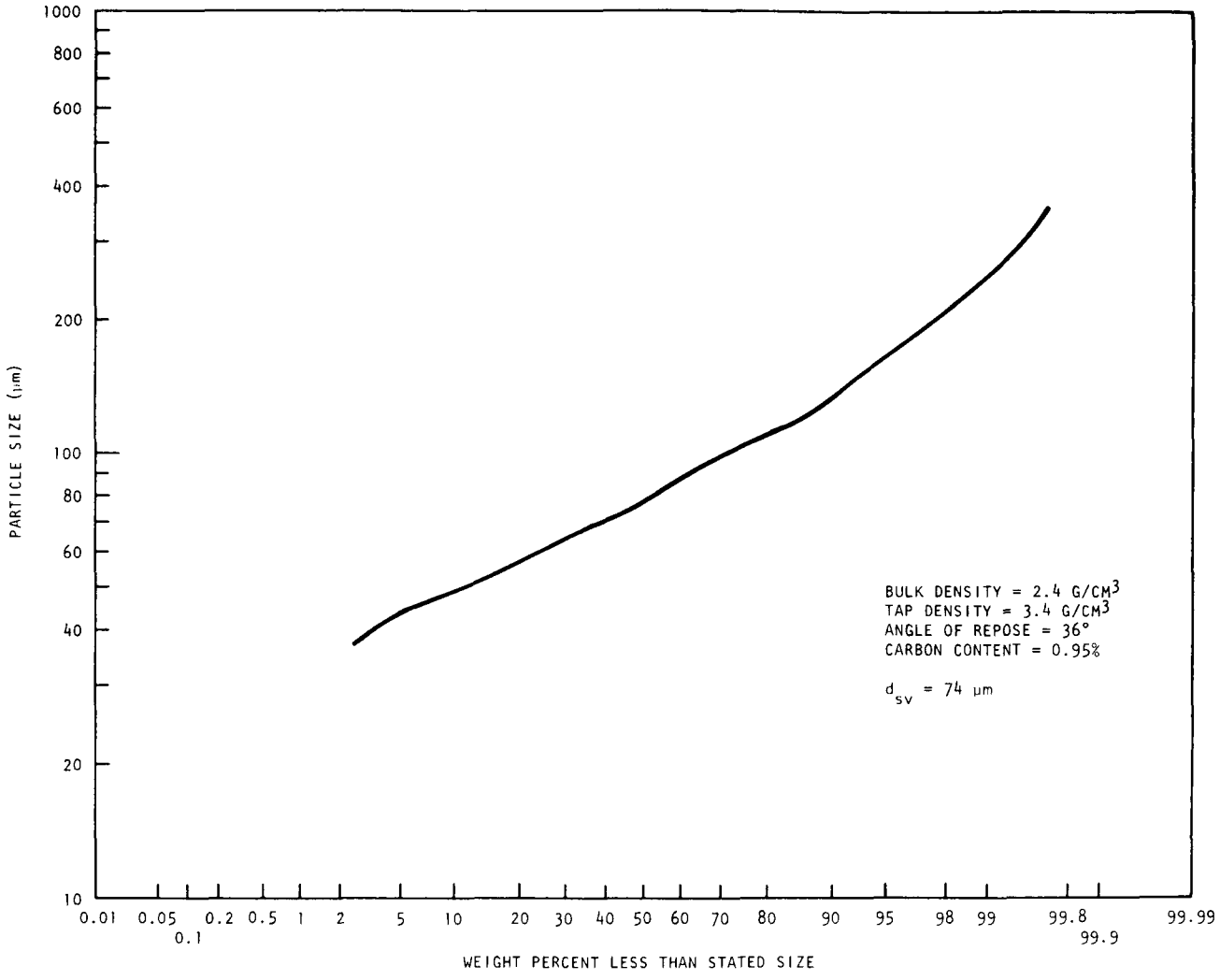

Fig. 4-21. Product size distribution, Run 47

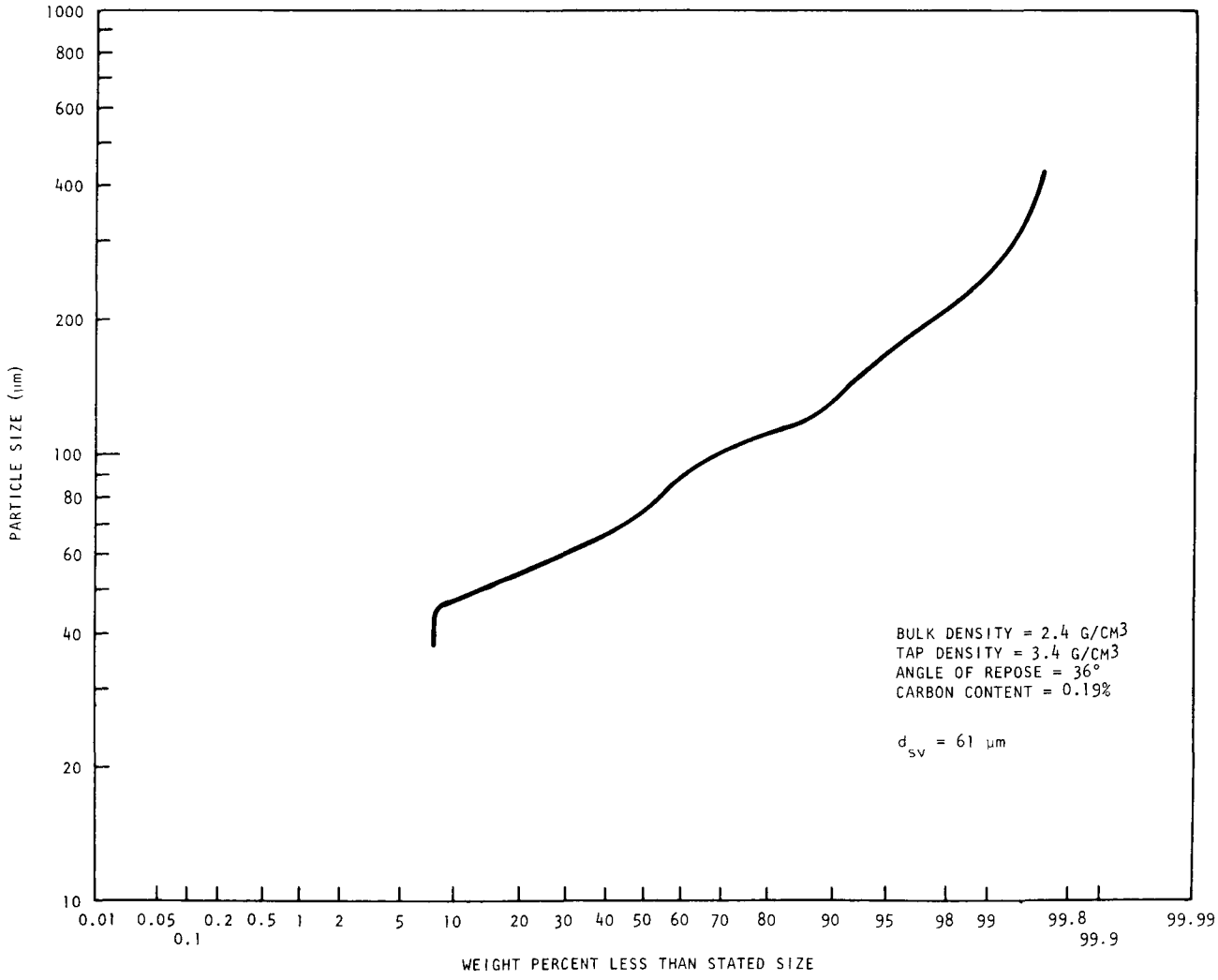

Fig. 4-22. Product size distribution, Run 48

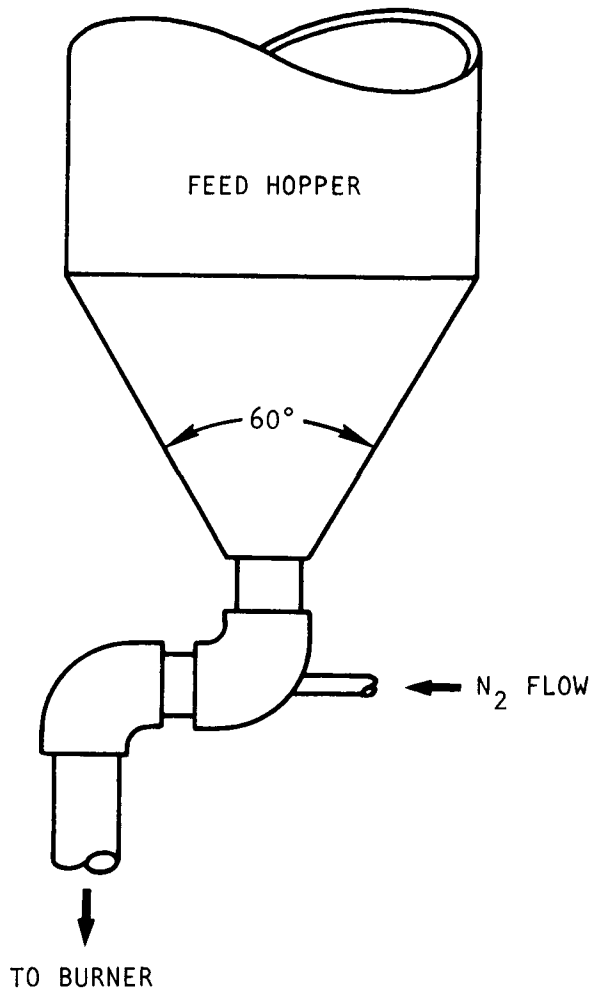

Fig. 4-23. Gravity-pneumatic feeder

preclude feed material from spilling over into the burner (determined by measuring the feed material angle of repose). When the N_2 flow is activated, material between the elbows is swept into the burner and is replenished by the gravity flow of feed from the hopper into the elbows.

This concept was tried using several different sizes of pipe, ranging from 1/2 in. to 4 in. Both 2-in. and 4-in. feeders were found to be erratic in their flow characteristics, with packing and uneven spurting of the material. The 1/2-in.-diameter feeder was not usable due to the tendency of the small pipe to clog with the -3/16-in. graphite mixture.

Feeders with diameters of 1 in. and 3/4 in. were both found to be suitable for use on the primary burner. The recommendation for their installation was not taken because the burner was subsequently deactivated for 18 months and has since been run with fresh feed added to the lower portion of the burner, a task for which this feeder is not suited.

A few months after the development work had been completed on the primary burner gravity-pneumatic feeder, the 10-cm secondary burner was relocated and extensively renovated. Up to that time, the secondary burner had been manually loaded via gravity and an automatic feeder was needed. A 1-in.-diameter gravity-pneumatic feeder was installed to allow top feed of crushed TRISO fertile particles to the secondary burner.

For about a year, the feeder was merely used and accepted because it never failed to add the feed material to the burner. Time was then allotted for some tests on larger feeders in order to achieve a shorter feed addition period in the burner cycle. This is a minor consideration in the 10-cm secondary burner because of the small bed sizes ($\sim$14 kg) but becomes more important in the 20-cm burner with bed sizes of up to 60 kg planned. The other purpose of the test was to gain further insight into the mechanism by which the feeder operates and to clearly establish the working range of the feeder.

All of the feeders used in the test program were of seamless butt-weld elbow construction with smooth inside surfaces unobstructed by pipe threads or similar rough edges that might cause material holdup. The centerline-to-centerline elbow spacing and the actual pipe inside diameter are given in Table 4-11 for various feeder sizes.

The elbow spacing was chosen to give 50% more horizontal length than required for the angle of repose (normally $\sim$38°). This was done to prevent solids from trickling over the edge after the N_2 flow was terminated.

As shown in Fig. 4-24, the feeders were fitted with a cleanout port aimed at the outer corner of the first elbow. This port was designed to remove any heel left by the normal feeder activation gas.

A cryogenic N_2 gas supply was used for the feeder activation flow and for feeder cleanout. An automatic timer was connected to a solenoid valve for setting the time duration of gas flow to the feeder.

Three kilograms of crushed TRISO fertile particles were used in the test program. The particle size distributions before and after crushing are shown in Fig. 4-25. This is typical of the feed material used in secondary burner experimental runs. The crushed particle angle of repose was 37°; the bulk density was 2.2 g/cm^3, and the tap density was 2.6 g/cm^3.

In the initial series of scoping tests, each of the three feeders was tested at 50 ft^3/hr (CFH) and 60 CFH N_2 activation flow for 5 sec in each test. Ten repetitions were made at each point to gain some repeatability data. Results of these tests (Table 4-12) indicated that the 1-1/2-in. feeder was well suited for future development from both the throughput and the repeatability standpoint.

The next set of tests was to determine heel weights, both with and without use of the cleanout port. The results (Table 4-13) indicate superiority of the smaller feeders, which is to be expected, and also that

TABLE 4-11
FEEDER GEOMETRIES

Nominal Feeder Size (in.)	Elbow Spacing, Centerline-to-Centerline (in.)	Feeder Inside Diameter (in.)
1	5.60	1.05
1-1/4	6.25	1.38
1-1/2	7.30	1.61
2	8.50	2.07

TABLE 4-12
FEEDER THROUGHPUTS

Nominal Feeder Size (in.)	Throughput (kg/min)	
	Activation Flow = 50 CFH	Activation Flow = 60 CFH
1	6.5 (σ=5.5%)[a]	6.0 (σ=7.6%)
1-1/4	10.6 (σ=4.0%)	10.2 (σ=6.0%)
1-1/2	12 (σ=8.7%)	13.7 (σ=5.9%)
2[b]		

[a] Standard deviation.

[b] Exhibited erratic flow characteristics at all flows.

TABLE 4-13
FEEDER HEEL WEIGHTS

Nominal Feeder Size (in.)	Heel Without Using Cleanout Port (g)	Heel Using Cleanout Port (g)
1	61	3
1-1/4	136	4
1-1/2	214	22

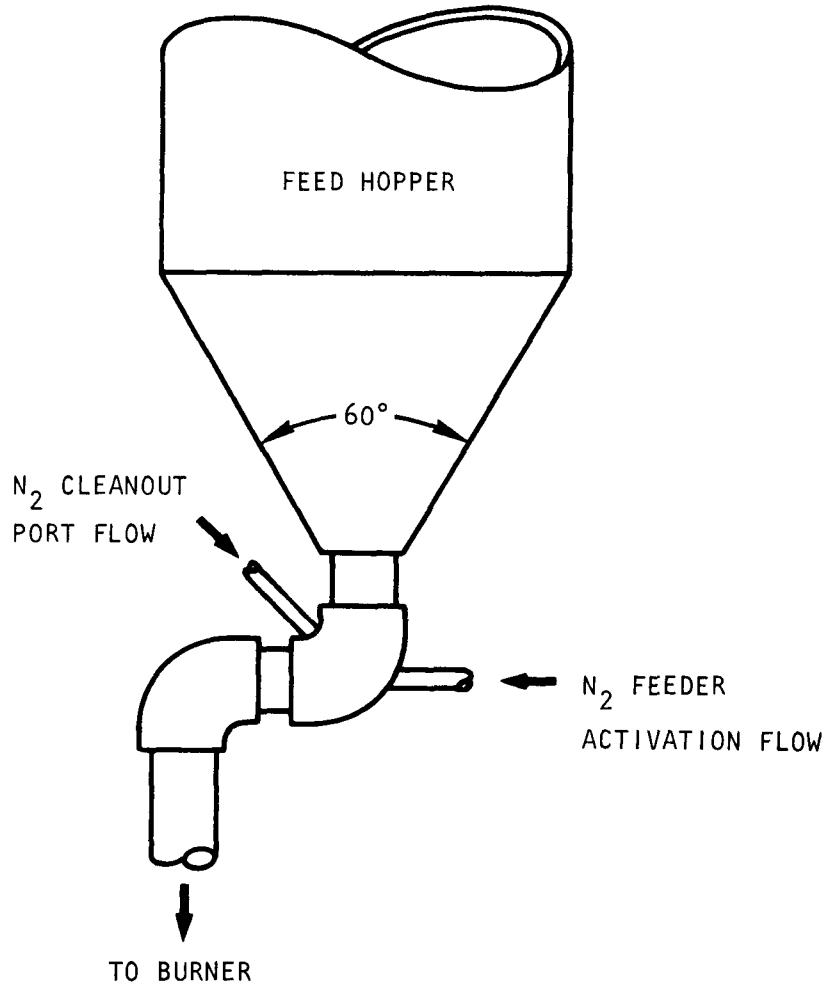

Fig. 4-24. Gravity-pneumatic feeder with cleanout port

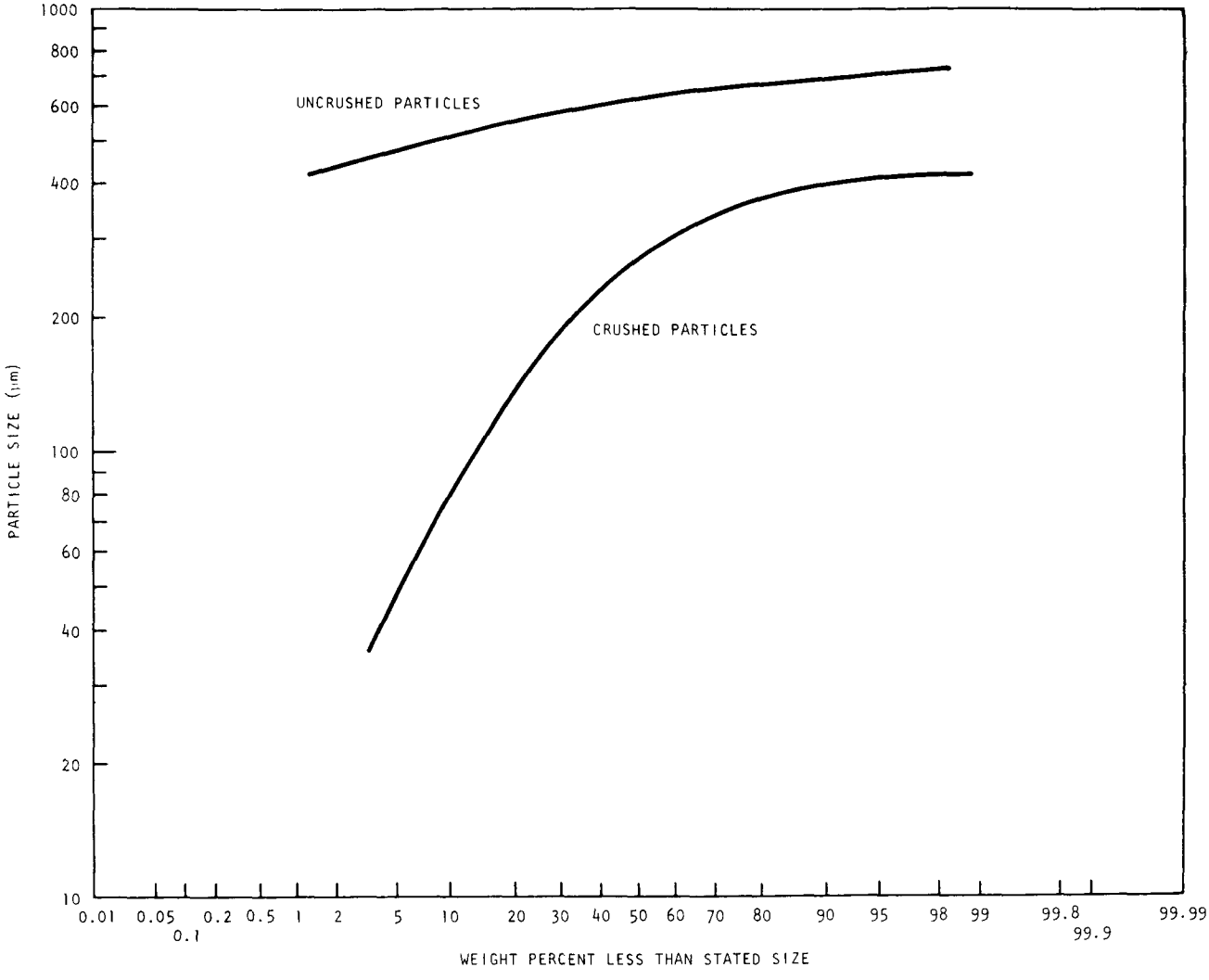

Fig. 4-25. Feed size distribution for tests of gravity-pneumatic feeder

the cleanout port worked well. The cleanout port activated at 30 psi inlet pressure for 10 sec after the feeder activation port had stopped blowing material out of the feeder. The 22-g heel on the 1-1/2-in. feeder was not seen to severely detract from its other attributes; thus, it was selected for more intensive study.

As shown in Fig. 4-26, the solids feed rate on the 1-1/2-in. feeder increases slightly with N_2 activation flow rate. Each plotted point represents the average of 10 tests performed under identical conditions.

Feeder cleanout capabilities were markedly improved by repeating the following cycle five times: 40 CFH gas flow through the feeder activation port for 5 sec followed by 70 CFH gas flow through the cleanout port for 5 sec. This procedure was tested 10 times, with heel weights averaging 3 g and no heel weights greater than 5 g.

The feeder with a nominal diameter of 1-1/2 in. has demonstrated the highest material throughput while providing excellent cleanout capabilities. It is therefore recommended for use on the 20-cm prototype secondary burner in the same configuration used in the test program.

Operation of the feeder at 40 CFH activation flow is recommended to minimize the gas requirements while maintaining a high throughput of 14 kg/min. The feeder cleanout procedures, as described in the discussion on the testing program, should be followed to ensure a minimum of heel.

4.2.2. 20-cm Prototype Secondary Fluidized-Bed Combustor

The following basic design parameters and the operational characteristics of the 20-cm prototype secondary have been analyzed in previous Quarterly Progress Reports (Refs. 4-2, 4-5):

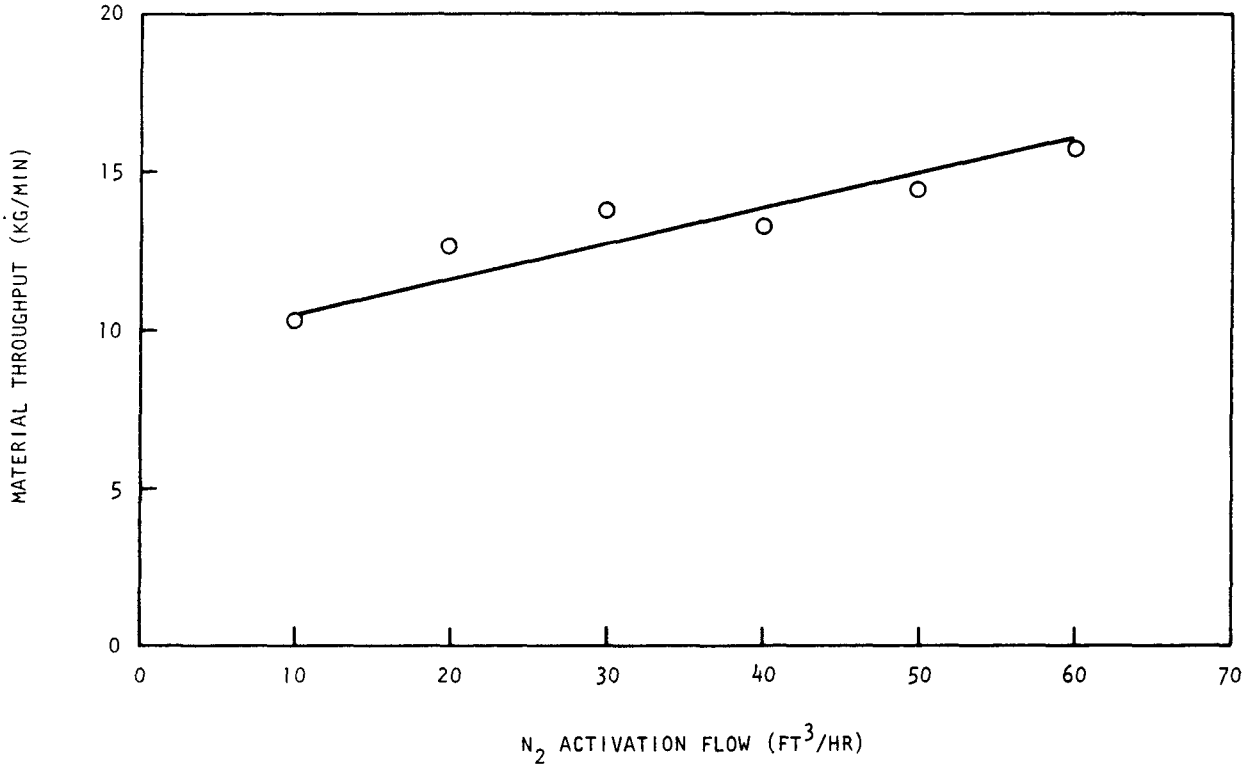

Fig. 4-26. Feeder throughput rates, 1-1/2-in.-diameter feeder

1. Feed and product characterization.

2. Fluidization characteristics.

3. Fluidizing velocity.

4. Heat transfer coefficient.

5. Induction heating for startup.

The basic operational cycle, the cooling and transient heating response characteristics, and the process controls are under study and will be included in future Quarterly Progress Reports.

Based on the above information and the experimental development data, specific design recommendations have been made for the ACC prototype secondary burner as per their request (Ref. 4-16). In connection with the design recommendations, the overall process and design have been reviewed. Six different heating methods have been evaluated (Section 4.3).

General Atomic has provided ACC with design recommendations for the prototype secondary burner per their request, which is included as Table 4-14. Responses to the specific data requests (items A-1 through A-12) are summarized below; the letter designations contained in the requests are included with each item.

4.2.2.1. Feeding (A-1)

A gravity-pneumatic feeder of 1-1/2 in. nominal diameter, as discussed in Section 4.2.1, with an activation flow of 40 CFH of N_2 gas is recommended for the following reasons:

TABLE 4-14
ACC REQUEST FOR SECONDARY BURNER DESIGN RECOMMENDATIONS

A. Please provide design recommendations based on GAC pilot plant experience on the following aspects of secondary burning:

	Priority	Need Date	Input to Node[a]
1. Feeding	II	2/1/75	224[b]
2. In-vessel filters	I	2/1/75	224
3. Distributor	I	2/1/75	224[b]
4. Product removal	I	2/1/75	224
5. Fluidizing velocity	I	2/1/75	224
6. Feed gas composition	I	2/1/75	224
7. Bed temperature	I	2/1/75	224
8. Wall temperature	I	2/1/75	224
9. Burn rate	I	2/1/75	224
10. Length-to-diameter ratio (L/D) for the beds excluding de-entrainment space	I	2/1/75	224
11. Ignition temperature	I	2/1/75	224
12. De-entrainment space size requirement	I	2/1/75	224

[a] As given in ORNL-4702 (Ref. 4-17).

[b] Input to Interim Title I.

1. Suitability of the gravity-pneumatic feeder to batch feeding.

2. Simplicity of the design and fabrication.

3. Proven reliability.

4. Sufficient capacity (∿14 kg/min) for a larger burner.

5. Relatively small requirement of pneumatic carrier gas.

Tests on the 10-cm secondary burner have been successful as shown by the results given in Ref. 4-18 and Section 4.2.1.

4.2.2.2. In-Vessel Filters (A-2)

The performance of in-vessel filters in a 10-cm secondary burner is analyzed in Ref. 4-19. Based on this analysis, in-vessel filters are recommended in the 20-cm prototype secondary burner.

A total of six filters, two in each compartment separated by three baffle plates, should provide adequate filtration without an excessive pressure drop across the filter. The dimensions of the filters are given in Table 4-15.

TABLE 4-15
SINTERED METAL FILTERS

Material	Hastelloy X
Diameter	3 in.
Length	36 in.
Thickness	1/8 in.
Total surface area for six filters	15.1 ft^2
Mean pore size	5 μm (Grade H)
Nominal particle removal ratings (98%)	0.4 μm
Absolute particle removal rating (100%)	1.0 μm

The forward linear velocity for the maximum flow of 110 ft^3/min (at a 3 ft/sec fluidizing velocity) at a maximum average filter temperature of 800°C will be 7.36 ft/min (or 3.74 cm/sec), which is comparable to the present 10-cm secondary burner filter capacity.

The blow-back of the filters will be accomplished by using compressed CO_2 gas (60 to 80 psi) through a venturi nozzle. Each filter compartment (two filters in a compartment) will be alternately blown-back every 2 or 3 minutes for a short duration (1 to 2 sec). A detailed drawing of a filter-venturi nozzle assembly is given in Ref. 4-2.

4.2.2.3. Gas Distributor (A-3)

Details on the distributor are given in Ref. 4-2, except that the product removal valve has been eliminated from the distributor plate for the reasons discussed in Ref. 4-5. This change increases the number of holes from 120 to 121, which makes a negligible difference in the pressure drop. All other dimensions remain the same. A revised drawing of the distributor without the valve is shown in Fig. 4-27.

4.2.2.4. Product Removal (A-4)

The basic arrangement of the product removal valve is the same as that used in the 10-cm secondary burner (Ref. 4-20), except that the valve is located on the side wall of the lower Gray-loc hub. Two different conceptual designs have been discussed in previous Quarterly Progress Reports (Refs. 4-2, 4-5); the final design is shown in Fig. 4-28.

The valve, which is operated by a three-position pneumatic actuator, opens 1/4 in. for the initial product withdrawal and 2 in. for the final withdrawal and cleanup. The product removal is achieved by a vacuum pneumatic transportation with about 15 in. Hg vacuum at the pump head. A further study of the pneumatic transport is under way. However, a

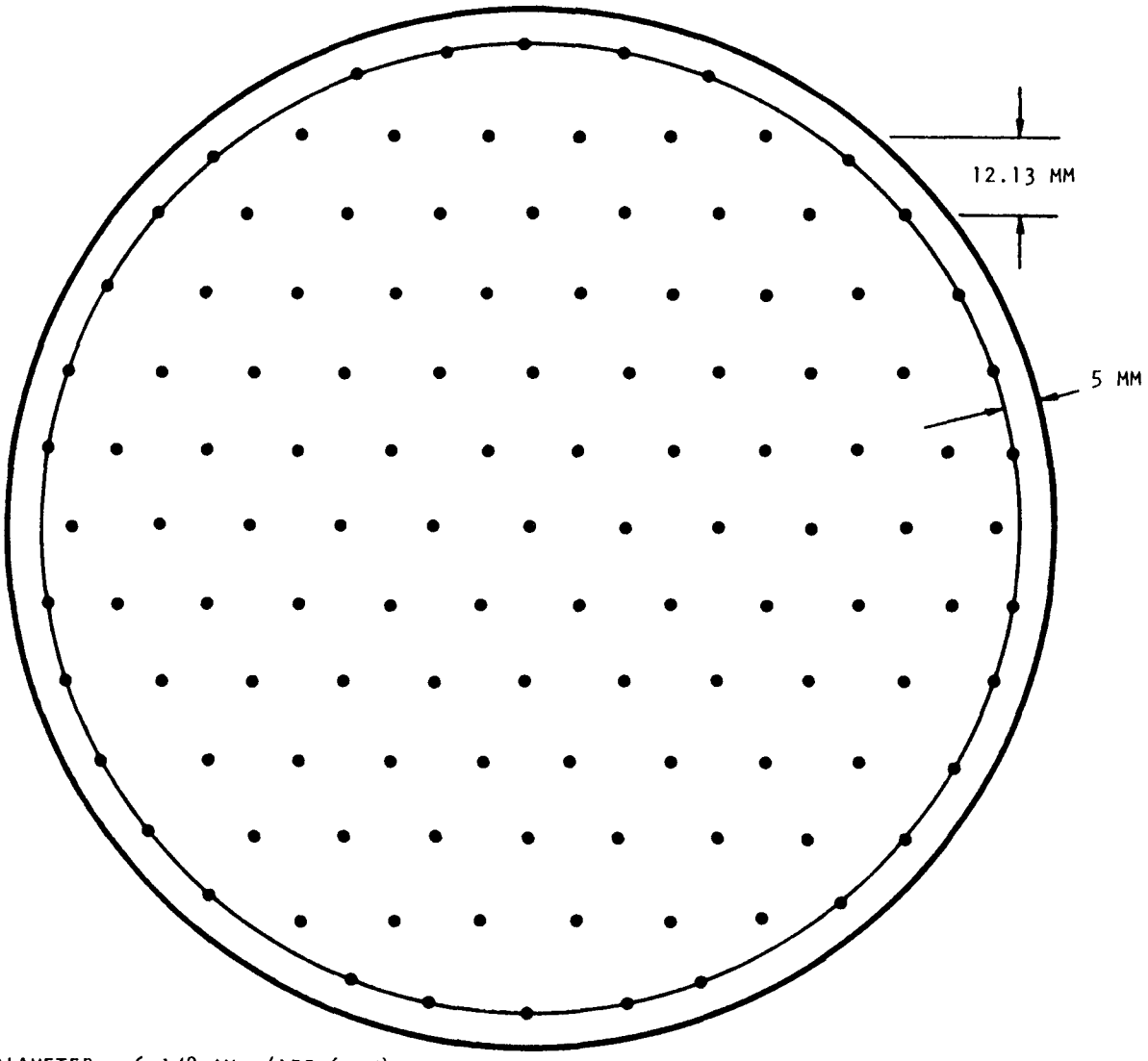

DIAMETER: 6-1/8 IN. (155.6 MM)
D_{OR} = 1.4 MM (55 MILS)
121 HOLES
ΔP = 35 CM H_2O

TRIANGULAR PITCH: 14 MM
OPEN AREA = 0.96%

Fig. 4-27. Distributor plate, 20-cm prototype secondary burner

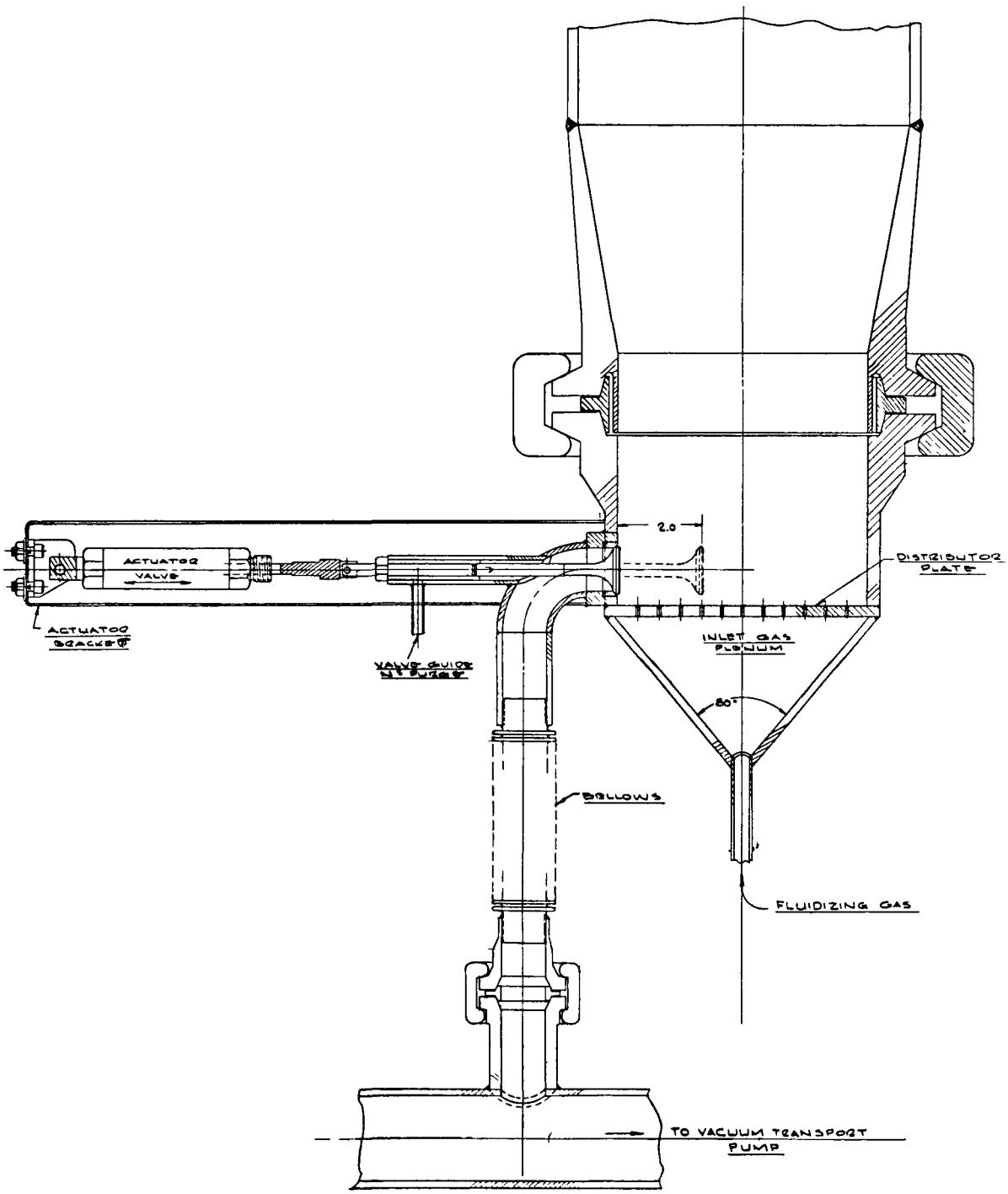

Fig. 4-28. Modified product removal valve

preliminary analysis and the operating experience on the 10-cm secondary burner show that a 1-1/2-in. to 2-in. pipe line with a solid loading of 0.5 to 1.0 lb of solids/lb of air at a velocity range of 100 to 200 ft/sec will be adequate.

4.2.2.5. Fluidizing Velocity (A-5)

The allowable burner operating velocity ranges from 15 to 80 cm/sec. Changing the velocity as the process goes on would be most ideal. However, a velocity in the range of 40 to 60 cm/sec appears to be optimum except at the end of the run, where the velocity may be reduced to 15 to 30 cm/sec. These velocities are based on:

1. Fluidization characteristics.
2. Elutriation of bed materials.
3. Heat transfer characteristics.
4. Burn rate.

Additional details on the fluidizing velocity are given in Ref. 4-5.

4.2.2.6. Feed Gas Composition (A-6)

During the period of feeding to the burner, the preheating period before ignition, and the burner idling period, the bed material will be fluidized by a 100% inert gas (in terms of oxidation*), N_2 or CO_2. From shortly after the ignition through the main burn period, the oxygen consumption is nearly complete and 100% O_2 can safely be used as the

---

*Oxidation of graphite by $C + CO_2 \rightleftarrows 2CO$ can be neglected compared to the reaction $C + O_2 \rightleftarrows CO_2$ (Ref. 4-21).

combustion gas and also as the fluidizing gas. This has been evidenced in secondary burner runs at GA and in work at KFA (Ref. 4-22). Diluent gases (N_2 or CO_2) can be used to control the bed temperature without altering the bed fluidization. At GA, 0 to 30% N_2 has been used in the feed gas during normal operation, and up to 60% N_2 at the end of the run, without any difficulty. KFA has used up to 45% CO_2 as a diluent gas. No difficulty in temperature control with either the O_2/CO_2 mixture or the pure oxygen was reported (Ref. 4-22).

During the tail burning period near the end of the run, the use of a diluent gas is necessary to protect the filters from the flash-burning of fine particles above the bed. Forty percent N_2 seems to be marginal and a 50:50 mixture of N_2/O_2 or CO_2/O_2 is recommended.

4.2.2.7. Bed Temperature (A-7)

The optimum range of bed temperature is governed by many factors:

1. Ignition temperature (discussed in Section 4.2.2.11).

2. Oxidation of CO into CO_2.

3. Maximum burner wall temperature (discussed in Section 4.2.2.8).

4. Heat removal capacity through the wall.

The threshold oxidation temperature of nuclear graphite in oxygen is around 530°C (Ref. 4-23). At this high temperature the amount of CO production is significant compared to the amount of CO_2, and at higher temperatures the main product becomes CO. Although the ignition temperature of CO is 609°C, a significant conversion reaction, $CO + 1/2O_2 \rightarrow CO_2$, occurs at a temperature above 750°C (Ref. 4-23). In order to reduce the CO production, the whole bed should be maintained above 750°C. Taking

the bed temperature fluctuation and the effect of frequent filter blow-back into consideration, a bed temperature (temperature at the burning zone) of 900 ± 50°C is considered adequate. This temperature has also been proven adequate by operations at GA.

The maximum allowable wall temperature limits the maximum allowable bed temperature. However, the wall temperature is determined by the wall cooling capacity and depends on the design. In any case, the maximum bed temperature should be kept lower than the sintering temperature of ThO_2 [1250°C in air, (Ref. 4-24)]. A higher bed temperature increases the heat removal capacity through the wall but does not help the combustion rate since the oxygen consumption is nearly complete even at a lower temperature.

4.2.2.8. Wall Temperature (A-8)

The wall temperature depends on both the bed temperature and the heat removal rate through the wall. As the heat removal rate is increased, the wall temperature decreases. For a given bed temperature, the wall temperature reaches its maximum when there is no cooling. Even for this case, the wall temperature will be substantially lower than the bed temperature, due to heat losses through the wall by radiation and conduction. The maximum allowable wall temperature depends on the burner vessel material. For Hastelloy-X the coded temperature for a pressure vessel is 900°C. Therefore, 900°C can safely be taken as an upper limit for the burner wall temperature. During the induction heating cycle before ignition and during tail burning and burner idling, the burner wall temperature will be maintained at 900°C and will be controlled by the thermocouples embedded on the tube wall.

4.2.2.9. Burn Rate (A-9)

The burn rate is determined by the following factors:

1. Reaction kinetics.

2. Oxygen supply (fluidizing gas velocity).

3. Heat removal capacity through the wall.

The graphite oxidation reaction is a very fast irreversible reaction; the reaction rate is not governed by the kinetics but by the oxygen supply in this burner. The maximum oxygen supply in turn is governed by the maximum allowable fluidizing velocity and the heat removal capacity. A preliminary calculation shows that the heat removal through the wall is limiting with a corresponding fluidizing velocity of 70 to 80 cm/sec (with 100% O_2).

The average burn rate is also a function of the batch operational cycle and the batch size. The batch size is discussed in Section 4.2.2.10. The operational cycle includes preheating of the burner (with or without a feed charge), ignition followed by the startup operation to a steady state, main burning, tail burning, burner idling (to release the volatile fission products), and burner cooling and discharge. With a 60-kg batch and a 5-hr batch cycle time, the burner will have a capacity of 1.2 blocks/hr (design capacity is 1 block/hr).

4.2.2.10. Length-to-Diameter Ratio (L/D) for the Beds Excluding De-entrainment Space (A-10)

The bed height decreases as the process continues; the height is also dependent on the fluidizing velocity. Since the bed height is largest at

the beginning of the process, the bed height, L, is defined as the static bed height with a fresh feed charge.

The L/D is not a well defined scale-up parameter, except that a higher L/D gives heavier slugging than a lower L/D. Generally, a higher bed height provides better heat transfer due to the increased heat transfer area. The effect, however, is not significant with a slugging bed due to a lower heat transfer coefficient resulting from poor solid mixing. At the top of the bed most of the gas moves upward in slugs, resulting in poor gas-solid contact. Therefore, added bed height and the resulting longer residence time of gas in the bed do not necessarily contribute to the process.

The determining factor for the bed height is the batch size, which in turn is determined by the bed fluidization characteristics, heater capacity, and the operating cycle. An L/D of up to 13 has been used in the 10-cm secondary burner without much difficulty in operation. With a 60-kg batch operation, the design burn rate (1 block/hr) can be achieved with the smallest physcial size of the burner and auxiliary equipment. This will give an L/D of 5, and no difficulty in fluidization is expected.

4.2.2.11. Ignition Temperature (A-11)

It is first necessary to distinguish the difference between the ignition temperature and the self-sustained burning temperature. To maintain the ignition temperature, a continued heat supply is necessary; the reaction rate depends on the rate of heat supply unless the heat of reaction is large enough to self-sustain the combustion. The self-sustained burning temperature, on the other hand, does not require a heat supply to the system and is a function of the heat generation rate, loss of heat to the surroundings, and the geometry.

The graphite-oxygen reaction becomes noticeable at temperatures above 300°C (Ref. 4-21). However, the reaction rate at this temperature is extremely low. The threshold oxidation temperature (at which a sample loses 1% of its weight in 24 hr) for nuclear graphite in oxygen is around 530°C (Ref. 4-21). Thermogravimetric analysis of the fuel element matrix carbon and the PyC coating (Ref. 4-25) shows that the matrix carbon can be ignited into a sustained burning at a temperature range of 450° to 630°C and the PyC at about 650°C. Thermogravimetric analysis of graphite and pyrolytic, SiC coated graphite disks (Ref. 4-26) shows burning at temperatures of 700° and 650°C, respectively. The results of the thermogravimetric analyses are shown in Figs. 4-29 through 4-35.

Thorium carbide is a pyrophoric material. Finely crushed thorium carbide spontaneously bursts into flame when exposed to air or oxygen at room temperature. The whole kernel, however, is not too reactive at room temperature (Ref. 4-27) and requires a higher temperature for ignition. The reactivity of ThC_2, therefore, depends largely on the relative surface area (particle size).

The self-sustained burning temperature is higher than the ignition temperature and depends on the rate of heat loss and the geometry. Work at ORNL with crushed particles burning in an alumina bed (Ref. 4-28) shows that the fuel ignites at 650°C and sustains burning at 700° to 750°C. The lowest ignition temperature attempted and achieved by GA is 480°C. Since the thorium carbide burns mainly in the first stage of the process (Ref. 4-5), the low ignition temperature was probably due to the high reactivity of thorium carbide. The safe ignition temperature for most runs, however, was 600°C. After the thorium carbide is depleted in the bed, the burner no longer sustains combustion at this temperature. Experience at GA shows that the self-sustained burning temperature is above 850°C for the 10-cm secondary burner. The relative heat loss per unit volume from the 20-cm secondary burner is lower than that from the 10-cm burner, and 850°C can be safely taken as the minimum bed temperature.

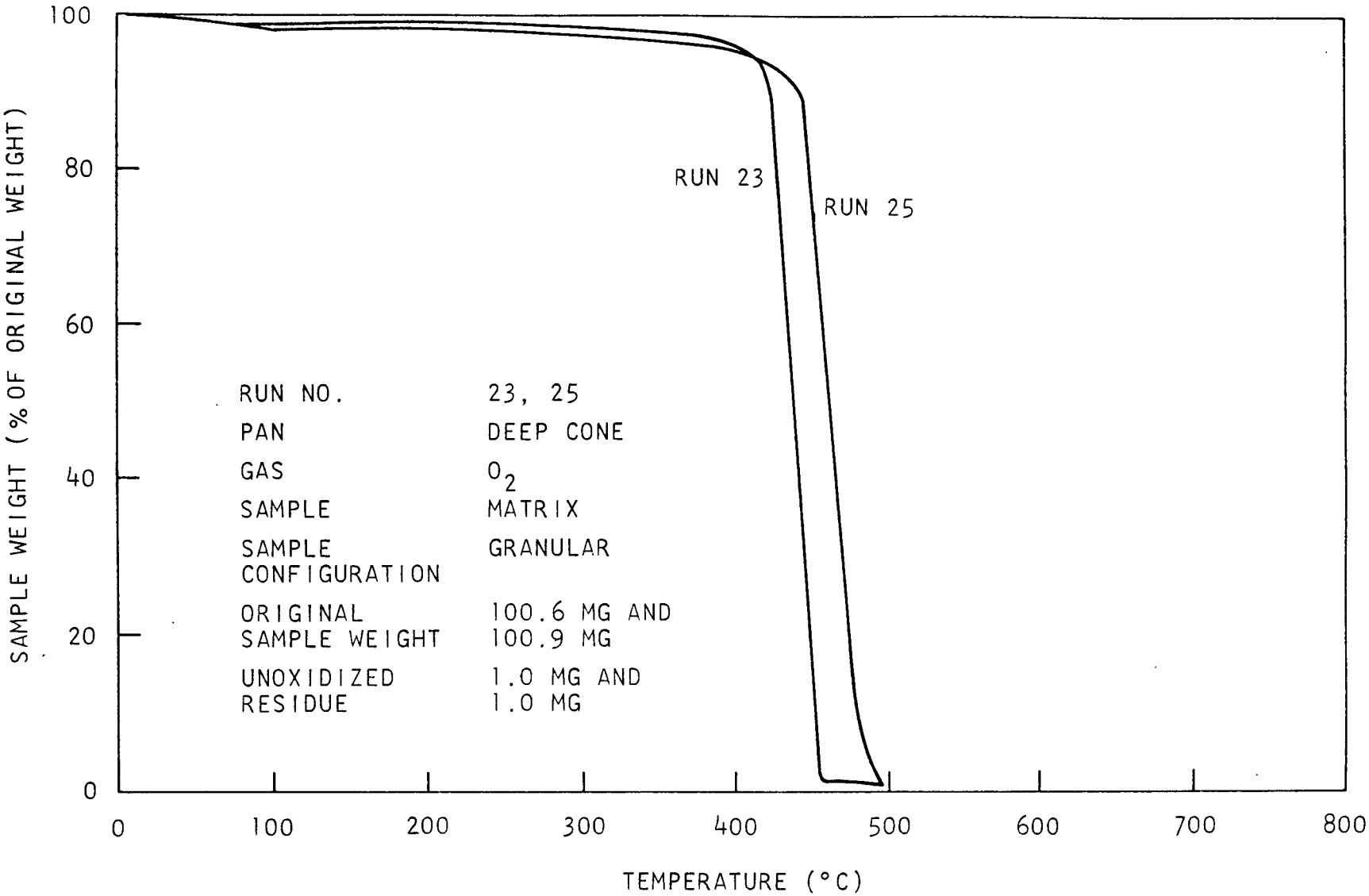

Fig. 4-29. Thermogram of granular matrix material in oxygen, 2.5°C/min temperature rise

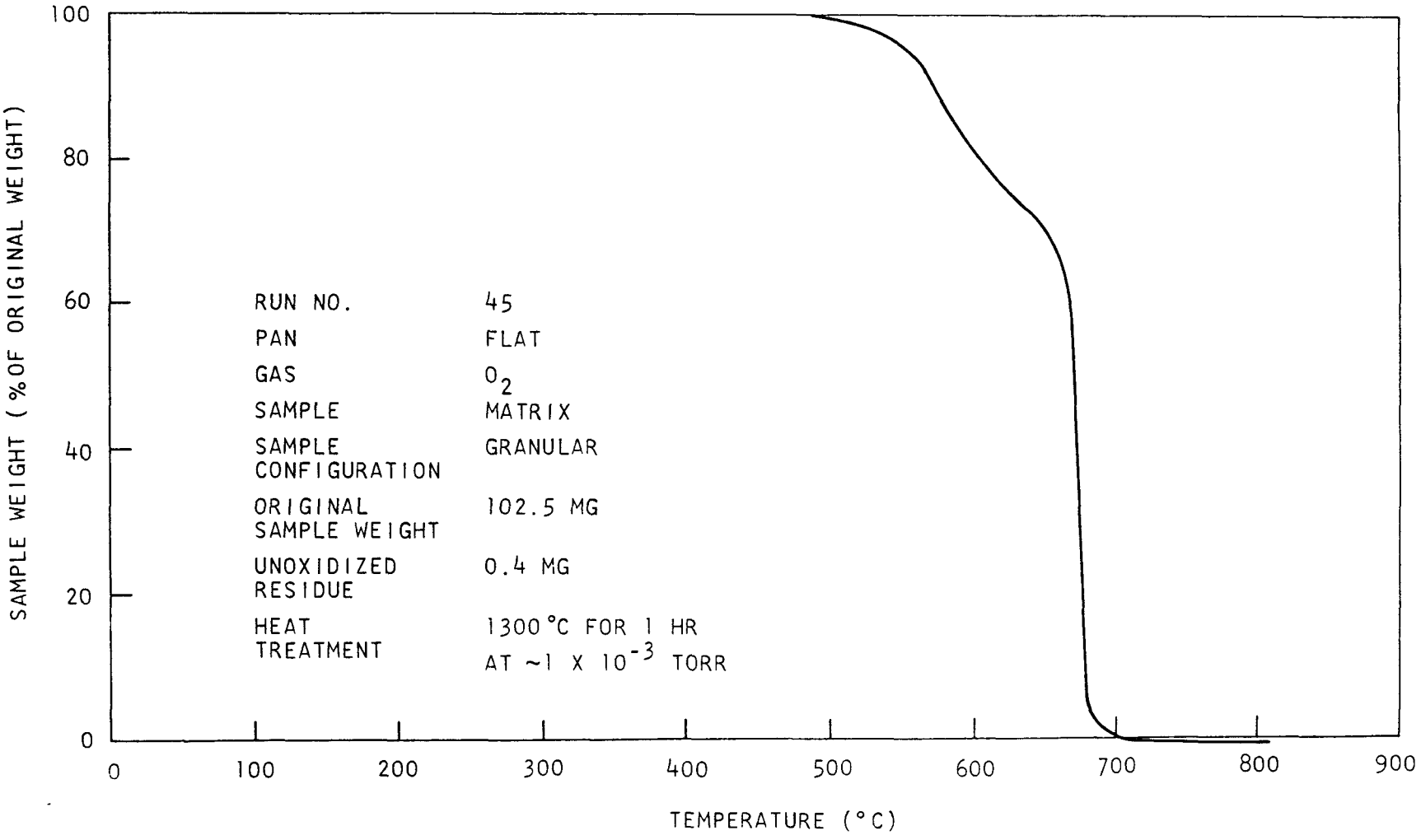

Fig. 4-30. Thermogram of matrix material in oxygen after outgassing at 1300°C, 2.5°C/min temperature rise

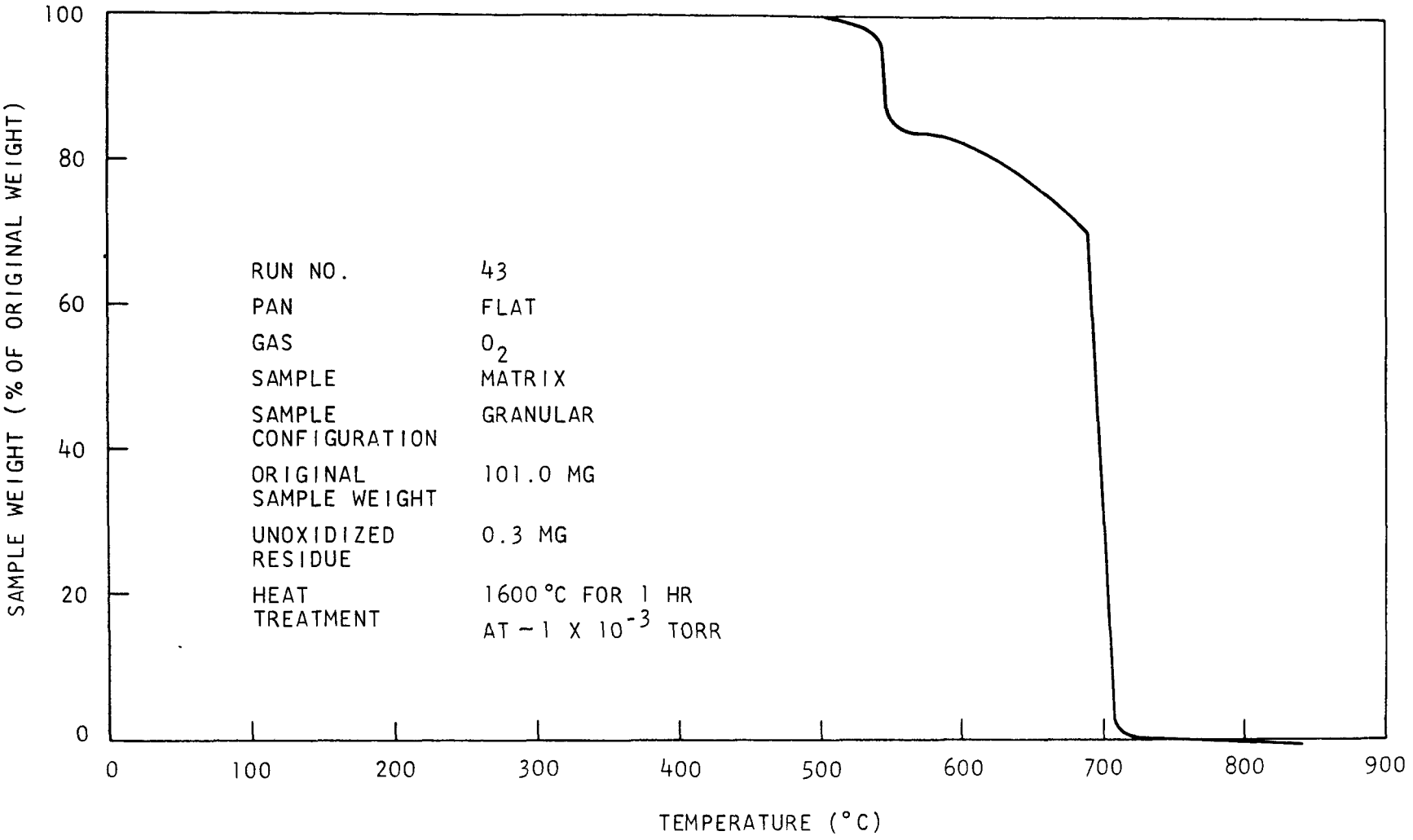

Fig. 4-31. Thermogram of matrix material in oxygen after outgassing at 1600°C, 2.5°C/min temperature rise

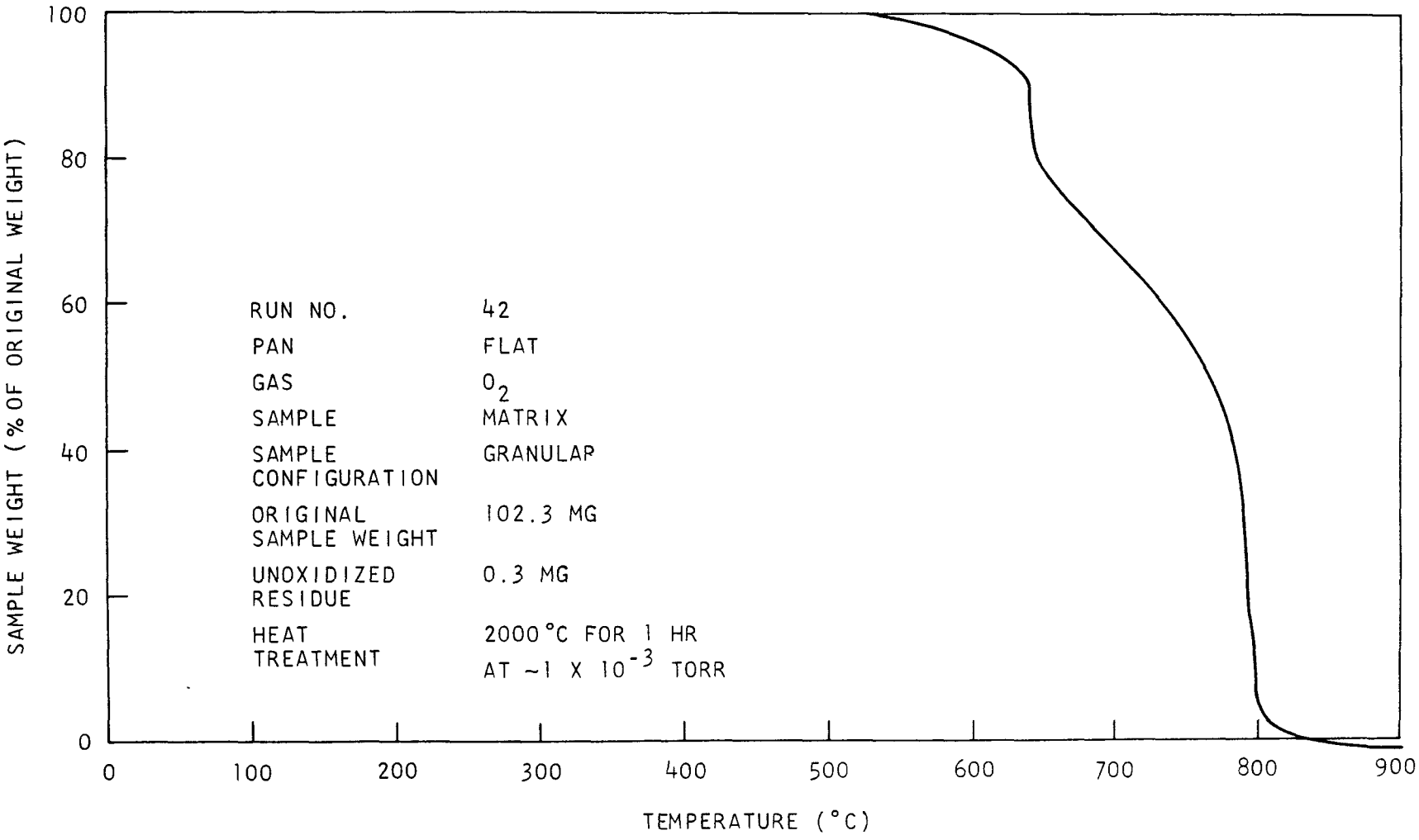

Fig. 4-32. Thermogram of matrix material in oxygen after outgassing at 2000°C, 2.5°C/min temperature rise

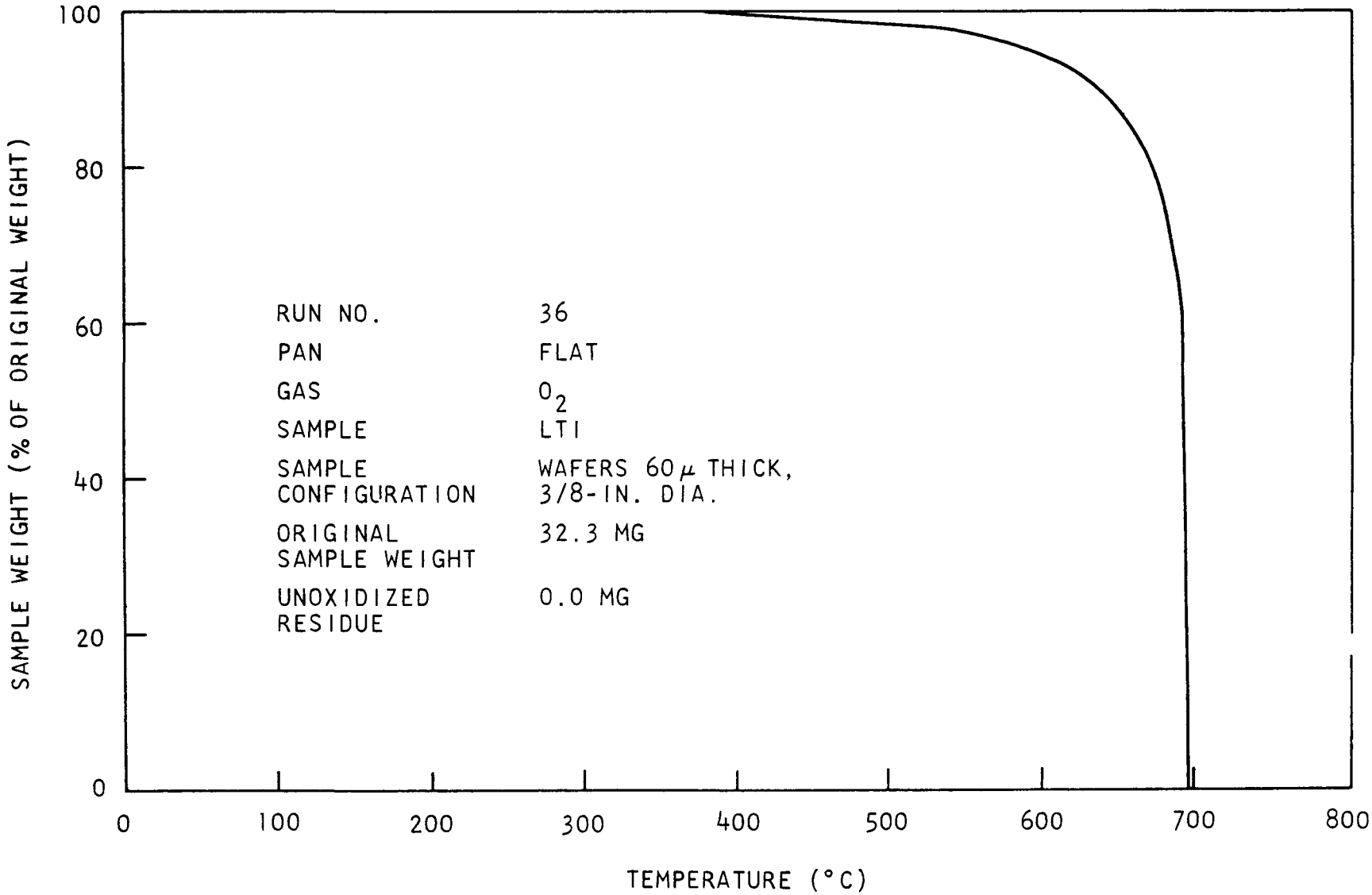

Fig. 4-33. Thermogram of LTI pyrocarbon in oxygen, 2.5°C/min temperature rise

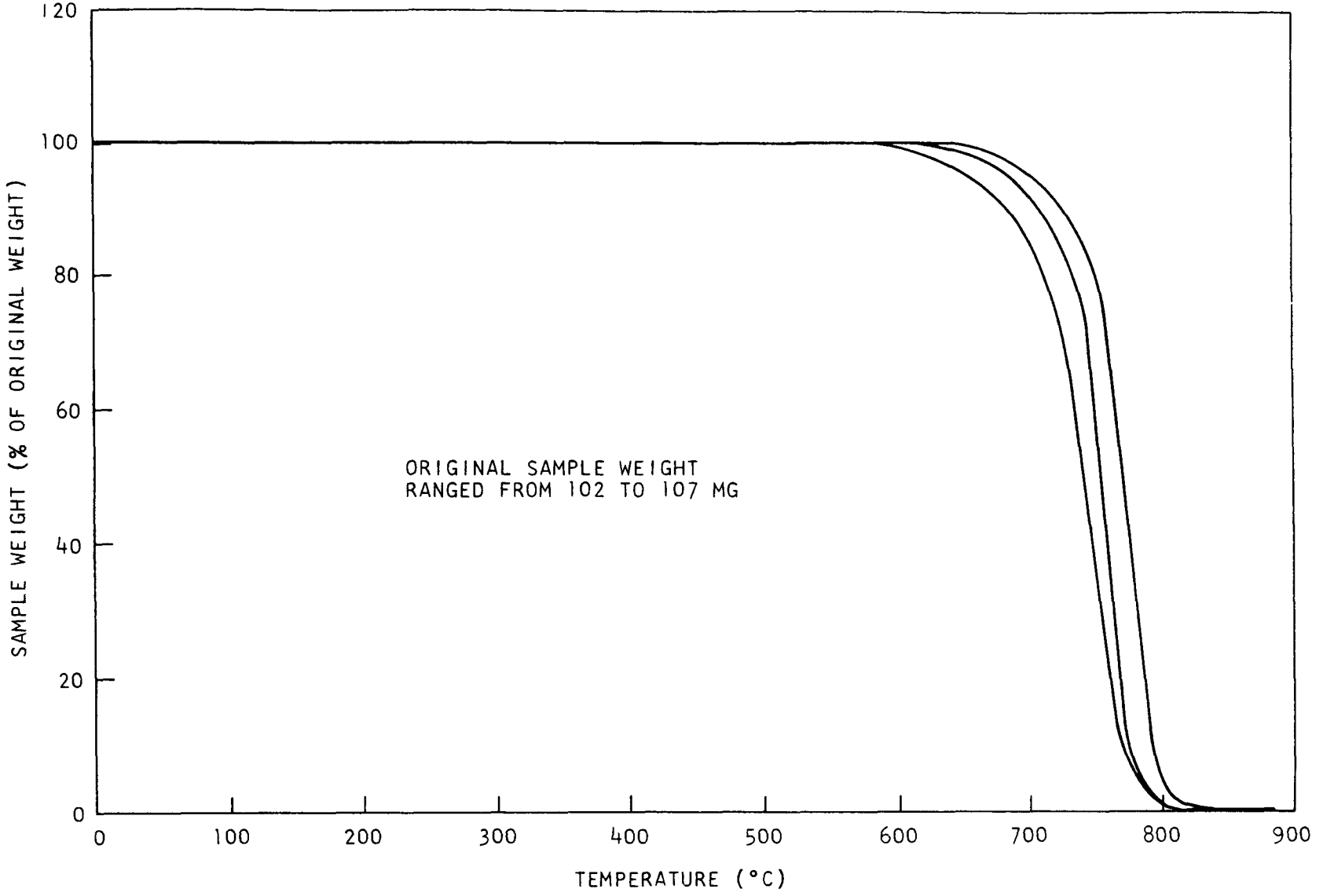

Fig. 4-34. Thermogram of graphite, 2.5°C/min temperature rise

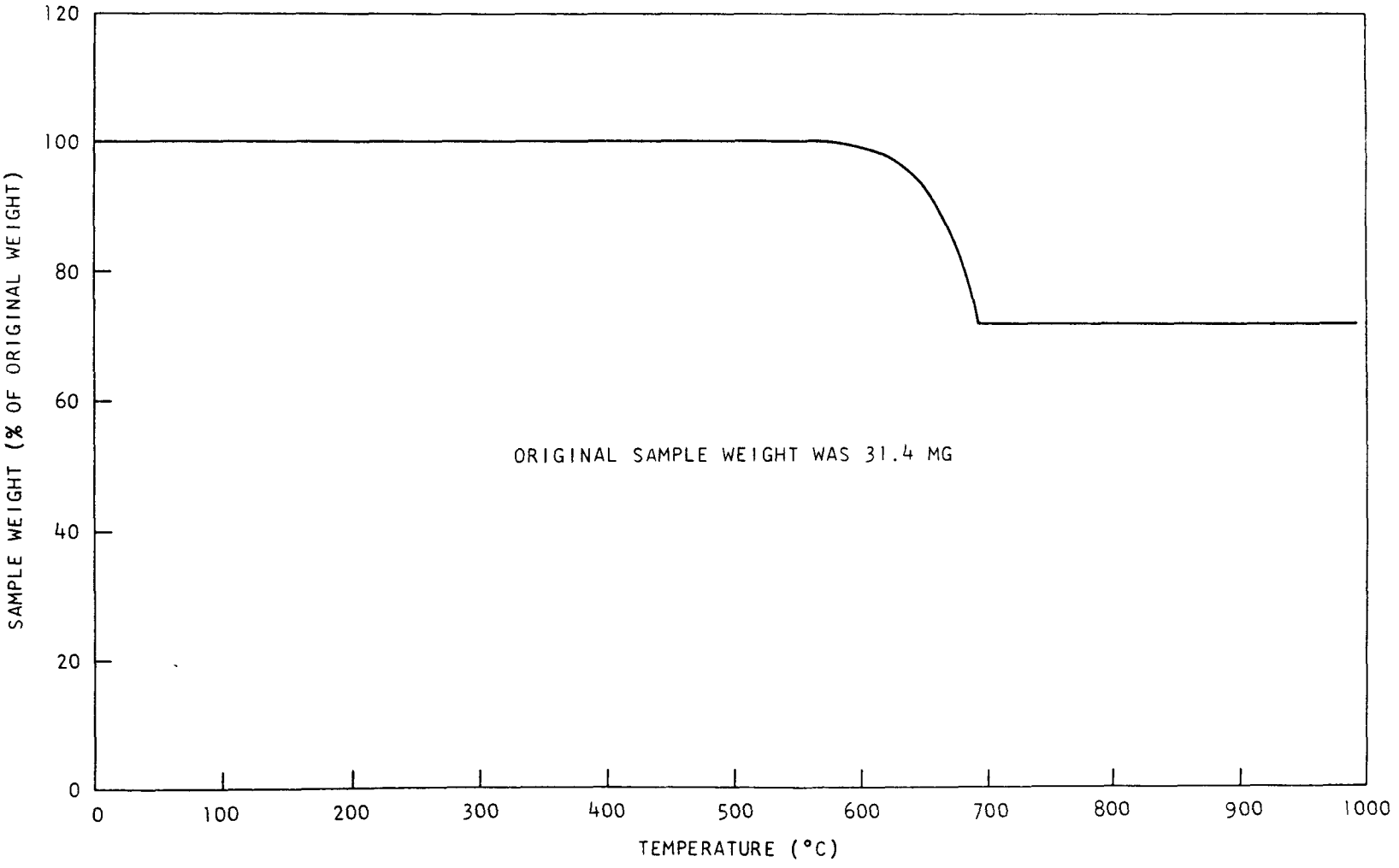

Fig. 4-35. Thermogram of a pyrolytic SiC coated graphite disk, 2.5°C/min temperature rise

From the above analysis, it is evident that the fuel can be ignited at 600°C but the self-sustained burning temperature will be substantially higher.

4.2.2.12. De-entrainment Space Size Requirement (A-12)

A de-entrainment space is allowed above the bed to return particles larger than the Stoke's diameter at the superficial velocity used. The minimum entrainment will be obtained when a space larger than the transport disengaging height (TDH) is allowed. No experimental data, however, are available for the TDH of secondary burner materials. The results from fluid catalytic cracking (FCC) catalyst of size between 20 and 150 μm show that a 20-cm burner will need a space of 150 cm at a superficial velocity of 60 cm/sec.

Not only is it difficult to afford this much space above the bed, but it is not necessary to minimize the entrainment with a large de-entrainment space for the following reasons:

1. The bed materials are confined in the burner by the use of in-vessel filters.

2. Since the bed height and the particle size change with the process and the final product is a fine powder, the entrainment of bed material is extremely difficult to reduce, even with a large de-entrainment space.

3. Even with a high entrainment rate, the particles can be returned to the bed effectively by the use of blow-back of filters.

4. A large de-entrainment space reduces the efficiency of returning fine particles to the bed.

5. A high filter pressure drop across the filter due to a high entrainment can be remedied by effective use of the blow-back technique.

In the 10-cm secondary burner, the de-entrainment space varied from 0 to 75 cm. With no de-entrainment space above the bed, the in-vessel filters were covered with fine powders. The filter pressure drop was excessive and stagnant burning of carbon fines on the surface of the filter eventually collapsed the filter. The carbon content in the final product, however, was lower with a larger bed size (a smaller de-entrainment space) (Ref. 4-19). In the 20-cm secondary burner, therefore, a space of 45 cm was allowed above the expanded bed. The effect of the de-entrainment space size is not considered critical unless the filters are submerged in the bed material or the space is too large for the back-blown particles to return to the bed.

4.3. FLUIDIZED-BED BURNER HEATING

Six different heating methods for fluidized-bed burners have been evaluated and, specifically, the induction heating method and the internal CO torch were compared (Ref. 4-29). The induction heating method shows an overall advantage over the internal CO torch. The application of an induction heating method, however, is limited to a moderate size burner due to its limited relative heat transfer area per unit bed volume. For a large-scale burner, an alternative hot gas heating method may be preferred, except that control of the fluidization might be difficult. A more extensive investigation of operational and economic considerations for this method is being pursued.

In order to optimize the induction heating system, including the minimization of power loss through the transmission line, a further system study was done (Ref. 4-30). This work includes the fundamental induction

coil design method, various factors affecting the power efficiency, and an analysis of the system power loss.

Detailed design of the burner vessel and the auxiliaries is progressing. The basic heating-cooling assembly design concept has been reaffirmed, and the design is progressing well into a detailed design stage.

4.3.1. Evaluation of Heating Methods

The primary and secondary burners both require a heating system to accomplish the following functional requirements:

1. Ignition of fresh feed material for startup.

2. Re-ignition of the bed materials after bed cooling (or quenching) due to process upsets.

3. Supply of heat to maintain the bed temperature during the tail-burning step.

4. Evaporation of fission products from the bed materials after the burning.

The burner heating methods proposed can be categorized as follows:

1. Internal heating by:

    a. Internal CO torch, ignition of coke.

    b. Internal CO torch, direct heating.

    c. High-temperature fluidizing gas.

2. External heating by:

   a. External flame torch.

   b. Resistance electric heating.

   c. Induction heating.

The various heating methods are compared in Table 4-16 and discussed below.

1. Internal CO torch to ignite a coke bed. A $CO-O_2$ torch can be used to ignite the coke bed, followed by the feeding of the bed material. Although this method has been used as a standard for the startup of both the 10-cm and 20-cm primary burners, it does not meet the heating system requirements listed above except for (1), i.e., ignition of feed material for startup. In addition, the formation of agglomerates has been attributed to a high local temperature and a lack of temperature control (Ref. 4-31). Also, this technique requires additional feed preparation and material transport steps.

2. Internal CO torch (direct heating). Direct heating with an internal CO torch has been proposed as a heating method. A low velocity flame is required to prevent particle sintering (Ref. 4-21). This technique must be used with high inert gas flows to maintain a low average bed temperature and to prevent particle sintering.

3. High-temperature fluidizing gas. Compared to other methods in which the heat flux is dependent on the relative surface area per unit bed volume, this method has a distinct advantage in scaling-up due to the invariance of the heat flux per unit volume with an

TABLE 4-16
COMPARISON OF VARIOUS HEATING METHODS

	Startup	Restart	Tail Burning	Soaking
Internal heating				
CO torch to ignite coke bed	Fairly fast, agglomeration.	Not practical	Not practical	Not practical
CO torch (direct heating)	Relatively fast, agglomeration, difficult to control the fluidization.	Same as startup	Same as startup	Same as startup
Hot-gas fluidization	Slow, easy to control, has advantages with a large burner.	Same as startup	Difficult to balance the fluidizing gas and the combustion gas, difficult to control.	Same as startup
External heating				
Wide flame torch	Moderately fast, temperature control is difficult, difficult to scale-up	Same as startup	Same as startup	Same as startup
Resistance heater	Very slow, needs frequent maintenance.	Same as startup	Not suitable due to slow response.	Same as startup
Induction heating	Moderately fast, easy to control both the temperature and fluidization.	Same as startup	Same as startup	Same as startup

increase in the burner diameter. One drawback of this method is difficulty in controlling the fluidization during tail burning, although this problem is not insurmountable. A separate combustion chamber for the generation of high-temperature gas is also required. A preliminary evaluation of this method (Ref. 4-32 indicates the necessity for further study to determine the operational and economic feasibility.

4. External flame torch (Ref. 4-33). The performance characteristics of an external flame torch are similar to those for induction heating. The temperature control, however, is more difficult in comparison with induction heating especially at high temperatures. The change of heating pattern with geometry makes scale-up very difficult. Due to these disadvantages and also lack of experience and development, further study of this method will not be undertaken.

5. Resistance heating. Although this method was used for some time at GA in the 10-cm secondary burner, a number of undesirable aspects were evident, such as a slow response, lack of cooling surface area, and a high maintenance frequency (Ref. 4-34). Therefore, this system is not recommended.

6. Induction heating. Induction heating has been demonstrated with the 10-cm secondary burner with proven reliability and ease of control. This method has been chosen as GA's reference heating method for both prototype burners.

The induction heating and CO torch methods represent the reference heating for the prototype burners and the system presently used for the primary burner. The performance characteristics of these two methods have been compared with respect to the following considerations:

1. Process.

2. Mechanical.

3. Safety.

4. Scale-up.

5. Economy.

The results of this comparison are summarized in Table 4-17.

Induction heating is the preferred method of the six methods evaluated and is recommended for use on both the primary and secondary prototype burners. The hot-gas fluidization method may be preferred for larger sized burners; a study is currently under way to evaluate the operational and economic considerations for this method.

4.3.2. Induction Heating Coil Design

The induction heating system is one of the most important parts of the integrated heating-cooling system for both the primary and secondary prototype burners and its design affects the entire system. The insulation thickness must be optimized according to the coil electrical efficiency, and the support rod and plate must be designed so as to minimize any magnetic susception on these parts. Susceptor temperature nonuniformity due to the coil end effects is also important in the control of the process. The following coil design method and the performance characteristics of the coil are presented to aid in understanding induction heating itself as well as to improve the overall system design.

TABLE 4-17
COMPARISON OF INDUCTION HEATING AND TORCH METHOD

	Induction Heating	Internal CO Torch
Process factors		
Heat flux (heatup cycle time)	Fairly high. Maximum flux is limited by the allowable burner wall or susceptor temperature. Total flux is limited by the available surface area.	Very high. Total flux is limited by the allowable flame temperature and the gas film to solid heat coefficient.
Temperature control	Relatively easy.	Difficult. Temperature fluctuations and nonuniformity expected.
Fluidization control	Independent from heating. Relatively easy due to even heating over the entire bed.	Influenced by the heating gas and the temperature distribution.
Fines elutriation	Small due to a low fluidizing velocity.	Very high due to high fluidizing velocity necessary to avoid local hot spots.
Segregation	Normal (because fines can easily be recycled without much effect on the heating).	Can be severe without fines recycle.
Agglomeration	None expected.	Formation of agglomerates has been continuously reported by GA and ICPP with CO torch operation. Excessive agglomeration can easily upset the process and cause a burn-through.
Fines recycle	Can be achieved without much influence on the heating operation (low recycle rate).	Impractical due to probable need for a high recycle rate.

TABLE 4-17 (Continued)

	Induction Heating	Internal CO Torch
Tail burning	Relatively easy; even temperature and fluidization control.	Difficult due to low residence time of carbon fines and temperature nonuniformity.
Soaking	Relatively easy; even temperature and fluidization control.	Difficult due to temperature non-uniformity and a high fines recycle rate.
Process analysis (off gas)	No effect.	Adds an additional uncertainty.
Off-gas treatment	No effect.	Increased load.
Automatic operation	Relatively easy.	Very difficult (torches backfire at low gas flow).
Mechanical factors		
Thermal stress	Even stress to the burner vessel (longer burner life).	Side penetration of the torches causes an uneven temperature distribution. Requires thermal shrouds in the torch.
Remote handling	Easier because heating system is handled separately from burner.	More complicated since the heating system is integrated into the burner assembly.
Maintenance	Relatively easy due to its inherent simple construction (a helically wound coil). Less maintenance is needed due to low-temperature operation.	Difficult especially with a large number of torches. More frequent maintenance is required due to high-temperature operation and the potential for bed material to back up into lines.

TABLE 4-17 (Continued

	Induction Heating	Internal CO Torch
Safety factors		
Criticality	Under examination. Potential problem due to water cooling of induction coil (see Safety).	Does not affect criticality.
Effect of radiation	Oil-filled capacitors need periodic replacement. (However, the capacitors can be located outside the hot cell or shielded.)	No effect.
Fire hazard	Low probability due to low-temperature operation and the lack of flammable materials.	Fire hazard due to handling of flammable gas with a high-temperature operation. High spark plug voltage (6000 volts) is another source of ignition. GA has experienced backfire and a detonation with a $CO-O_2$ torch, which pressurize the vessel.
Safety	Indirect heating with a susceptor plate provides an additional safeguard to the burner system. (Use of a susceptor plate also increases the coil electrical efficiency and reduces the coil conduction loss.)	Needs a secondary containment for protection from an explosion and an extremely careful operation to prevent backfire.
System reliability	Induction heating has been used in many fluidized-bed heating applications; the induction heating operation in the Hanford hot cell has proven its reliability.	Particle sintering has been observed when high flame temperatures and velocities exist.

TABLE 4-17 (Continued)

	Induction Heating	Internal CO Torch
Scale-up factors		
Heatup cycle time	Increases with burner size (diameter).	Does not increase with burner size. Due to the low gas-solid heat transfer coefficient, a larger burner requires more torches.
Mechanical complexity (remote handling)	Not affected by the burner size.	Complex; more torches need more in-cell gas lines, wires, and accessories. Remote handling is more difficult.
Temperature control	Control is relatively easy due to an even temperature distribution. Not much affected by the burner size.	Temperature nonuniformity increases when the number of torch penetrations is limited. Local hot spots facilitate the formation of agglomerates, and the temperature control is more difficult with a larger burner due to the larger number of torches needed.
Fines burning	The carbon can be burned out by maintaining a hot bed at a low fluidizing velocity.	At a higher fluidizing velocity, fines elutriation increases with the burner size due to temperature nonuniformity.
Criticality	May require poisoned water; however, a small-volume closed-loop system will be used.	No effect.

TABLE 4-17 (Continued)

	Induction Heating	Internal CO Torch
Economy factors		
Capital cost	The motor-generator (M-G) is expensive.	Safety equipment represents added cost.
Operational	Automatic operation lowers overall cost.	Manual operation can be costly.
Maintenance	Very low.	A higher frequency and degree of maintenance or repair for the ignitor. Potential line plugging can be very costly due to an expensive hot cell operation.
Space requirement	Requires space for the work station and M-G set. The M-G set can be outside the facility.	Less space is required. A CO storage tank can be installed outside the facility.

4.3.2.1. Equivalent Circuit Coil Design Method (Ref. 4-35)

The basis of this method is the reduction of the induction heating coil and workpiece to their equivalent resistances and inductances. Figure 4-36 shows the current paths in a solenoid work coil, as well as the distribution of the flux that induces the current. The symbols used in Fig. 4-36 are defined as follows:

A_g = cross-sectional area of the air gap, $in.^2$
d_c = coil inside diameter, in.
d_w = workpiece outside diameter, in.
I_c = coil current, amp
I_w = induced current in workpiece, amp
l_c = projected length of coil section, in.
l_w = length of workpiece, in.
δ_c = coil reference depth, in.
δ_w = workpiece reference depth, in.
ϕ_c = magnetic flux through coil, maxwells
ϕ_e = magnetic flux through external flux path, maxwells
ϕ_g = magnetic flux through air gap, maxwells
ϕ_w = magnetic flux through workpiece, maxwells

The reference depth δ is defined as

$$\delta = 3.16\sqrt{\frac{\rho}{\mu f}} \qquad (4\text{-}4)$$

where ρ = electrical resistivity, microhm-in.
μ = relative magnetic permeability
f = frequency of current, cps

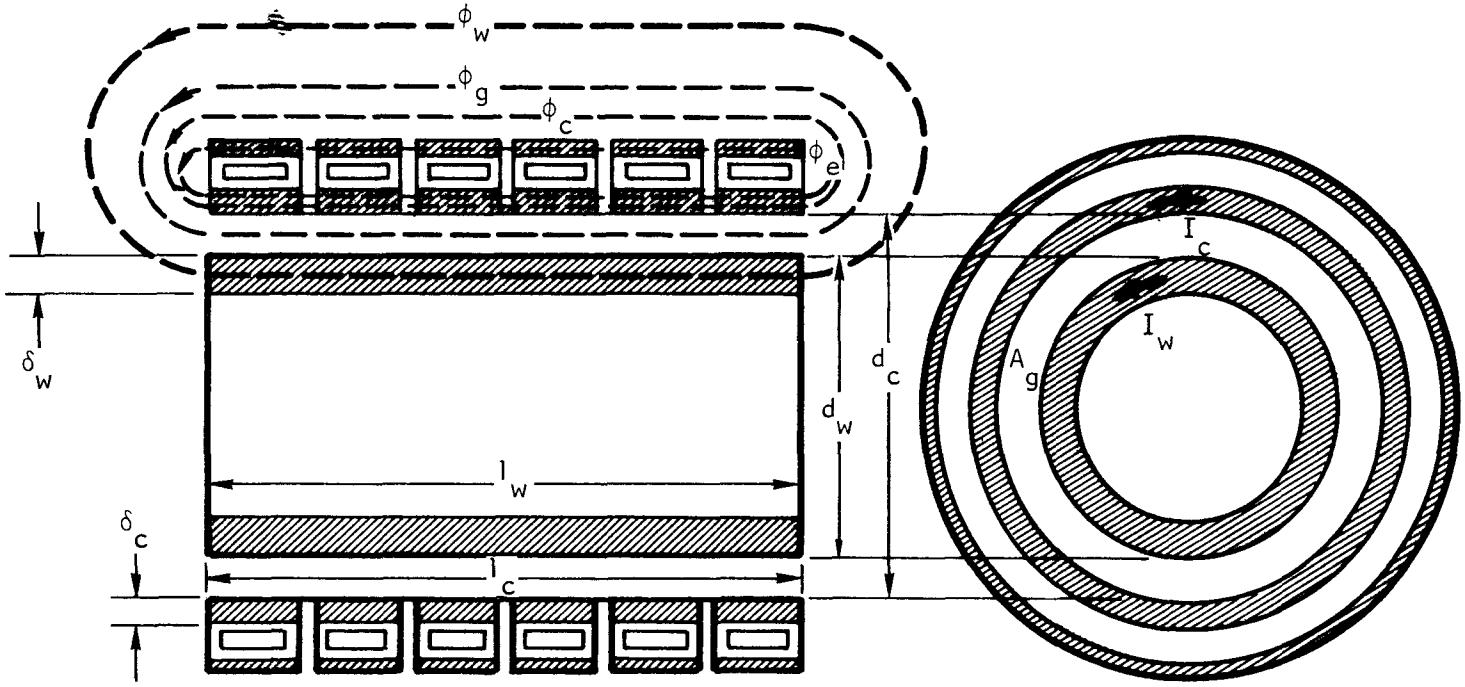

Fig. 4-36. Flux and current paths in a solenoid coil

Electrically, the system in Fig. 4-36 is equivalent to the circuit shown in Fig. 4-37. By equating the current densities to the magnetic flux densities using Ohm's law, the circuit components in Fig. 4-37 can be obtained from the physical dimensions and electrical properties of the coil and workpiece as follows (for details, see Ref. 4-30):

$$R_w = \frac{15.8f\ d_w^2\ \mu_w\ Q \times 10^{-8}}{l_c} N^2 \tag{4-5}$$

$$X_w = \frac{15.8f\ d_w^2\ \mu_w\ P \times 10^{-8}}{l_c} N^2 \tag{4-6}$$

$$R_c = X_c = \frac{k_r 63.2\ d_c\ (f\rho_c)^{1/2} \times 10^{-8}}{l_c} N^2 \tag{4-7}$$

$$X_g = \frac{20.1f\ A_g \times 10^{-8}}{l_c} N^2 \tag{4-8}$$

$$X_e = 35.3f\ d_c \times 10^{-8}\ N^2 \tag{4-9}$$

where R_w = work resistance, ohms
X_w = work rectance, ohms
R_c = coil resistance, ohms
X_c = coil reactance, ohms
X_g = air-gap reactance, ohms
X_e = external flux-path reactance, ohms
k_r = coil resistance correction factor
N = number of coil turns
P,Q = correction factors
ρ_c = coil electric resistivity, microhm-cm

The circuit in Fig. 4-37 can further be reduced into a simplified circuit as shown in Fig. 4-38. The equivalent reduced circuit components, R'_w and X_o, can be obtained from the following equations:

$$\frac{R'_w}{N^2} = \frac{(R_w/N^2)(X_e/N^2)^2}{(R_w/N^2)^2 + (X_1/N^2 + X_e/N^2)^2} \tag{4-10}$$

$$\frac{X_o}{N^2} = \frac{(X_e/N^2)[(R_w/N^2)^2 + (X_1/N^2)^2 + (X_e/N^2)(X_1/N^2)]}{(R_w/N^2)^2 + (X_1/N^2 + X_e/N^2)^2} \quad , \tag{4-11}$$

where $X_1 = X_w + X_c + X_g$ (4-12)

$$R_o = R'_w + R_c \tag{4-13}$$

Additional relevant equations are:

Total impedance:

$$Z_o = \sqrt{R_o^2 + X_o^2} \tag{4-14}$$

Coil efficiency:

$$\eta = \frac{R'_w}{R_o} \tag{4-15}$$

Coil power factor:

$$\text{Cos } \phi_c = \frac{R_o}{Z_o} \tag{4-16}$$

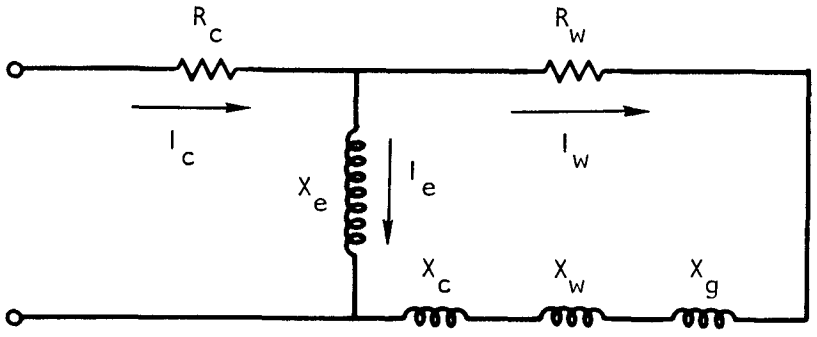

Fig. 4-37. Full coil and work equivalent circuit

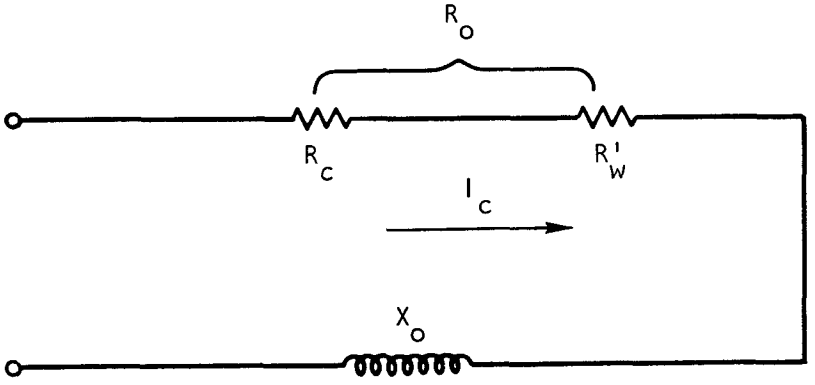

Fig. 4-38. Reduced equivalent circuit

Coil power and KVA:

$$P_o = \frac{P_w}{\eta} \tag{4-17}$$

$$KVA_c = \frac{P_o}{\cos \phi_c} \tag{4-18}$$

Coil volts per turn and ampere turns:

$$\frac{\text{volts}}{\text{turn}} = \frac{E_c}{N} \left[(KVA_c)\left(\frac{Z_o}{N^2}\right)(10^3) \right]^{1/2} \tag{4-19}$$

$$\text{amp-turns} = I_c N = \left(\frac{KVA_c \times 10^3}{Z_o/N^2} \right)^{1/2} \tag{4-20}$$

Coil power loss:

$$P_c = P_o - P_w = (1 - \eta)P_o \tag{4-21}$$

Coil cooling water requirement (gallons per minute):

$$GPM_c = \frac{P_c}{(0.147)(\Delta\theta_c)} \tag{4-22}$$

where P_c = coil loss, kilowatts

$\Delta\theta_c$ = specified cooling water temperature rise, °F (in general, $\Delta\theta_c$ is 40°F maximum, with the upper temperature of the coil outlet water fixed at 130°F)

4.3.2.2. Capacitor Corrections

In the circuit shown in Figs. 4-37 and 4-38, the current lags in phase with the voltage due to the reactive inductance. In order to minimize the reactive power loss, the circuit must be balanced as shown in Fig. 4-39. The following symbols are used in Fig. 4-39:

E_t = terminal voltage to the coil
I_t = current from motor-generator set to capacitor
I_L = current from capacitor to load
I_{cap} = current through the capacitor

Figure 4-40 further shows the vector diagrams for the change of phase angle, ϕ, with an addition of capacitors.

When the coil is properly balanced with capacitors, the power factor becomes unity and Eqs. 4-19 and 4-20 become

$$\frac{\text{volts}}{\text{turn}} = \frac{E_c}{N} = \left[(KVA_c \times 10^3) \frac{\left(\frac{Z_o}{N^2}\right)^2}{\left(\frac{R_o}{N^2}\right)} \right]^{1/2} \tag{4-23}$$

$$\text{amp-turn} = I_c N = \left[KVA_c \times 10^3 / (R_o/N^2) \right]^{1/2} \tag{4-24}$$

For a given coil and workpiece configuration, R_o/N_2 and Z_o/N_2 can be obtained from Eqs. 4-13 and 4-14. Since the KVA_c of the motor-generator set is known, the volts per turn is obtained using Eq. 4-23. The required number of coil turns is obtained simply by dividing the coil terminal voltage by the volts per turn.

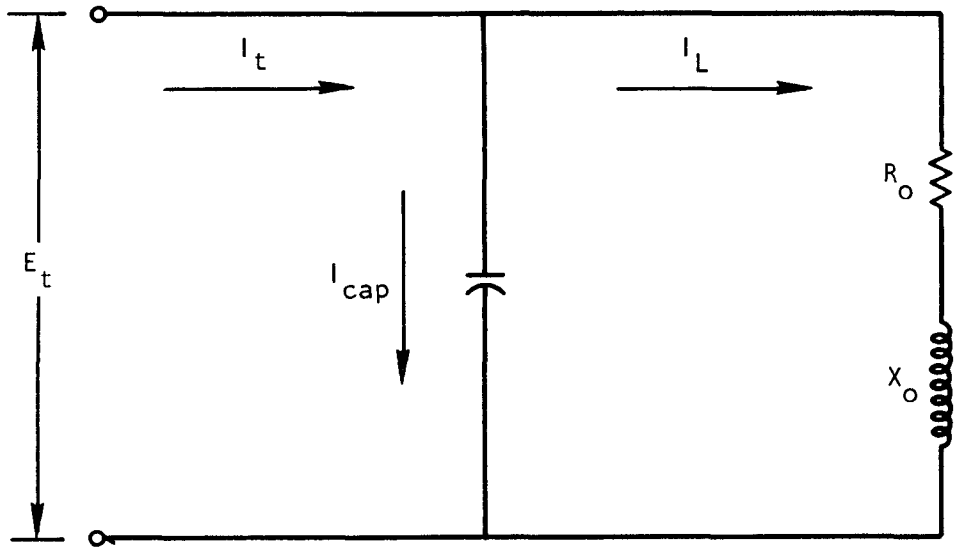

Fig. 4-39. Simplified equivalent circuit

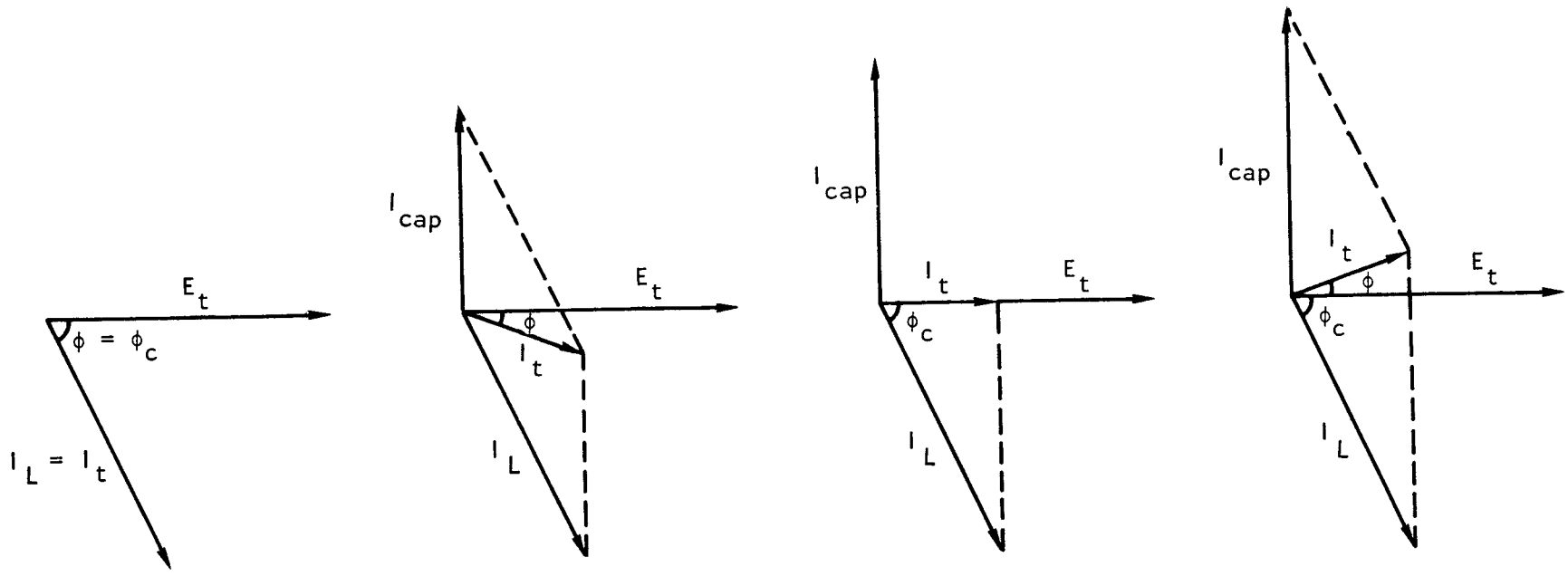

Fig. 4-40. Capacitor corrections

The amount of capacitors required to balance the circuit can be estimated as follows:

$$I_{cap}N = \frac{E_c/N}{X_o/N^2} \tag{4-25}$$

$$KVAR_c = \frac{(I_{cap}N)(E_c/N)}{1000} \tag{4-26}$$

where $KVAR_c$ = amount of capacitors, KVA.

In actual cases the amount of capacitors needed to balance the circuit exceeds the amount given by Eq. 4-26 due to an added inductive reactance of the transmission lines.

Generally, a perfect balance is difficult to maintain due to the change of electrical resistivity and magnetic permeability of the workpiece with a temperature change. When the load resistivity (thus the power) changes, the terminal voltage of the motor-generator set changes as shown in Fig. 4-41. The curves show that the least terminal voltage drop is obtained with a slightly leading power factor. A value of 0.9 (lead) is usually recommended in practice. Excessive capacitance should be avoided, as the terminal voltage rises with a large leading power factor.

4.3.2.3. Determination of P and Q Factors (Hollow Cylinders)

The P and Q factors in Eqs. 4-5 and 4-6, respectively, take account of the effect of the change of magnetic flux densities in the workpiece. The detailed derivation and the solution of the magnetic flux equation are not presented here due to their longevity and mathematical complexities. Details are given in Ref. 4-30; the final results are given in the following equations.

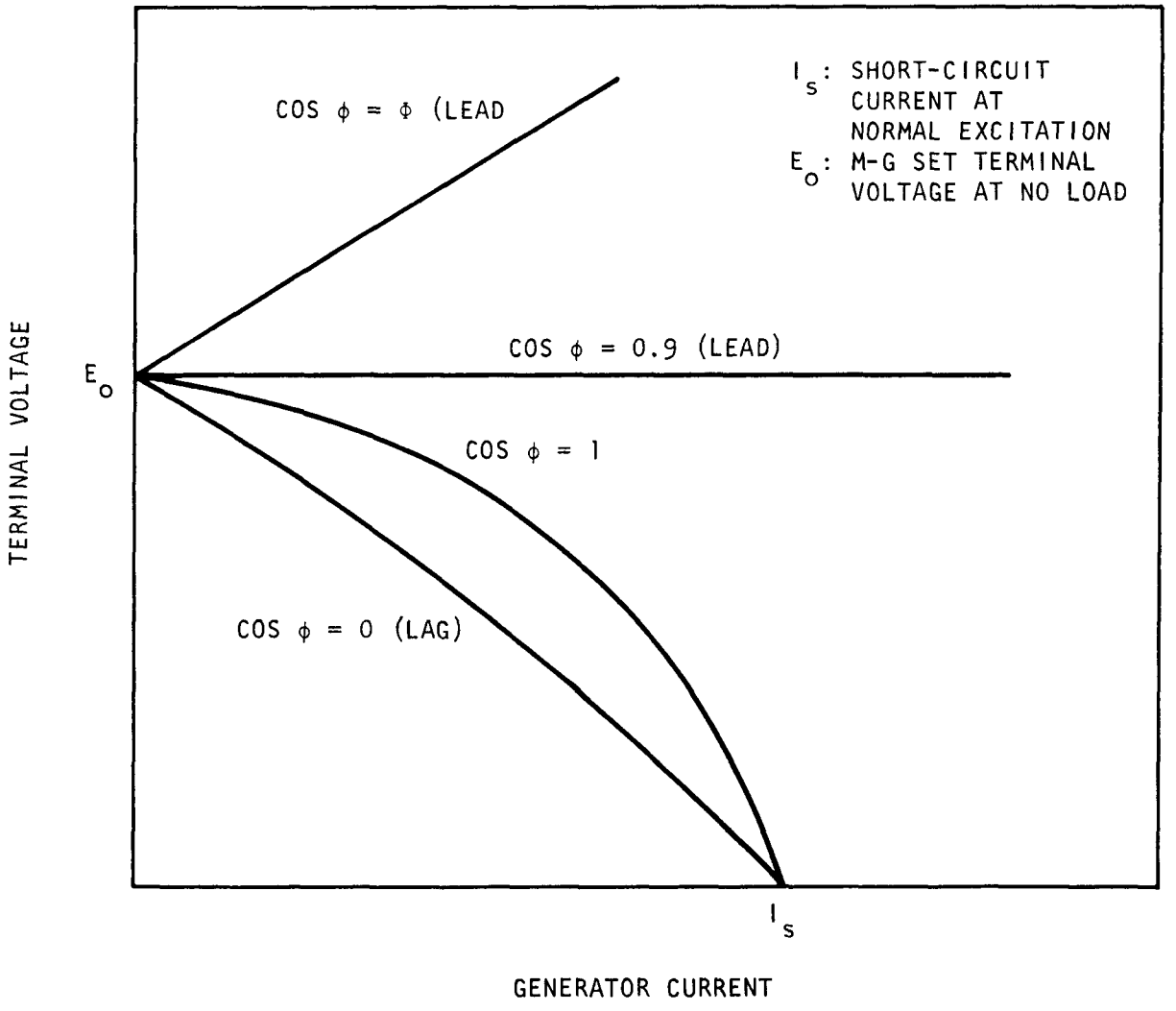

Fig. 4-41. Generator voltage-current characteristics

Thin-walled cylinder, i.e., $t < \delta_w/3$

$$P = \frac{1}{1 + \gamma^2} \tag{4-27}$$

$$Q = \frac{\gamma^2}{1 + \gamma^2} \tag{4-28}$$

where $\gamma = \dfrac{2\pi^2 d_w f t}{\rho_w}$

ρ_w = workpiece electrical resistivity in abohm-cm

Relatively thick-walled cylinder, i.e., $t > \dfrac{\delta_w}{3}$

$$P = \frac{2}{ka}\left(\frac{cd + ef}{d^2 + f^2}\right) \tag{4-29}$$

$$Q = \frac{2}{ka}\left(\frac{cf - de}{d^2 + f^2}\right) \tag{4-30}$$

where a = outer radius of cylinder

b = inner radius of cylinder

$$\left.\begin{aligned} c &= \text{bei' ka} - \alpha\ \text{kei' ka} - \beta\ \text{ker' ka} \\ d &= \text{ber ka} - \alpha\ \text{ker ka} + \beta\ \text{kei ka} \\ e &= \alpha\ \text{ker' ka} - \beta\ \text{kei' ka} - \text{ker' ka} \\ f &= \text{bei ka} - \alpha\ \text{kei ka} - \beta\ \text{ker ka} \end{aligned}\right\} \tag{4-31}$$

and $$\alpha = \frac{gh + ij}{g^2 + j^2} \tag{4-32}$$

$$\beta = \frac{gi - hj}{g^2 + j^2} \tag{4-33}$$

$$
\left.
\begin{aligned}
g &= \text{ker } kb - \frac{2\mu}{kb} \text{ kei' } kb \\
h &= \text{ber } kb - \frac{2\mu}{kb} \text{ bei' } kb \\
i &= \text{bei } kb + \frac{2\mu}{kb} \text{ ber' } kb \\
j &= \text{kei } kb + \frac{2\mu}{kb} \text{ ker' } kb
\end{aligned}
\right\} \qquad (4\text{-}34)
$$

The ber, bei, ker, and kei are the Thomson functions of the first and second kinds, and the prime represents their first derivatives (Ref. 4-36). Typical curves for the P and Q factors are given in Figs. 4-42 and 4-43.

4.3.2.4. Coil End Effect

The magnetic flux density at the ends of the coil drops to one half of its maximum value at the center due to the fringing effect, as shown in Fig. 4-44. Since this effect affects the temperature distribution of the workpiece (Fig. 4-45) as well as the susceptance on the end support plates, a quantitative prediction of the change of the magnetic flux density at the coil ends is necessary.

In general, the fringing effect depends on the coupling distance between the workpiece and the coil.

Assuming that (1) the ratio of the radial air gap to the radius of the load is small enough that curvature effects can be neglected, (2) the reference depth δ is small in relation to h and the radii (see Fig. 4-46), and (3) the coil ampere-turn per inch is constant, the field intensity H/NI/L is given by the following equation:

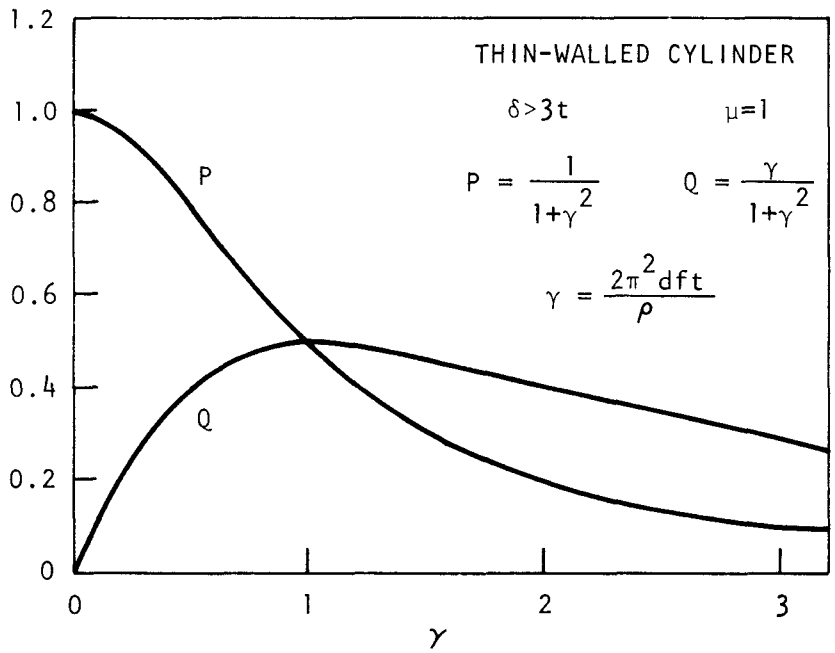

Fig. 4-42. P and Q functions, thin-walled cylinder

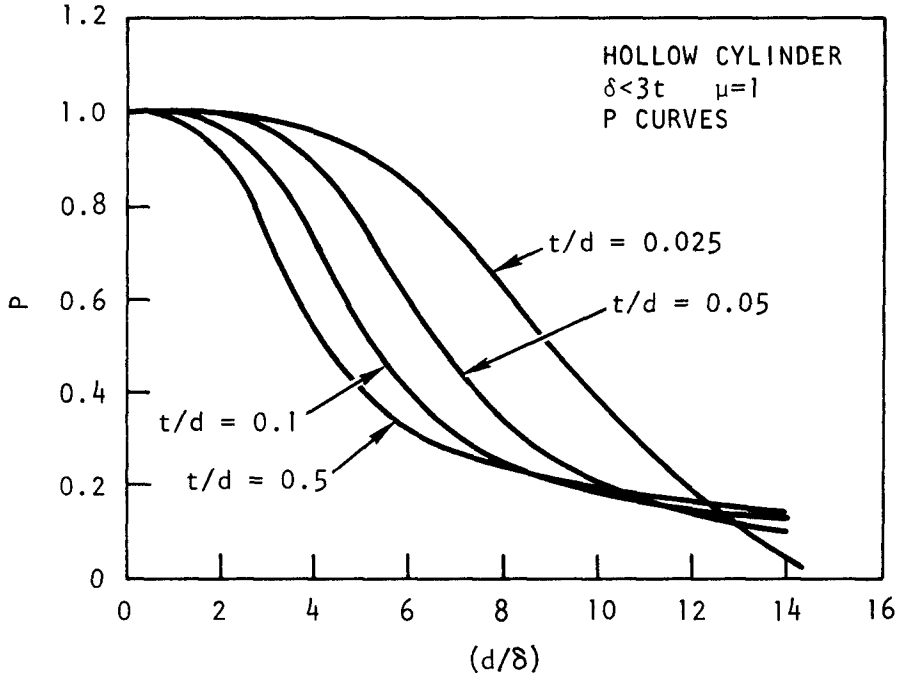

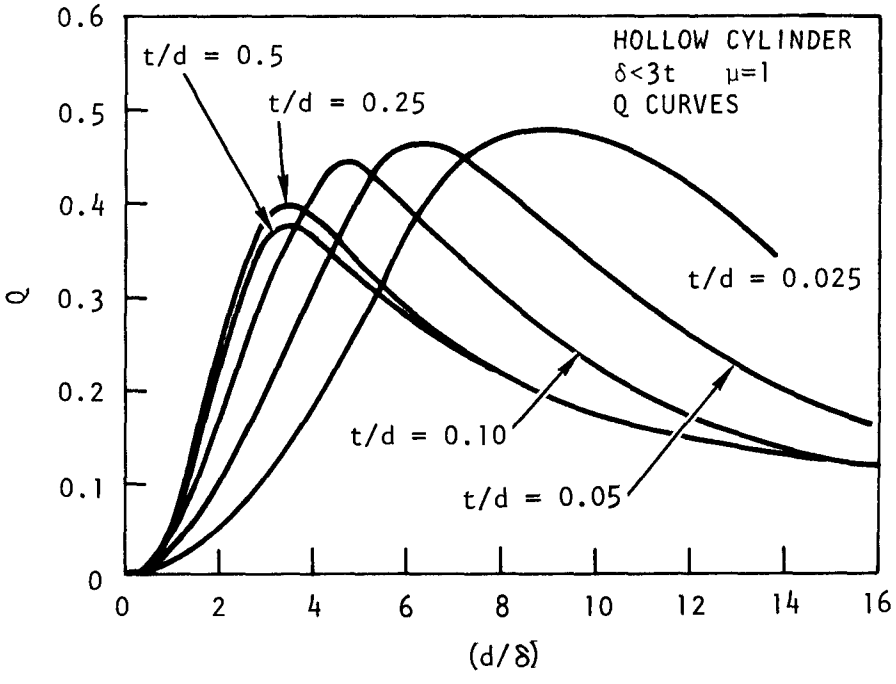

Fig. 4-43. P and Q functions, hollow cylinder

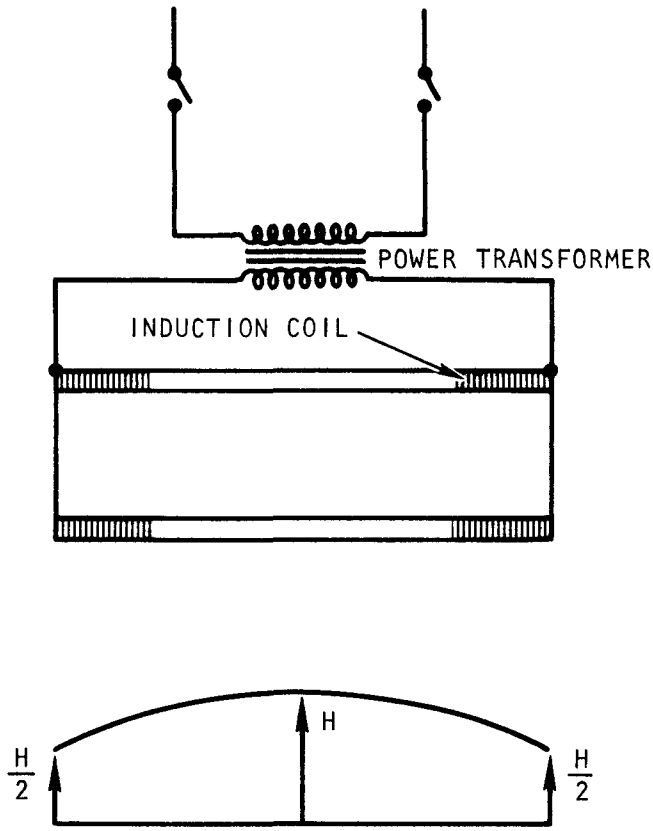

Fig. 4-44. Single-phase coil (top) and corresponding field intensity (bottom)

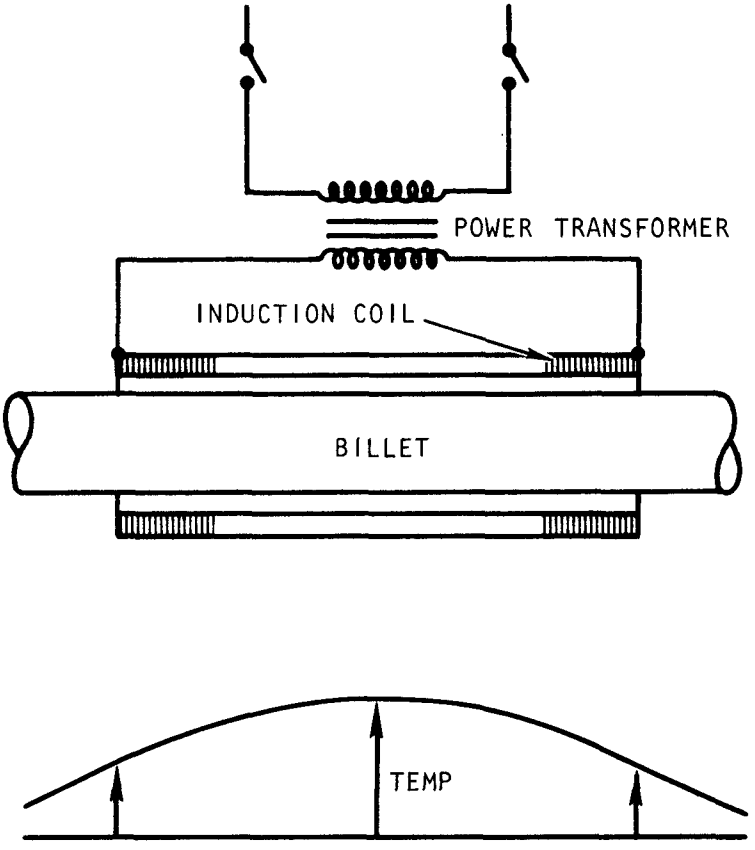

Fig. 4-45. Single-phase coil with long billet (top) and corresponding temperature pattern (bottom)

$$\frac{H}{NI/L} = \frac{1}{2} + \frac{1}{\pi} \tan^{-1}\left(\frac{x}{h}\right) \qquad (4\text{-}35)$$

where NI/L = ampere-turn/unit length.

Equation 4-35 is plotted in Fig. 4-47. The curve shows that the field intensity reaches 90% of its maximum value (at the center) at a distance of three times the coupling distance between the coil and the workpiece, i.e., 3h. Conversely, the field intensity drops rapidly outside the coil and reaches a 10% value at a distance of -3h.

For the prototype burners the induction coil packages are supported by end plates. Figure 4-48 allows an estimation of the magnetic field susception on the end plates from the distance of the end of the coil to the end support plate.

4.3.2.5. Transmission Line Power Loss

When a high-frequency current flows through two parallel conductors, there is a line loss due to the high reactance in addition to the resistive loss. For an induction heating system, as shown in Fig. 4-48, line loss occurs between the motor-generator set and the capacitors and between the capacitors and the coil. An equivalent electrical circuit of the system is shown in Fig. 4-49. In general, the loss between the motor-generator set and the capacitor is not very significant as long as a low impedance coaxial cable is used. The loss between the capacitor and the coil, however, becomes very significant due to its high current. The amount of this line loss greatly depends on the spacing between the conductors and on the frequency of the current. For a frequency less than 100,000 cps, the capacitive reactance between the two conductors can be ignored and the line loss decreases with a decreasing conductor spacing. The dependence of the loss on the frequency is almost linear, and the loss can be minimized by using a low frequency when the line length is large or the current is too high.

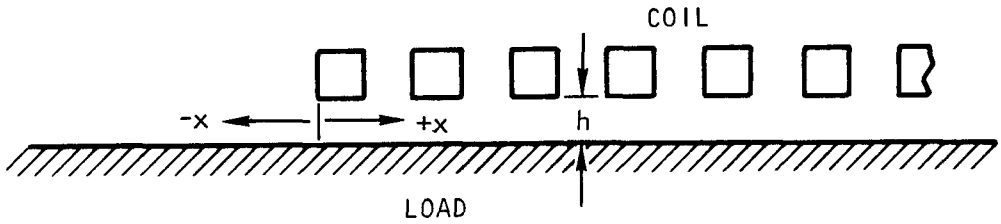

Fig. 4-46. Diagram for calculating field intensity near end of long cylindrical coil

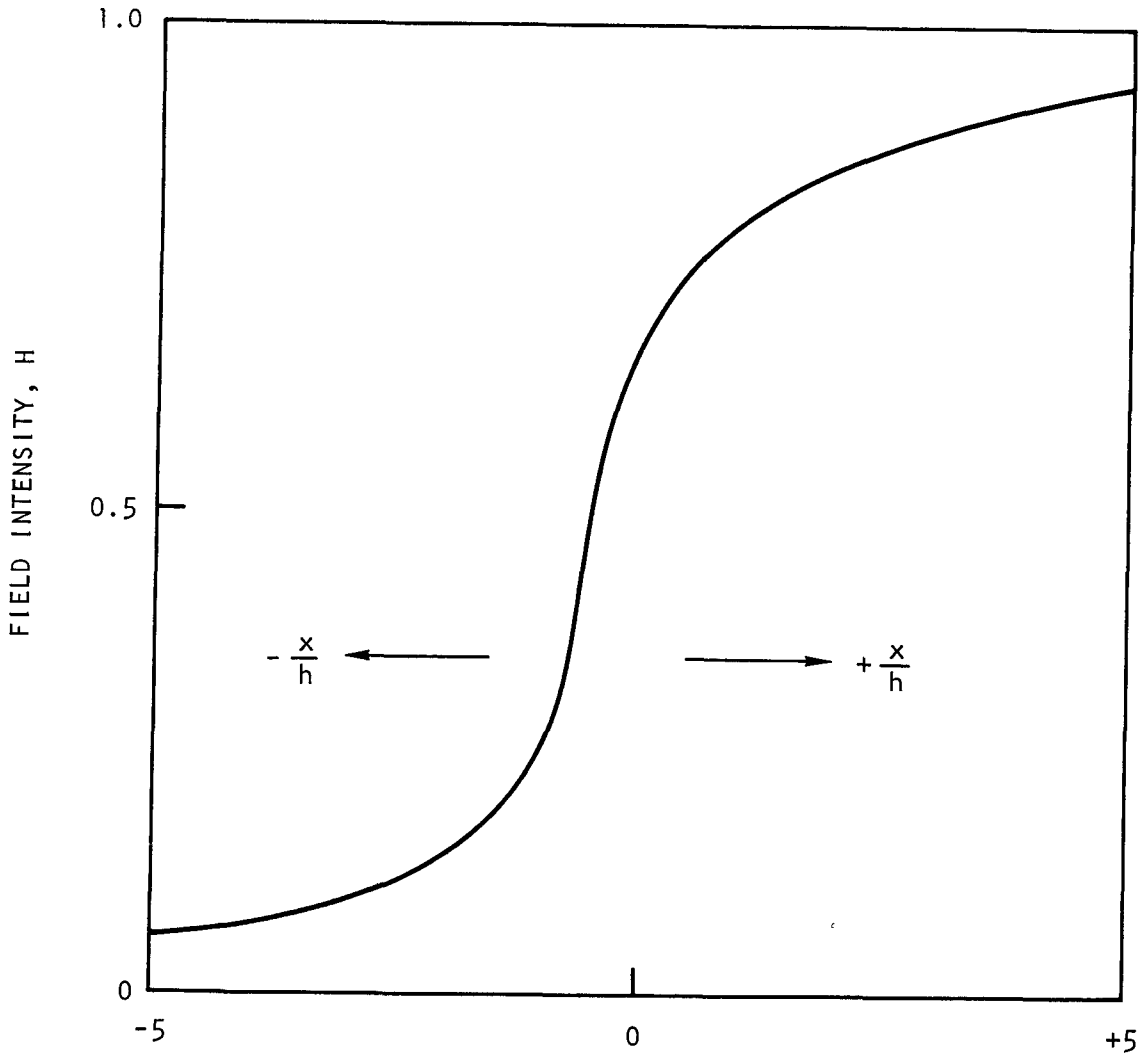

Fig. 4-47. Magnetic field intensity near end of coil

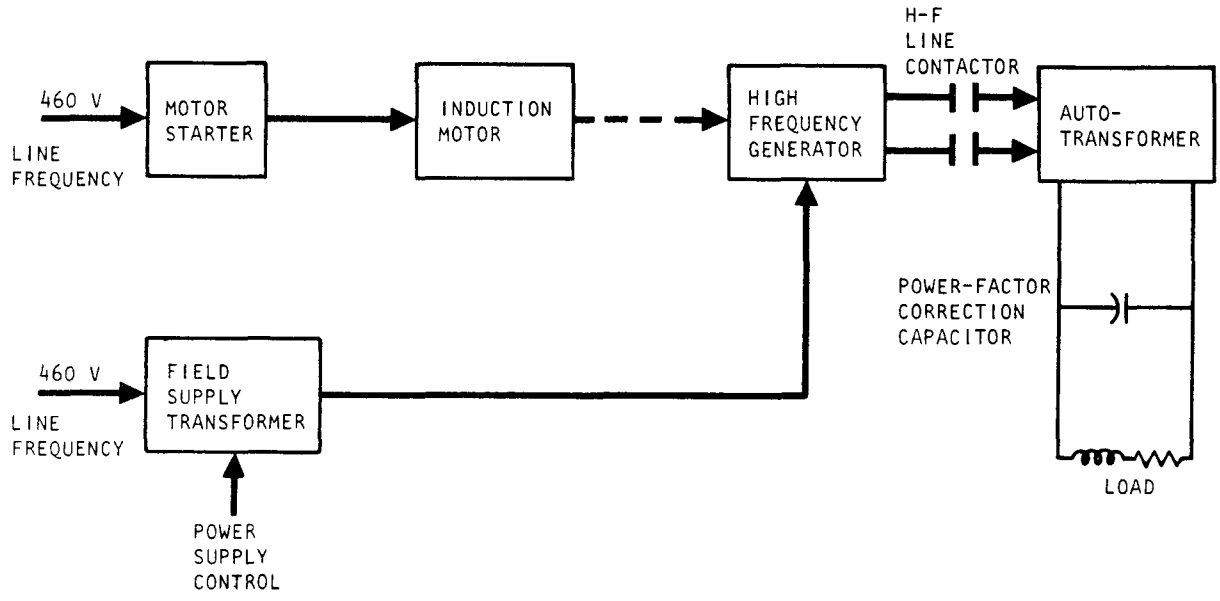

Fig. 4-48. Typical induction heating system

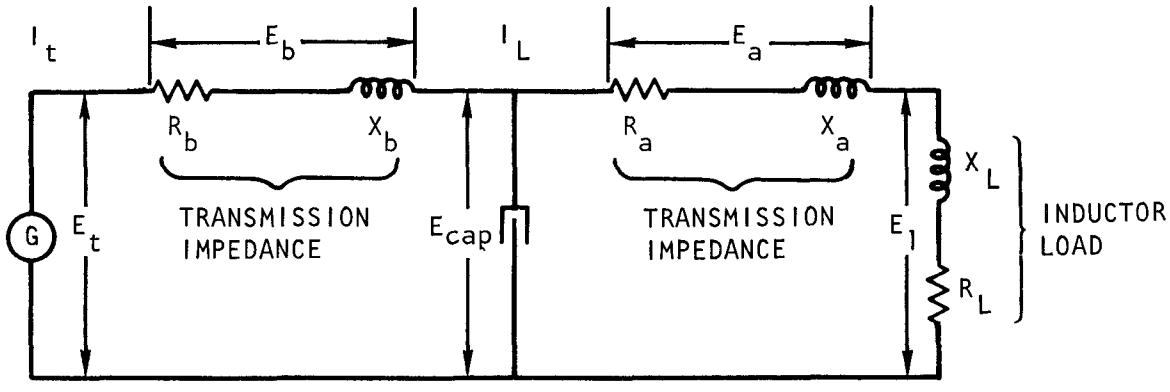

Fig. 4-49. Equivalent circuit of induction heating system

Figure 4-50 shows the line losses in vector diagram form to aid in understanding the overall phase relation and the line voltage drops. Generally the conductor between the capacitor and the coil is designed such that the line voltage drop does not exceed 10% of the terminal voltage.

REFERENCES

4-1. Young, D. T., to R. D. Zinnerman, General Atomic Company, "20-cm Primary Burner Runs 1-11 and Their Correlation With Other Primary Burner Work," private communication, January 31, 1975.

4-1a. Palmer, W. B., "Interium Results of Fines Recycle Testing Using Primary Graphite Burner," ICP-1069.

4-2. "Thorium Utilization Program Quarterly Progress Report for the Period Ending August 31, 1974," USAEC Report GA-A13178, General Atomic Company, October 31, 1974.

4-3. "HTGR Base Program Quarterly Report for the Period Ending May 31, 1973," USAEC Report Gulf-GA-A12599, Gulf General Atomic, June 30, 1973.

4-4. Wender, L., and G. Cooper, A.I.Ch.E. J. 4, 15 (1958).

4-5. "Thorium Utilization Program Quarterly Progress Report for the Period Ending November 30, 1974," USAEC Report GA-A13255, General Atomic Company, February 15, 1975.

4-6. "Bed-to-Wall Heat Transfer Coefficient for Fort St. Vrain Pilot Plant Primary Burner," ICPP Memo DLA-5-74.

4-7. Jakob, M., Heat Transfer, Vol I, John Wiley and Sons, New York (1949), p. 552.

4-8. Kerns, D., Process Heat Transfer, McGraw-Hill Book Company, New York, 1970, p. 525, Fig. 16.10.

4-9. Norris, R. H., and W. A. Spofford, Trans. ASME 64, 489, (1942).

4-10. McAdams, W. H., Heat Transmission, 3rd ed. McGraw-Hill Book Company, New York (1954), p. 269.

4-11. Kays, W., and A. L. London, Compact Heat Exchangers, 2nd ed., McGraw-Hill Book Company (1964), p. 33.

4-12. Botterill, J.S.M., A.I.Ch.E. Symp. Ser. 128 69, 26 (1973).

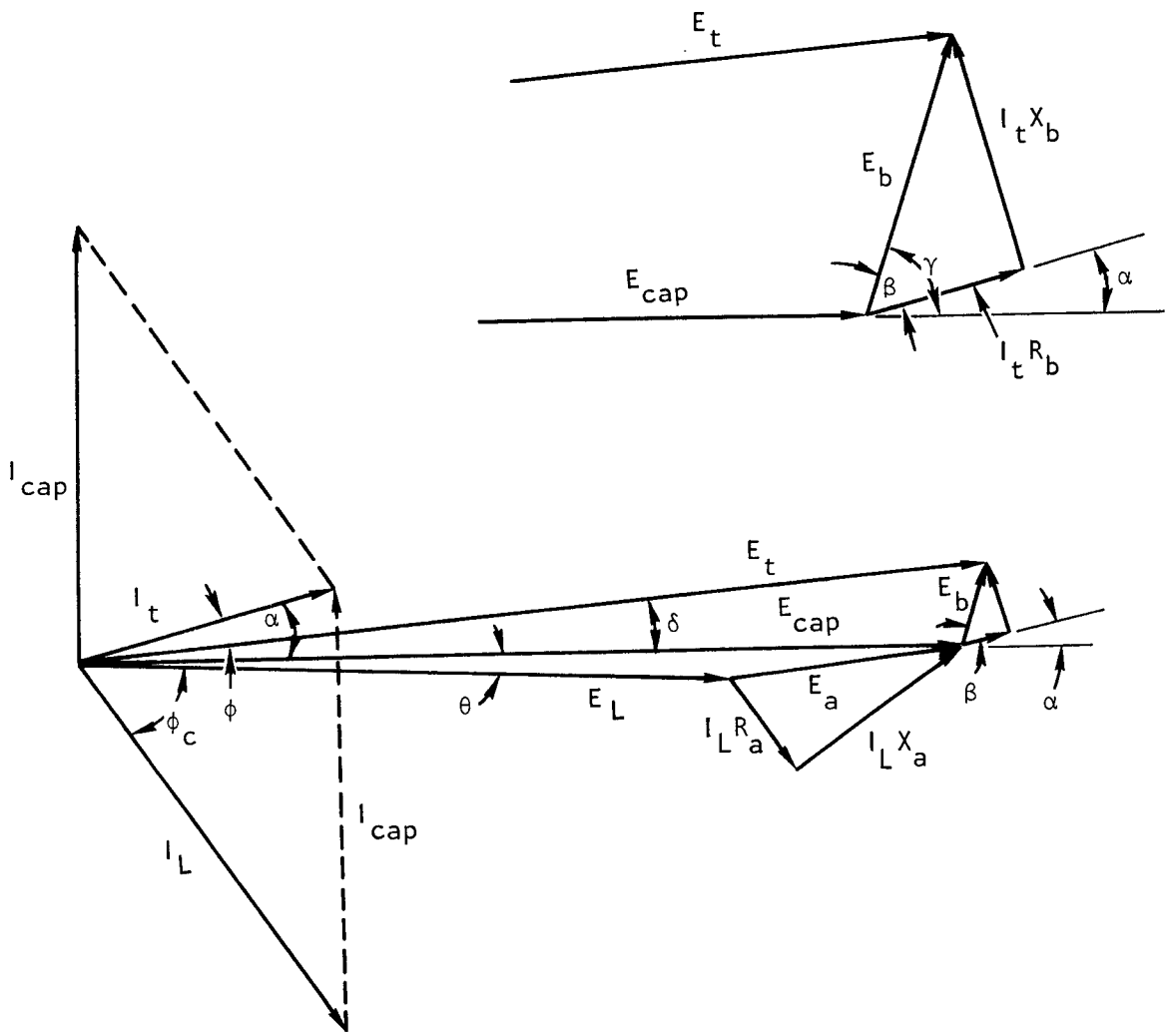

Fig. 4-50. Phase relations of current and voltage (with a leading power factor)

4-13. "HTGR Base Program Quarterly Progress Report for the Period Ending August 31, 1970," USAEC Report GA-10288, Gulf General Atomic, September 30, 1970.

4-14. "HTGR Base Program Quarterly Progress Report for the Period Ending February 29, 1972," USAEC Report Gulf-GA-A10999, Gulf General Atomic, March 31, 1972.

4-15. Rice, R. L., and N. H. Coates, "Combustion of Coals in Fluidized Beds of Limestone," paper presented at the Third International Conference on Fluidized Bed Combustion, October 29-November 1, 1972, Hueston Woods, Ohio, Paper No. EPH-65012-73-053.

4-16. Park, U., "ACC Data Request (ACC-GAC-5)," General Atomic unpublished data, 1975.

4-17. "National HTGR Fuel Recycle Development Program Plan," USAEC Report ORNL-4702, Oak Ridge National Laboratory, August 1971.

4-18. Rickman, W. S., "Evaluation of a Gravity-Pneumatic System for Secondary Burners," General Atomic unpublished data, 1975.

4-19. Park, U., "Performance of In-Vessel Filters in Secondary Burner," General Atomic unpublished data, 1974.

4-20. Rickman, W. S., "10-cm Secondary Burner High-Temperature Bed Removal System," General Atomic unpublished data, 1973.

4-21. Clark, T. J., et al., Nuclear Graphite, R. E. Nightingale, Ed., Academic Press, New York (1962), Chapter 14.

4-22. Wetzler, K. T., H. Wirth, and H. Witte, KFA Report, 1970.

4-23. Snider, J. W., and D. C. Watkin, "An Evaluation of HTGR Primary Burning," USAEC Report ORNL-TM-4520, Oak Ridge National Laboratory, November 8, 1974.

4-24. HOBEG Monthly Report, October 1974.

4-25. "HTGR Base Program Quarterly Progress Report for the Period Ending February 29, 1968," USAEC Report GA-8530, Gulf General Atomic, March 29, 1968.

4-26. "HTGR Base Program Quarterly Progress Report for the Period Ending May 31, 1968," USAEC Report GA-8662, General Atomic Company, June 28, 1968.

4-27. Leary, D., to U. Park, General Atomic Company private communication, 1975.

4-28. Nicholson, E. L., L. M. Ferris, and J. T. Roberts, "Burn-Leach Process for Graphite-Base Reactor Fuels Containing Carbon-Coated Carbide or Oxide Particles," USAEC Report ORNL-TM-1096, Oak Ridge National Laboratory, April 2, 1965.

4-29. Park, U., "Evaluation of Different Heating Methods," General Atomic unpublished data, 1975.

4-30. Park, U., "Induction Heating Coil Design," General Atomic unpublished data, 1975.

4-31. Young, D. T., to U. Park, General Atomic Company, private communication, 1975.

4-32. Johanson, N. W., "Estimate of Hot-Gas Startup Time for 16-in. Primary Burner," General Atomic unpublished data, 1975.

4-33. Rickman, W. S., "Alternate Burner Heating Method," General Atomic unpublished data, 1974.

4-34. Rickman, W. S., "Secondary Burner Heating and Cooling Methods," General Atomic unpublished data, 1973.

4-35. Simpson, P. G., Induction Heating, McGraw-Hill Book Company, New York (1960).

4-36. Nosova, L. N., "Tables of Thomson Functions and Their First Derivatives," translated from the Russian by Prasenjit Basu, Pergamon Press, New York (1961).

5. AQUEOUS SEPARATION

5.1. LEACHING

5.1.1. Summary

Leaching Runs 82, 83, and 85 through 93 were conducted during the quarter to investigate the dissolution of crushed burned-back TRISO fertile particles with a larger size distribution than utilized previously (page 65 of Ref. 5-1). The larger size distribution arises from a modified double-roll particle crusher, which essentially cracks the SiC hull and allows the kernel to fall out rather than pulverizing the entire particle. As expected, the larger ThO_2 size distribution resulted in longer dissolution times (Fig. 5-1).

Several operational difficulties were encountered during the course of the leacher runs. These difficulties have either been corrected by equipment modifications or are believed to be characteristic of the pilot plant unit design and operation and not characteristic of a production plant unit.

5.1.2. Discussion

The eleven test runs were conducted with the 13-cm-diameter leacher. All of the tests were made on a batch basis using a composite mixture of secondary burner product. The burner ash utilized in these leaching runs results from the fluidized bed combustion of crushed TRISO ThC_2 particles, which were crushed in a double-roll crusher. The roll gap was set to break only the SiC coats and thus release the ThC_2 kernel uncrushed. Further details are available in the secondary burner run summary on page 110 of Ref. 5-2.

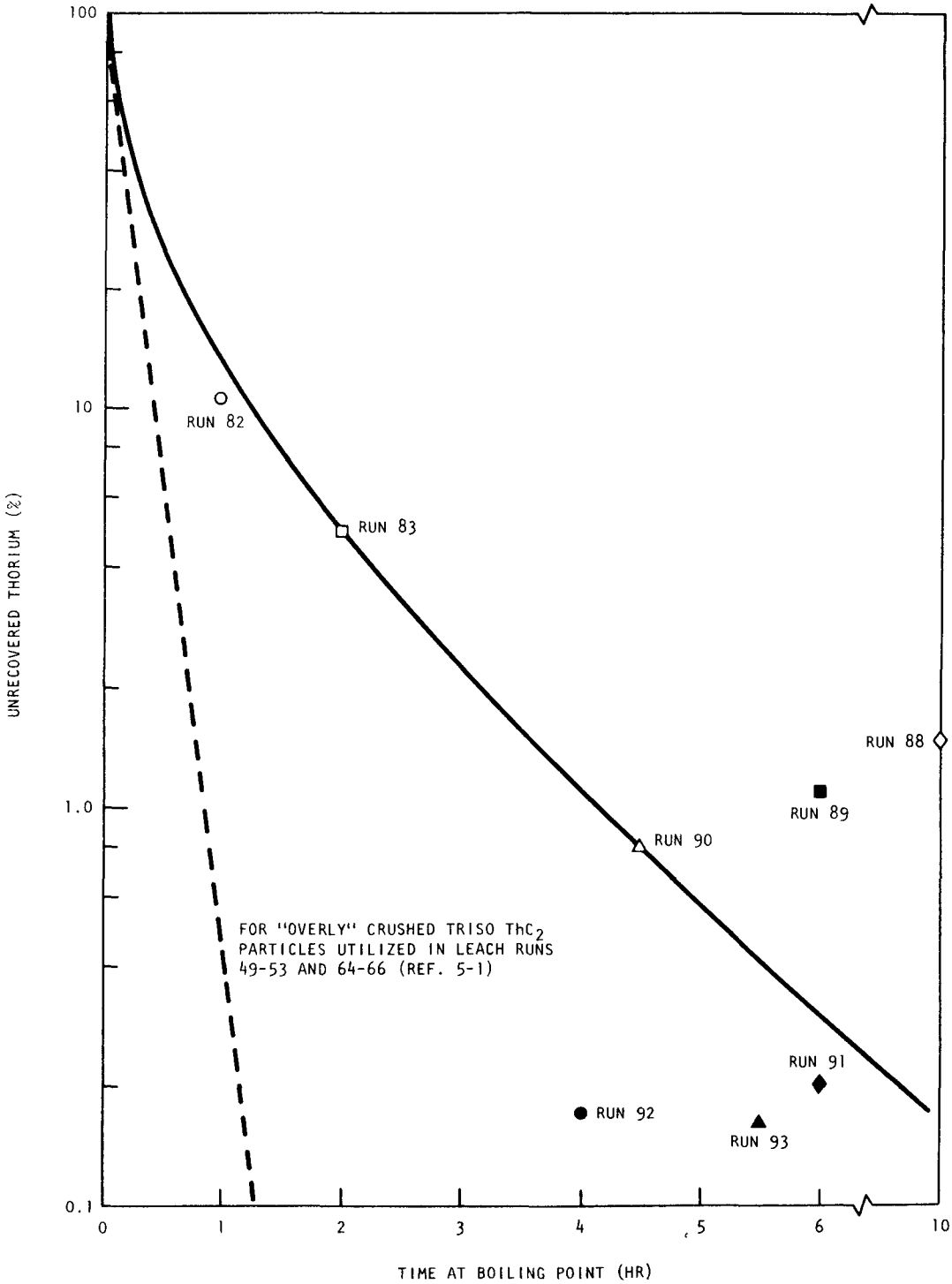

Fig. 5-1. Dissolution of larger size secondary burner ash in 13-cm-diameter leacher

The properties of the burner ash from eight separate burner runs are given in Table 5-1. This material was composited into a single batch of burner ash to eliminate variations resulting from changes in composition of solids fed to the leacher. The burner ash was composited by three separate passes of the total amount of ash through a 10-way cone-type sample splitter. The properties of the burner ash composite are also included in Table 5-1. The size distribution of the resulting composite is shown in Fig. 5-2. The size distribution for burner ash utilized in past leaching studies (Ref. 5-1, pp. 65 and 112) is also included in Fig. 5-2 for comparison.

All tests were conducted with about 3 liters of Thorex [13$\underline{M}$ HNO_3/0.05$\underline{M}$ HF/0.1$\underline{M}$ $Al(NO_3)_3$] per kilogram of the secondary burner ash. Operating data are shown in Table 5-2. All of the runs were conducted with 4 kg of burner ash, 12 liters of Thorex, and an air sparge rate of 2.83 liters/min [6 standard cubic feet per hour (SCFH)]. The leaching time (time of boiling point) was varied for each run.

The liquid-solid separation of the leacher product was accomplished with a batch centrifuge. Centrifuge data for all runs are as follows:

1. 30-cm-diameter perforate basket.

2. Polypropylene filter bag (5- to 6-μm openings).

3. Purging force of 42 g at basket sheet (500 rpm) during slurry loading.

4. Purging force of 1100 g at basket sheet (2500 rpm) during water washing.

5. Filter cake spin dryed for about 5 min after washing.

The quantity and specific gravity of liquids in all storage tanks and the leacher were continuously and automatically monitored and recorded.

TABLE 5-1
SECONDARY BURNER PRODUCT CHARACTERISTICS

Secondary Burner Run No. F4RHBM-	Burner Product Used (g)	Product d_{SV}[a] (μm)	ThO_2 (%)	C (%)	SiC and Unbroken Particles (%)	Product Bulk Density (g/cm^3)	Product Tap Density (g/cm^3)	Product Angle of Repose (degrees)
				Product				
24 & 26	8829	56	84.0	0.7	15.3	2.92	3.22	40
29	9601	59	74.2	0.8	25.0	--	--	--
30	11,561	56	76.7	0.5	22.8	2.46	3.01	--
31	12,449	51	75.7	0.3	24.0	--	--	--
32	11,793	48	68.7	0.4	30.9	2.4	2.8	--
33	12,788	49	65.6	0.3	34.1	--	--	--
35	16,227	45	76.1	0.7	23.2	--	--	--
				82-kg Composite of Secondary Burner Product				
Total Amount (g)								
83,248		66	73.68[b]	0.6[c]	25.72	2.39	3.05	40.7

[a] Average particle size, defined in Ref. 5-3.

[b] Average based on analysis of four samples: 65.36, 64.95, 64.24, and 64.45% Th.

[c] Average based on pan burn of three samples: 0.97, 0.23, and 0.59% combustibles.

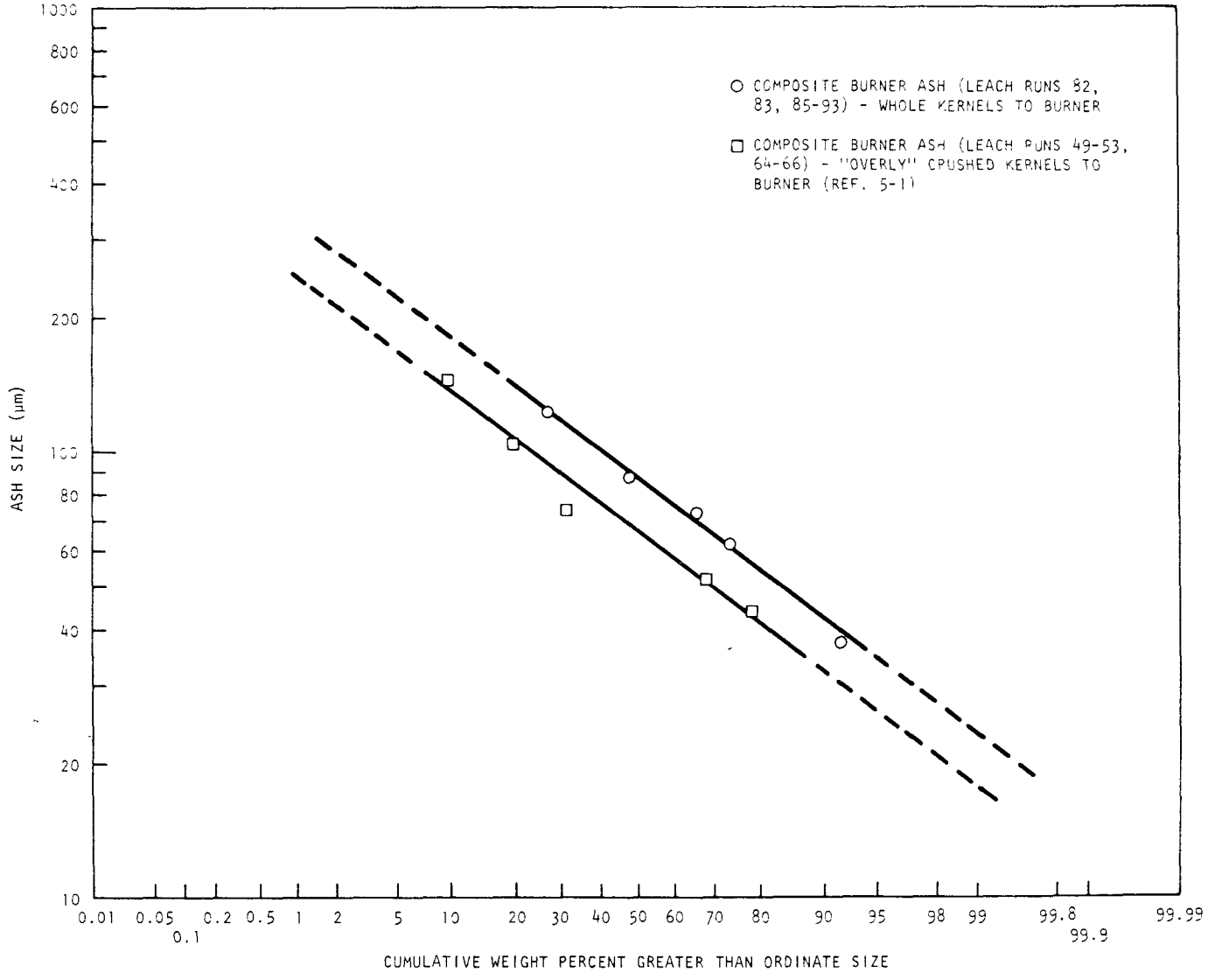

Fig. 5-2. Burner ash size distribution

TABLE 5-2
LEACHER OPERATING DATA, 13-CM-DIAMETER LEACHER

	82[a]	83	85	86	87	88	89	90	91	92	93
Burner ash charged, kg	4.0	4.0	4.0	4.0	4.0	4.0	4.0	4.0	4.0	4.0	4.0
Thorex charged, liters	12.0	12.0	12.0	12.0	12.0	12.0	12.0	12.0	12.0	12.0	12.0
Air sparge rate, liters/min	2.83	2.83	2.83	2.83	2.83	2.83	2.83	2.83	2.83	2.83	2.83
Leaching time at boiling point, hr	1.0	2.0	6.0	4.5	6.0	10.0	6.0	4.5	6.0	4.0	5.5
Insolubles after leach (dry wt), g	1275	1123	1235	1216	1126	1074	1061	1018	1082	935	1036
Mother liquor,[b] liters	14.14	15.45	13.59	11.95	10.61	15.49	12.56	13.07	14.93	15.42	19.33

[a] Leach run number; leach run 84 included in previous run summary (see Ref. 5-1).

[b] Includes some wash water.

Tank calibration relationships were not utilized for material balance purposes. All volumetric determinations for liquids were accomplished with graduated cylinders. Analyses of samples submitted to the Analytical Chemistry Department are given in Table 5-3. These data were utilized in material balance calculations (see Table 5-4).

Details of the results of these runs and associated problems are presented below:

1. As expected, the larger ThO_2 size distribution resulted in longer dissolution times.

2. It is not clear to what extent the increased dissolution time may be the result of less than optimum mixing. All of the runs were carried out utilizing the same sparge rate, and it is therefore not possible to establish to what degree insufficient sparging might have contributed to the increase in overall dissolution time. It is pointed out, however, that for the burner ash utilized previously (dissolution time and size distribution included in Figs. 5-1 and 5-2, respectively) the dissolution rate was found to be independent of the sparge rate (Ref. 5-1).

3. The differential pressure purgerator and dip leg system plugged repeatedly during the runs. This system is utilized to measure specific gravity and the weight factor using a nitrogen purge into the leacher solution (Ref. 5-4, p. 51). In most cases the plug or restriction was believed to be a buildup of $Th(NO_3)_4$ formed at the end of the purge dip leg. The restriction was easily removed by injecting several milliliters of water into the dip legs. However, these restrictions would slowly reform. The number of times the restriction formed (and thus had to be removed) was a function of the overall dissolution time. This problem was not encountered in previous dissolution runs (Ref. 5-1) because the smaller size burner ash required only 1 to 2 hr to dissolve. However, with the longer dissolution times required

TABLE 5-3
SAMPLE ANALYSIS RESULTS

	82[a]	83	85	86	87	88	89	90	91	92	93
Burner ash,[b] wt % Th	64.75	64.75	64.75	64.75	64.75	64.75	64.75	64.75	64.75	64.75	64.75
Insolubles,[c] wt % Th	21.35	10.97	19.99	14.4	13.75	3.55	2.56	1.88	0.46	0.49	0.38
Mother liquor[c] g Th/liter	163.5	156.5	164.95	177.21	169.36	159.52	198.1	182.52	167.7	170.96	129.09

[a] Leach run number.

[b] Analysis based on a gravimetric determination using an oxalate precipitation of the thorium.

[c] Analysis based on Th colorimetry for Th wt % < 2%; all others same as (b).

TABLE 5-4
THORIUM MATERIAL BALANCE

	82[a]	83	85	86	87	88	89	90	91	92	93
Thorium input, g in burner ash	2590	2590	2590	2590	2590	2590	2590	2590	2590	2590	2590
Thorium output, g in mother liquor	2311.7	2418.2	2143.0	2117.6	1797.4	2506.1	2487.5	2385.7	2504.8	2636.7	2494.7
Insolubles	272.2	123.2	246.8	175.1	154.8	38.1	27.2	19.1	5.0	4.6	3.9
Total output	2583.9	2541.4	2389.8	2292.8	1952.2	2544.2	2514.7	2404.8	2509.8	2641.3	2498.6
Material balance closure,[b] wt %	99.76	98.12	92.28	88.52	75.38	98.23	97.09	92.85	96.90	101.9	96.50
Thorium recovery,[c] wt %	89.47	95.15	90.54[d]	93.24[d]	94.02[d]	98.50	98.92	99.20	99.8	99.83	99.84

[a] Leach run number.

[b] Output/input.

[c] Based on output quantities.

[d] Because of poor material balance closure, thorium recoveries were calculated based on insolubles composition, i.e., 100 - (Th in insolubles/Th in feed) x 100.

for the larger size distribution burner ash, there is an opportunity for the restriction to form.

During Run 90 the problem was compounded. The standard procedure for washing out the dip legs was to disconnect the nitrogen purge line at the top of the leacher to allow water injections.

However, in this run some of the burner ash was pushed from the solution head up into the dip legs and could not be removed by water washing. The solids could not be removed during the run, even though an attempt was made to force a rod down the dip legs. Thus, the specific gravity and weight factor readings were not available during the remainder of the run. It was found later that the dip legs could only be cleared by removing the dip legs from the leacher and drilling out the dry compacted burner ash. It is not evident why the solids completely plugged the dip legs only during Run 90 as the same technique was used in the other runs to wash out the dip legs. These dip tubes were 1/4-in. tubing. They have subsequently been replaced with 3/8-in. tubing and pluggage problems have since been minimal.

4. For Runs 82 and 83, the centrifuge speed was initially set at 2500 rpm. In both cases the centrifuge off-loaded (high vibrations occurred), and the feeding of slurry to the centrifuge had to be stopped. It was possible to resume and complete the leacher dump in Run 83, but the tygon line connecting the leacher to the centrifuge plugged in Run 82. The line plug was removed and cleared by hand. Thus, plugged lines can occur when transferring the leacher slurry if the flow stops before the transfer is complete. To reduce the problem with centrifuge off-loading, the centrifuge was loaded at only 500 rpm in all subsequent runs. No further problems with off-loading occurred. Following the leacher runs reported here, the centrifuge mounting was modified, which eliminated the vibration problems even at high speeds.

5. In Runs 82 and 83, the flow of slurry to the centrifuge was very slow and unsteady. Also, the initial slurry was very high in solids content (50 to 80 wt %). A dilution tube and two additional air sparge inlets were installed for Run 85 to help alleviate this problem. Figure 5-3 shows the configuration of the dilution tube and air sparge rings. These changes were initially thought to improve the slurry flow characteristics. However, the dilution tube allowed the sparge air to bubble up through the dilution tube rather than the burner ash. (The solids mixing obtained during this run is not felt representative of the other runs, and the thorium recovery for Run 85 is therefore not included in Fig. 5-1.) The dilution tube has since been removed.

   In a production plant, it is very likely a steam jet mounted above the leacher would be used. Preliminary slurry transfer tests with a steam jet (to be reported next quarter) have demonstrated a reduced propensity to line pluggage,

6. For Runs 86 through 93, the sparge air was introduced through three separate sparge lines, i.e., the bottom dump valve, bottom sparge ring, and top sparge ring. During the leaching time most of the sparge air was introduced through the bottom dump valve. This was an attempt to carry out runs that were directly comparable to previous runs (Ref. 5-1). Therefore, 4 SCFH (1.90 standard liters/min) were introduced through the bottom dump valve and 1 SCFH (0.47 standard liters/min) through both the bottom and top sparge rings. This flow rate for the sparge rings was the minimum controllable flow; some sparge flow was felt desirable at all times to keep the sparge rings from plugging with solids. The sparge air was increased as required during the period of feeding the slurry to the centrifuge.

7. The large discrepancy in the material balance closure for Runs 86 and 87 (Table 5-4) is not completely explainable. Because of

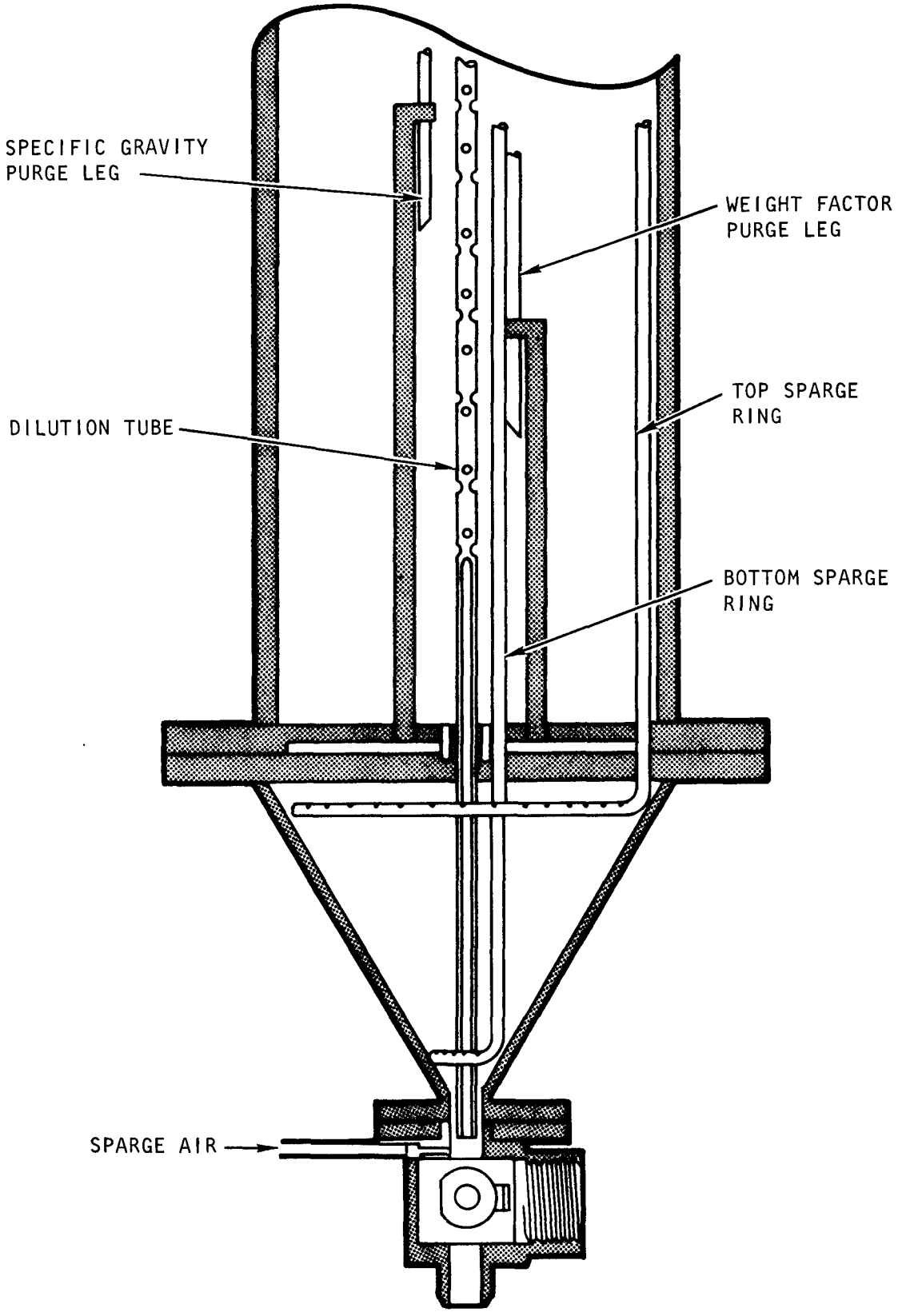

Fig. 5-3. Location of leacher dilution tube and sparge rings

these discrepancies, the data for Runs 86 and 87 are not included in Fig. 5-1. Several possible problems that may contribute to errors in the material balance are:

a. Solids sample splitting, i.e., ability to obtain representative samples of solids for analytical analysis.

b. Burner ash compositing, i.e., ability to composite burner ash from large number of burner runs into a uniform composite.

c. Materials accountability, i.e., accurate measurement of the quantity of liquids and solids.

Steps are being taken to obtain improved equipment for solids splitting and sampling.

8. There is some scatter of the data for Runs 82, 83, and 86 through 93 (Fig. 5-1). Some possible causes for this scatter are:

a. The three items listed above as possible causes for material balance errors.

b. The air sparging rate used was exactly at (or below) the minimum required for the size distribution burner ash utilized.

c. After feeding Thorex to the leacher and then burner ash to the leacher, some time lapse occurred before the sparge air was introduced. This could have caused some degree of solids compaction. Beginning with Run 90, considerable effort was exerted to minimize the time of contact between liquid and solids without air sparging.

d. Interference of corrosion coupons with liquid-solids contact (unlikely).

e. Variation in the composition of the Thorex used, i.e., composition of Thorex was not exactly 13M HNO_3/0.05M HF/0.1M $Al(NO_3)_3$. This is not believed to be a likely cause.

9. In Runs 89 through 91, there was some difficulty in removing the slurry from the leacher. The leacher dump valve was either stuck and would not open or was plugged. It is suspected that the plug was the result of a combination of SiC solids buildup and $Th(NO_3)_4$ formation at the dump valve opening. At the end of a leach run, the leacher solution is about 1M in thorium concentration, and is cooled by a cooling water jacket around the leacher. In addition, the majority of the sparge air is injected into the dump valve at the top of the valve ball. In the presence of the sparge air and as the temperature of the solution drops, it is likely that $Th(NO_3)_4$ precipitates out. The flow of slurry out of the leacher was eventually achieved by repeated opening and closing of the dump valve and increasing and reducing the sparge air flow.

   As discussed above, the use of a steam jet rather than a dump valve for slurry removal is expected to minimize this difficulty.

   No problems with dumping the leacher contents were experienced in subsequent Runs 92 and 93. In these runs the dump was initiated when the leacher contents were at about 82°C.

5.2. INSOLS DRYER

Installation of the insols dryer described in the previous Quarterly Progress Report (Ref. 5-5) was completed and shakedown testing of the components was initiated.

5.3. FEED ADJUSTMENT

The equipment for adjustment of leacher solution to solvent extraction feed requirements (Ref. 5-6) was installed. Feed adjustment requires a substantial reduction in the nitric acid concentration of the leacher solution. The installed equipment consists of an evaporator with steam sparging capability to remove the excess nitric acid by distillation. The equipment is designed to permit either batch or continuous operation. Component checkout has been started.

5.4. SOLIDS WASHING REQUIREMENTS IN SOLID BOWL CENTRIFUGES

Separated solids retain residual amounts of uranium and thorium, some of which is in the retained liquid and some of which may be in insoluble form. Washing or repulping of the separated solids is necessary to recover as much of the dissolved fertile and fissile material as is practicable.

An estimation of the washing requirements can be made, based on repulping the solids from either batch or continuous centrifuges. Figure 5-4 shows the effect of reslurrying a saturated cake of insoluble silicon carbide shells on the decontamination factor and the dilution of original leacher product. Complete mixing and complete dissolution of the fuel material are assumed.

It can be seen from these curves that to achieve the same decontamination factor (i.e., 10^5), the number of reslurry operations decreases from A to C with increasing reslurry volume, the dilution effect increases from A to C, and the slurry solids loading for subsequent transfer decreases from A to C.

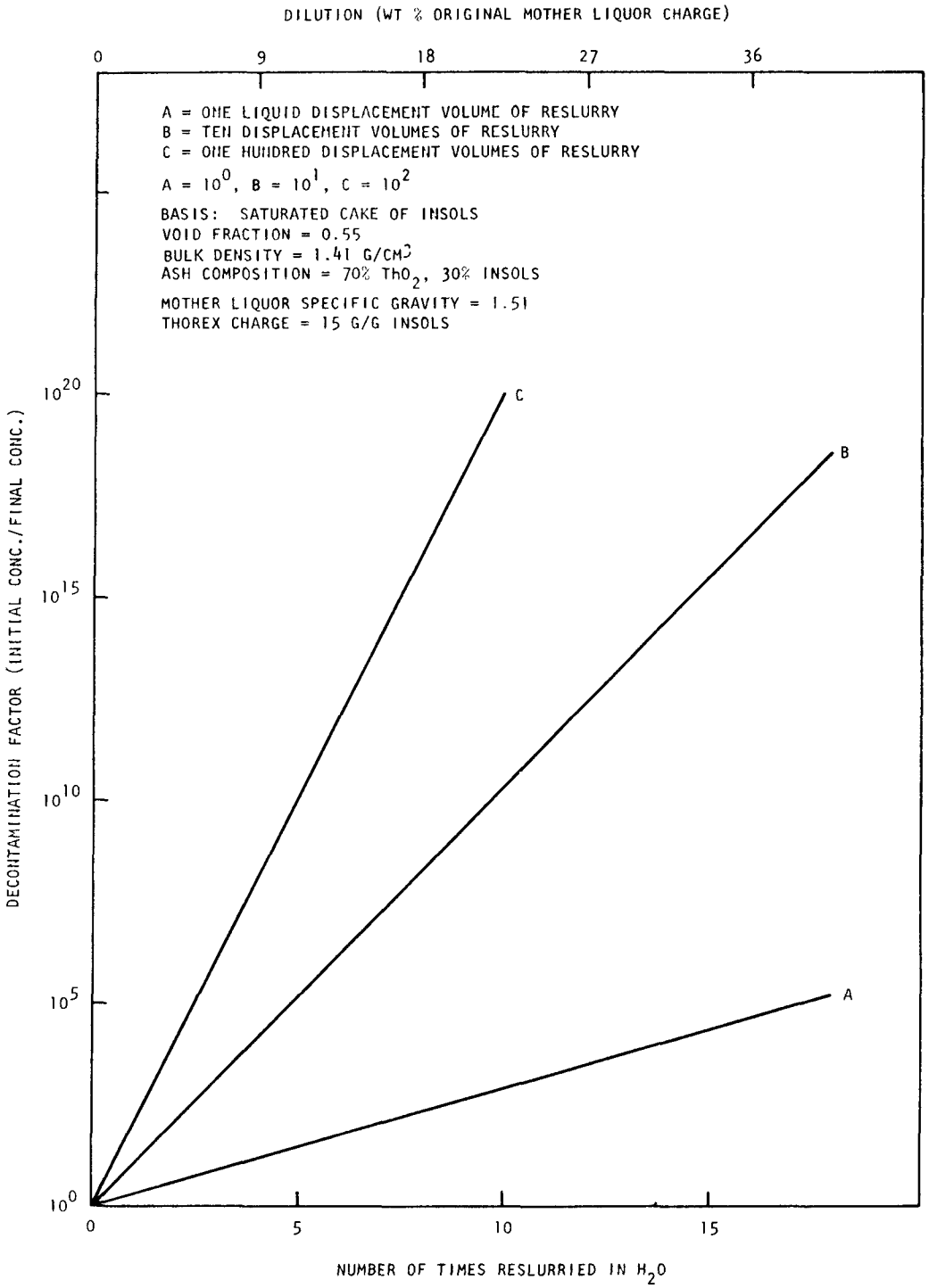

Fig. 5-4. Effect of reslurry on decontamination factor of insolubles and dilution of mother liquor

5.5. BENCH-SCALE TESTS WITH NONRADIOACTIVE MATERIALS

5.5.1. Effect of Fission Products on Thoria Dissolution Rate

A study was completed on the effect of fission product spikes on the dissolution of ThO_2 in the normal Thorex dissolvent [13M HNO_3/0.05M HF/0.1M $Al(NO_3)_3$]. Nonradioactive fission product isotopes were used. If zirconium is added as a solution to the dissolver system, the thorium oxide dissolution rate is lowered significantly. However, if the zirconium is added as a solid compound, a lesser effect is noted. These effects are attributed to the formation of zirconium fluoride complexes. The data for the various cases are shown in Fig. 5-5.

5.5.2. Effect of Fission Products on Solvent Extraction Feed Adjustment

In the feed concentration and nitric acid steam stripping step, bench-scale test with nonradioactive zirconium have confirmed that zirconium precipitates in low-acid solutions at zirconium concentrations above 2.1 g/liter (final 1M thorium nitrate solution) (Refs. 5-7, 5-8). The difficulty of separating this finely divided zirconium precipitate, and the high specific radioactivity of this solid from irradiated fuel, reinforces the conclusion in the referenced reports that feeds below 0.6M for nitric acid should not be used when the zirconium-to-thorium ratio exceeds 1:100.

REFERENCES

5-1. "HTGR Base Program Quarterly Progress Report for the Period Ending August 31, 1973," USAEC Report Gulf-GA-A12725, Gulf General Atomic Company, September 8, 1973.

5-2. "HTGR Base Program Quarterly Progress Report for the Period Ending February 28, 1974," USAEC Report GA-A12916, General Atomic Company, March 29, 1974.

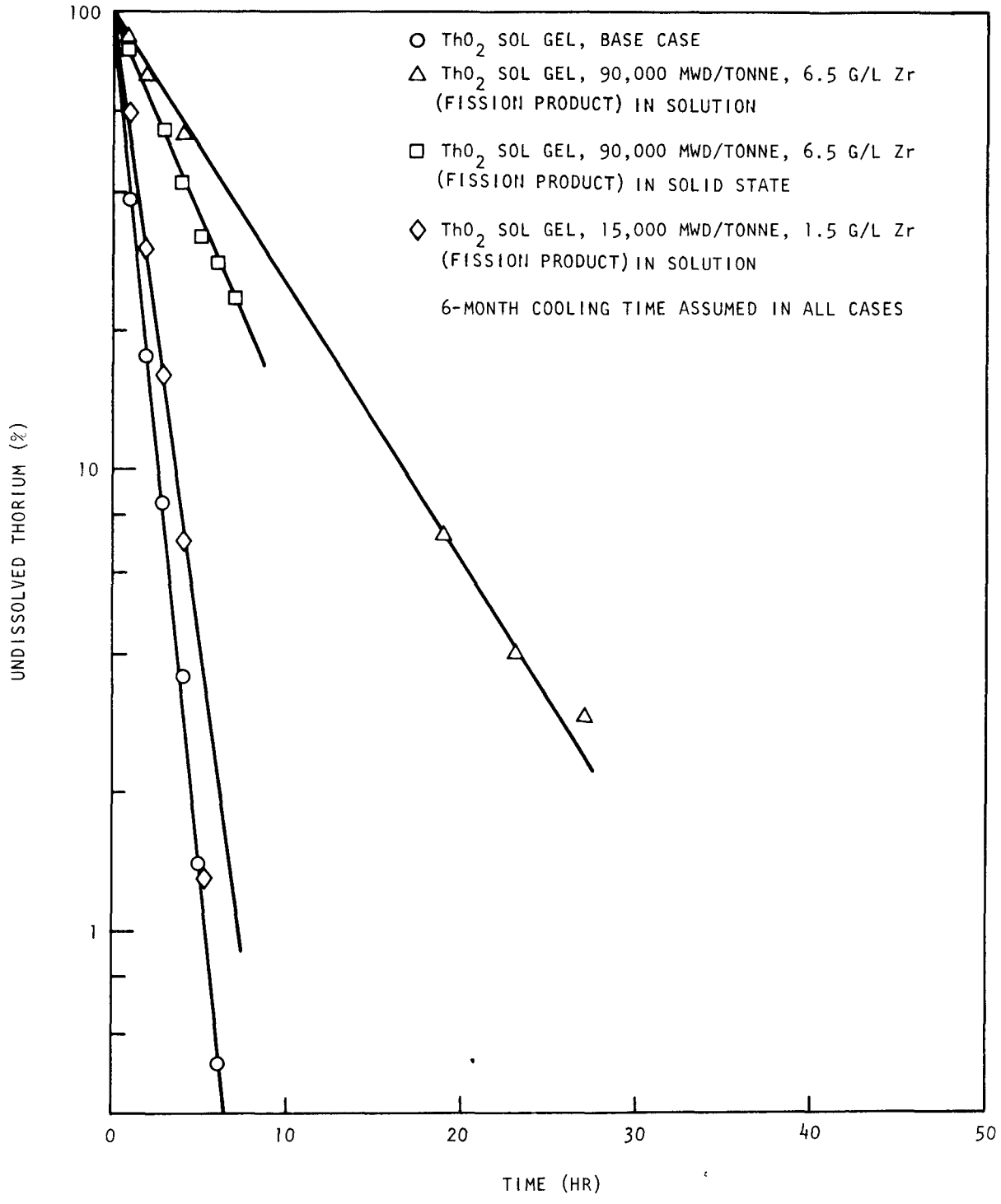

Fig. 5-5. Undissolved thorium versus time

5-3. Geldart, D., "The Effect of Particle Size and Size Distribution on Behavior of Gas-Fluidized Beds," Powder Technol. 6, 201 (1972).

5-4. "HTGR Base Program Quarterly Progress Report for the Period Ending May 31, 1973," USAEC Report Gulf-GA-A12599, Gulf General Atomic, June 30, 1973.

5-5. "Thorium Utilization Program Quarterly Progress Report for the Period Ending November 30, 1974," USAEC Report GA-A13255, General Atomic Company, February 15, 1975.

5-6. "HTGR Base Program Quarterly Progress Report for the Period Ending May 31, 1974," USAEC Report GA-A13030, General Atomic Company, June 28, 1974.

5-7. Küchler, L., L. Schäfer, and B. Wojtech, "Thorex Two-Stage Process for Reprocessing Thorium Reactor Fuel With High Burnup," Kerntecknik 13, 319 (1971).

5-8. Küchler, L., L. Schäfer, and B. Wojtech, "Laboratory and Hot-Cell Experiments on the Applicability of the Acid-Thorex Process for Recovery of Thorium Reactor Fuel With High Burnup," Kerntecknik 12, 327 (1970).

6. SOLVENT EXTRACTION

Four solvent extraction runs were completed during the quarter. The flowsheets under investigation are related to HTGR reprocessing and the Idaho HTGR fuel reprocessing pilot plant.

6.1. RUNS 11 AND 12

Runs 11 and 12 consisted of uranium and thorium extraction, partitioning, and uranium stripping. A partition-scrub step for Run 11 was also run. These runs were conducted in the pilot plant two-column system to obtain efficiency and capacity data.

The flowsheet tested was the first cycle of Fig. 6-1, except Run 12 did not include partition-scrub (1BS column) operation. Table 6-1 shows the stream analyses and flow for each operation. Table 6-2 contains the percent loss data and height equivalent to a theoretical stage (HETS) at the observed percentage of flooding frequency. Flooding data at additional flow rates are given in parentheses. The HETS is an average value for the length of column used; additional column length is expected to change the HETS value.

Co-extraction and partitioning were run through the two-column system the first day, followed by partition-scrub and uranium stripping in the second column on successive days. As noted above, in Run 12 only the uranium stripping run was made after the first day.

As indicated by the HETS values in Table 6-2, the sieve plate cartridge in Run 12 was slightly more efficient than the nozzle plate cartridge in Run 11. However, the throughput rates for the sieve plate

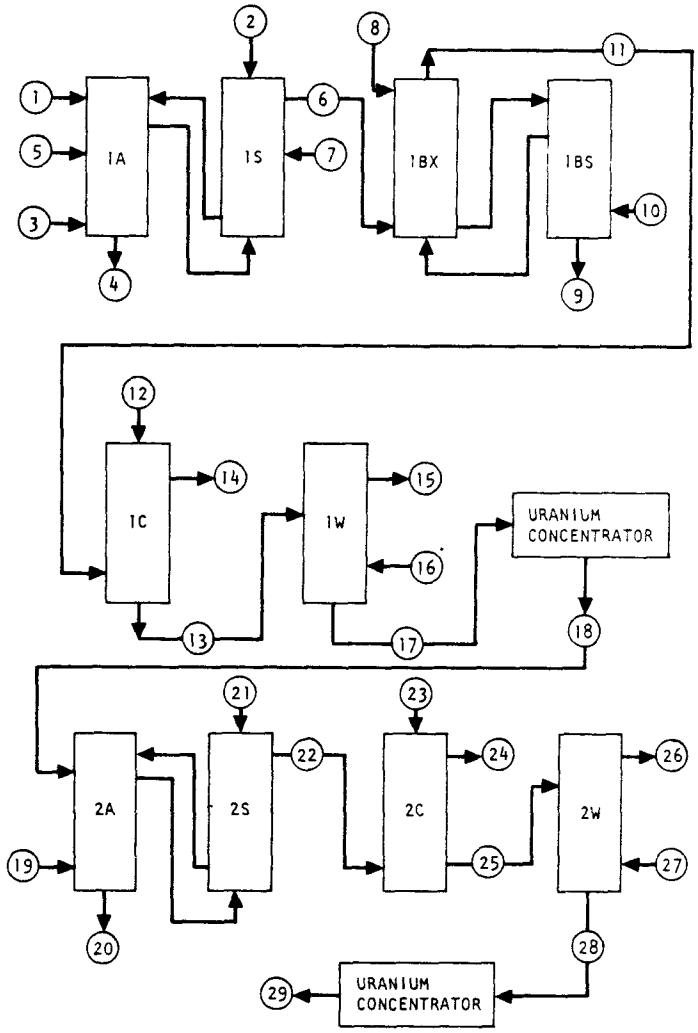

STREAM NO.	FLOW (L/DAY)	COMPOSITION U (G/L)	Th (G/L)	HNO_3 (M)
1	725	14	348	<1.0
2	754			0.01
3	7250		(30% TBP)	
4	1903		(FISSION PRODUCTS)	
5	234			13.0
6	7250	1.4	35	
7	190			5.0
8	4350			0.2
9	4350	Trace	102	
10	1300		(30% TBP)	
11	8550	1.19		
12	4300			0.01
13	4300	2.37		
14	8550		(30% TBP)	
15	430		(NPH)	
16	430		(NPH)	
17	4300	2.37		
18	43.6	233		
19	858		(5% TBP)	
20	294		(WASTE)	
21	243			2.0
22	858	11.8		
23	430			0.01
24	858		(ORGANIC)	
25	430	23.6		
26	43		(NPH)	
27	43		(NPH)	
28	430	27.5		
29	43.6	233		

Fig. 6-1. Partition flowsheet

TABLE 6-1
ANALYTICAL DATA AND STREAM FLOWS, RUNS 11 AND 12

Stream	Stream No.[a]	Run 11				Run 12			
		Th (g/liter)	U (g/liter)	HNO_3 (M)	Flow ml/min	Th (g/liter)	U (g/liter)	HNO_3 (M)	Flow (ml/min)
1AF	1	350.8	38.2	1.10	128	353.5	34.78	1.02	75
1AS	2			1.0	166			1.0	100
1AX	3			30% TBP	1151			30% TBP	750
1AIS	7	--	--	--	--			1.7M ANN[c]	4.36
1AA	5			13	30			13.5	18.8
1AW	4	0.154	3.12×10^{-3}	1.72	--	5.9×10^{-2}	4.1×10^{-4}	1.75	--
1AP	6	37.10	3.95	0.158	--	35.04[b]	3.06[b]	0.180[b]	--
1BX	8			0.2	740			0.2	450
1BXT		60.18	0.774	0.44	--	62.96	0.382	0.515	--
1BU	11	5.4×10^{-3}	3.55	0.015	--	2×10^{-4}	3.68	0.017	--
1BXT (avg)		57.74	1.38	0.413	742	--	--	--	--
1BS	10	--	--	30% TBP	240	--	--	--	--
1BT	9	49.15	3.79×10^{-3}	0.403	--	--	--	--	--
1BSU		24.26	3.85	0.073	--	--	--	--	--
1BU (avg)		--	3.16	0.042	1448	6.1×10^{-2}	1.84	0.019	813
1CX	12			0.01	746			0.01	377
1CW	14	--	1.16×10^{-3}	6.3×10^{-4}	--	--	9.31×10^{-4}	--	--
1CU	13	--	6.03	0.098	--	0.266	3.84	0.06	--

[a] See Fig. 6-1.

[b] Calculated; a second organic phase was present in this sample.

[c] 1.7M aluminum nitrate.

TABLE 6-2
COLUMN HETS, LOSS, AND FLOODING DATA, RUNS 11 AND 12[a]

Column	Purpose	Volume Velocity (gal/hr/ft)	Flooding Frequency (cpm)	Continuous Phase	HETS (ft)	Loss (%)		Flooding Frequency (%)	Temp (°F)
						Th	U		
				RUN 11					
1A	Extraction	1072	147	Organic	--	0.11	0.02	79	90
1BX	Partition	1375	30	Aqueous	3.3 (Th)	--	--	82	85
1BS	Partition scrub	714	82	Aqueous	2.0 (U)	--	--	∿82	81
1C	Strip	1595 (1290)	42 (58)	Aqueous	3.5-4 (U)	--	0.04	92 (95)	112 (115)
				RUN 12					
1A	Extraction	690	158	Organic	--	0.044	3.1×10^{-3}	76	95
1BX	Partition	872	48	Aqueous	3.0 (Th)	--	--	81	87
1C	Strip	872	67	Aqueous	3.0 (U)	--	0.05	84	107
		(1090)	(66)		--	--	--	--	110
		(654)	(77)		--	--	--	--	105
		(1310)	(45)		--	--	--	--	112

[a] Extraction column: 23% free area, 1/8-in.-diameter-hole nozzle plates, nozzles down, 2-in. plate spacing, 22-ft length, (9 ft scrub and 13 ft extraction), 1-in. pulse amplitude.
Partition, partition-scrub, stripping columns: 23% free area, 3/16-in.-diameter-hole nozzle plates, spacing from column bottom, 8-1/2 ft of 4-in. spacing, 1-1/2 ft of 3-in. spacing, 5 ft of 2-in. spacing, 1-in. pulse amplitude for Run 11, nozzles up.

Run 12 had 40% free area sieve plates with spacing and amplitude the same as Run 11.

cartridge are much less. The presence of a more predominate third phase (second organic phase) in Run 11 may have also contributed somewhat to the lower apparent efficiency of the partition column in that run.

A comparison of the stripping operation results also indicates a higher efficiency with the sieve plate cartridge. The following factors must be considered when making this comparison: (1) operation with the sieve plate cartridge was at lower throughput rates to prevent flooding, (2) the uranium and nitric acid concentrations of the solvent [1BU (avg)] were a factor of about two lower in Run 12, and (3) in Run 11, the solvent [1BU (avg)] was stored an additional day before processing due to the partition-scrub operation. Therefore, the difference in calculated efficiency may not be significant.

The visible third phase (cloudy emulsion in the scrub section) noted in the extraction column of Run 11 cleared when the solvent flow rate was increased in the latter part of the run. The third phase was not as distinct in Run 12, but a second organic phase was reported in the 1AP sample (see Table 6-1) during analysis.

6.2. RUN 21

Run 21 consisted of uranium-thorium extraction and costripping. This run was conducted in the pilot plant two-column system to provide efficiency and capacity data. The flowsheet tested was the first cycle of Fig. 6-2, except stream 7 contained 3.87M HNO_3 and 0.159M ANN (aluminum nitrate). Table 6-3 contains the analyses and flow rates for each stream. The data in parentheses resulted from a second set of operating conditions. Table 6-4 contains the percent loss data and HETS at the observed percentage of flooding frequency. In this run the stripping column contained 40% free area sieve plates.

The stripping column flooding point with sieve plates was at a lower pulse frequency than with the 3/16-in.-diameter nozzle plates, which had

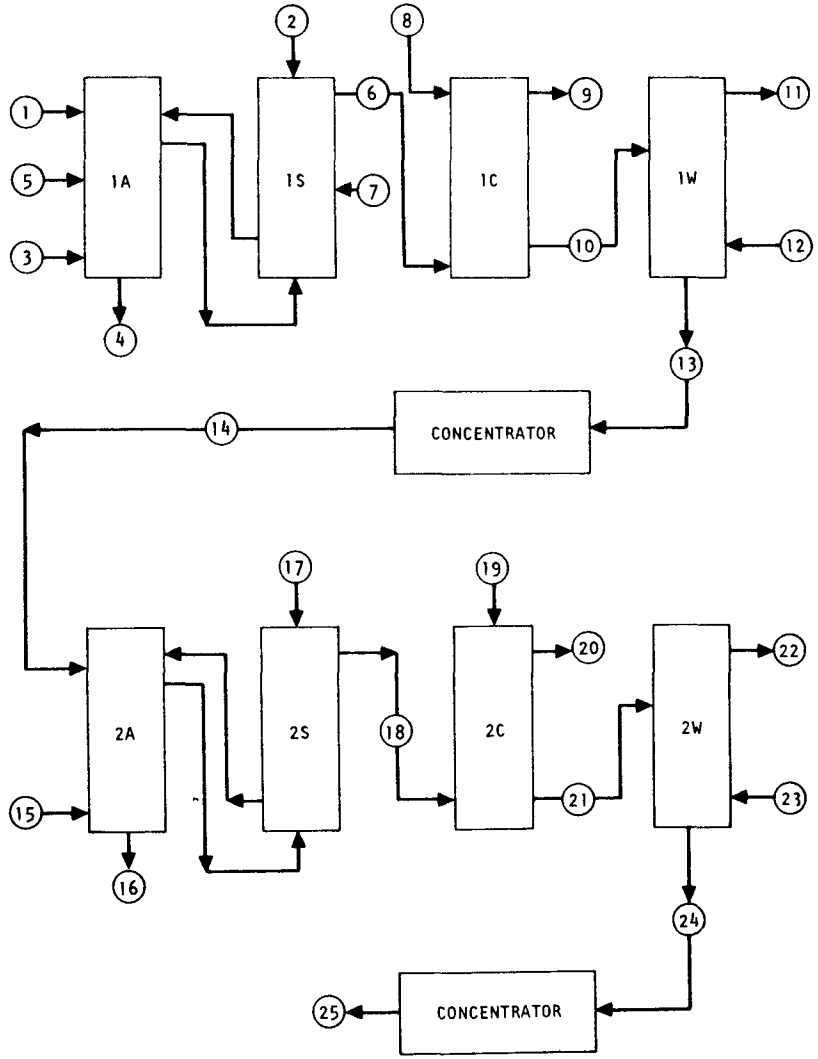

STREAM NO.	FLOW (L/DAY)	COMPOSITION U (G/L)	Th (G/L)	HNO_3 (M)
1	725	14	348	<1.0
2	754			0.01
3	7250		(30% TBP)	
4	1903		(FISSION PRODUCTS)	
5	234			13.0
6	7250	1.4	35	
7	190			5.0
8	7250			0.01
9	7250		(ORGANIC)	
10	7250	1.4	35	
11	725		(NPH)	
12	725		(NPH)	
13	7250	1.4	35	
14	725	14	348	
15	940		(5% TBP)	
16	1007		255	
17	282			2.0
18	940	10.8		
19	470			0.01
20	940		(ORGANIC)	
21	470	21.6		
22	47		(NPH)	
23	47		(NPH)	
24	470	21.6		
25	43.6	233		

Fig. 6-2. Co-strip flowsheet

TABLE 6-3
ANALYTICAL DATA AND STREAM FLOWS, RUN 21

Stream	Stream No.[a]	Th (g/liter)	U (g/liter)	HNO_3 (M)	Flow (ml/min)
1AF	1	353.1	35.7	1.18	106 (110)
1AS	2			0.008	100 (102)
1AA	7			3.87[b]	22 (23)
1A1S	5			13.6	34 (33)
1AX	3			30% TBP	1009 (1035)
1AW	4	0.03 (0.04)	1.58×10^{-4} (2.6×10^{-5})	2.21 (2.28)	--
1AP	6	34.62 (40.55)[c]	3.23 (4.29)[c]	0.16 (0.097)	--
1CX	8			0.008	980 (1023)
1CW	9	1.23×10^{-3} (7.4×10^{-4})	1.11×10^{-4} (9.7×10^{-5})	--	--
1CP	10	34.51 (41.03)	3.38 (4.34)	0.17 (0.12)	--

[a] See Fig. 4 of Ref. 6-1.

[b] 3.87M HNO_3, 0.159M aluminum nitrate.

[c] Calculated from material balance.

TABLE 6-4
COLUMN HETS, LOSS, AND FLOODING DATA, RUN 21[a]

Column	Purpose	Volume Velocity (gal/hr/ft^2)	Continuous Phase	Flooding Pulse Frequency (cpm)	Loss (%) or Estimated HETS (ft)	Frequency (%)	Temp (°C)
1A	Extraction	925	Organic	145[b]	0.02 % (Th) 0.0011% (U)	80	32
1C	Strip	1450	Aqueous	45	3.5 ft (Th) 2 ft (U)	78	52

[a] Extraction column: 23% free area, 1/8-in.-diameter-hole nozzle plates, nozzles down, 2-in. plate spacing, 22-ft length, 13 ft extraction and 9 ft scrub, 1-in. pulse amplitude.
Strip column: 40% free area 1/8-in.-diameter-hole sieve plates, spacing from column bottom, 8-1/2 ft of 4-in. spacing, 1-1/2 ft of 3-in. spacing, 5 ft of 2-in. spacing, 1-in. pulse amplitude.

[b] Estimated from data from Runs 13 and 14.

been tested previously. However, the column efficiency was comparable to other cartridges that were operated at higher pulse frequencies. This statement is based on the visual appearance of the column, along with analytical data and the estimated HETS values.

A third phase was present in the extraction column during the latter part of the run. The third phase was indicated by cloudiness in the scrub section of the column and was confirmed by samples from that section of the column. Some inconsistencies were noted in the analyses of samples of the scrub section product stream (1AP). These inconsistencies in the uranium-to-thorium ratios may have resulted from instability created by the third phase. The set of 1AP samples taken before the development of the third phase had the expected uranium-to-thorium ratio.

Significant difficulties with the 1AF flow control system may have contributed to the fluctuations of the third phase and to the high concentration of thorium in the 1AP stream. Use of aluminum nitrate in the scrub stream in a test of this addition for fluoride scrubbing caused no problems in extracting the thorium or uranium.

All HETS data will be recalculated to confirm the equilibrium data selected here when the SEPHIS program for uranium-thorium stage calculation is made available by HNL.

6.3. RUN 22

Run 22 consisted of uranium and thorium extraction, partitioning, and uranium stripping. These runs were made in the pilot plant two-column system to obtain efficiency and capacity data. The flowsheet tested was the first cycle of Fig. 6-1, except the partition-scrub operation (1BS column) was excluded. Both the extraction column and the partition column were operated with a continuous organic phase. Table 6-5 shows the stream

TABLE 6-5
ANALYTICAL DATA AND STREAM FLOWS, RUN 22

Stream	Stream No.[a]	U (g/liter)	Th (g/liter)	HNO_3 (M)	Flow (ml/min)
1AF	1	34.78	353.5	1.02	106
1AS	2			0.984	132
1AIS	7			1.7M ANN[b]	7.3
1AA	5			13	33
1AW	4	3.2×10^{-2}	6.74×10^{-2}	1.74	
1AX	3			30% TBP	980
1AP	6	3.14	38.04	0.171	
1BX	8			0.21	599
1BU	11	3.81	0.370	0.016	
1BXT		0.598	63.19	0.434	
1BU (avg)	11	--	--	--	2100 (2447)[c]
1CX	12	--	--	--	988 (1134)[c]

[a] See Fig. 6-1.

[b] 1.7M aluminum nitrate.

[c] Second flow conditions.

analyses and flow rates for each operation. Table 6-6 shows the flooding and percent loss data and HETS at the observed percentage of flooding frequency. As indicated above, the partition column was operated organic phase continuous and with 3/16-in.-diameter nozzle plates having 23% free area. The partition column did not exhibit significant stability or mixing efficiency at flow rates greater than those indicated in Table 6-5 and 6-6. The recovery from flooding of the partition column at these rates was also difficult.

The stripping operation was run in the same column as that used for partitioning on a separate day. No samples were taken, but flooding tests were run at the rates indicated in Table 6-6.

The high thorium loss to the 1BU stream in the partition column confirms the higher HETS observed in earlier runs with organic continuous operation (Runs 6 and 7). However, the Run 22 results may be partially incorrect. The high thorium values could be partially attributed to residual thorium remaining from the flooding and column instability in the early part of this run.

When flooding occurs in the organic continuous partition column, the flood lowers the countercurrent aqueous flow in the column mixing area. The organic stream flows unhindered up through the column, carrying all of the uranium and much of the thorium with it. In a plant operation, this amount of thorium being misdirected for a short time could contaminate the uranium product enough to require reworking.

Flooding in an aqueous continuous partition column results in a holdup of the organic stream developing near the bottom of the cartridge mixing area. Not only is the operational recovery from this type of flood easier, but the thorium does not significantly follow the normal uranium path and would not require reworking in the magnitude mentioned for organic

TABLE 6-6
COLUMN HETS, LOSS, AND FLOODING DATA,[a] RUN 22

Column	Purpose	Volume Velocity (gal/hr/ft^2)	Flooding Frequency (cpm)	Continuous Phase	HETS (ft) or Loss (%)	Flooding Frequency (%)	Temp (°F)
1A	Extraction	915	(140)[b]	Organic	0.05% (Th)	80	83
1BX	Partition	1148	115	Organic	4+ ft	80	70
1C	Strip	2245 2603	94 65+	Organic Organic	--	--	110 105

[a] Extraction column: 23% free area, 1/8-in.-diameter-hole nozzle plates, nozzles down, 2-in. specing (13 ft extraction and 9 ft scrub), 1-in. pulse amplitude.

Other columns: 23% free area, 3/16-in.-diameter-hole nozzle plates, nozzles down, 2-in. spacing (15 ft), 1-in. pulse amplitude.

[b] Estimated from previously reported flooding data.

continuous operation. Additionally, if the uranium concentration increases in the 1BXT stream, the uranium would be separated from the thorium in the 1BS column.

The HETS value for partitioning was obtained from a McCabe-Thiele diagram using the best estimate available for equilibrium lines. The HETS is an average number for the length of column used; additional column length will change the HETS value.

6.4. SOLVENT EXTRACTION FACILITY EXPANSION

The expansion of the two-column solvent extraction system to a five-column system has been completed. Initial shakedown runs in the five-column system have begun.

REFERENCE

6-1. Benedict, G. E., General Atomic Company, "Solvent Extraction Experimental Run Plan," private communication, 1974.

7. SYSTEMS DESIGN

7.1. PROTOTYPE SIZE REDUCTION SYSTEM

Remote maintenance concepts for the fuel element size reduction system were presented in a joint meeting with GA, ERDA, ACC-ICPP, and Parsons Company on January 16, 1975. General Atomic's revised design, schedule, and cost proposal based on ACC's System Design Description was presented and discussed. Approval of the program plan was obtained from ACC. Remote handling and maintenance are being factored into each component of the new design, i.e., remotely operated lift fixtures for the last-stage crusher, the total frame, movable and stationary jaws, roll crushers, lift fixture and horizontal transfer cart for screener, and jet grinders.

7.2. PROTOTYPE BURNER SYSTEM

Remote maintenance concepts for the primary and secondary burners were presented in a joint meeting with GA, ACC-ICPP, and ERDA-ID on February 20 and 21, 1975. It was again agreed that full demonstration of remote maintenance, disassembly, and decontamination would not be required for the burner system and that a demonstration of a semi-remote assembly and disassembly operation should be accomplished. The following features have been designed into the system and will be demonstrated: swinging the burner installation away for burner removal, semi-remote removal of the bottom spool, swing out and remote removal of the hopper and filter box, and semi-remote removal of the burners from the platform.

7.3. PROTOTYPE PLANT SYSTEMS, GENERAL

Detailed facility plans were prepared and approved. A detailed plan view of the reference plan for the E-Building facilities is shown in Fig. 7-1.

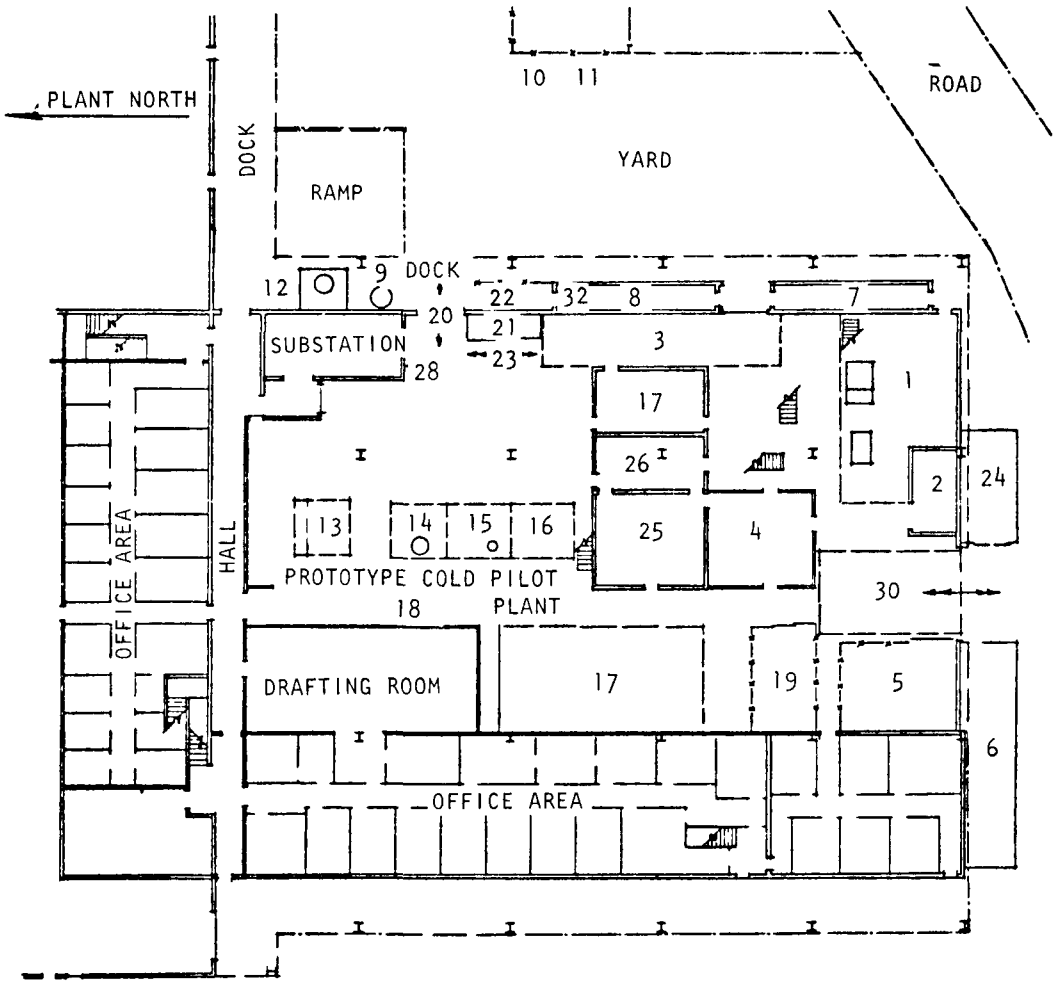

1. BURNER TEST AND LABORATORY AREA
2. LEACHING FACILITY
3. SOLVENT EXTRACTION FACILITY
4. EXISTING CONTROL ROOM
5. SHOP
6. EXISTING VENTILATION SYSTEM
7. SOUTH VAULT
8. NORTH VAULT
9. EXISTING N_2 TANK
10. EXISTING LOX TANK
11. CO_2 TANK
12. M-G SET FOR PROTOTYPE BURNERS
13. PROTOTYPE CRUSHER UNIFRAME
14. 16-IN. PROTOTYPE PRIMARY BURNER
15. 8-IN. PROTOTYPE SECONDARY BURNER
16. FUTURE DISSOLVER -- CENTRIFUGE
17. SPECIAL TESTS AREA
18. REPAIR AREA FOR PROTOTYPE COMPONENTS
19. CENTRAL STORAGE AREA
20. PRIMARY ACCESS FOR PROCESS MATERIALS AND WASTE REMOVAL
21. DRY-CHEMICALS STORAGE
22. PETROCHEMICAL AND BARRELED-WASTE STORAGE
23. BARRELED-WASTE REMOVAL AISLE
24. STORAGE ENCLOSURE
25. TECHNICIAN'S OFFICE
26. WASH AND LOCKER ROOM
27. EXTENDED RUNWAY FOR EXISTING 1-TON EOT CRANE
28. DECONTAMINATION HOOD
29. NEW CONTROL ROOM
30. TRUCK UNLOADING AREA
31. NEW VENTING SYSTEMS
32. COOLING-AIR BLOWER FOR PROTOTYPE BURNERS
33. STORAGE RACK

Fig. 7-1. Reprocessing development cold pilot plant, E-building

The five-column solvent extraction system was completed. The two-story office and control area, with a one-story wash and locker room, was approved with a completion date scheduled for April 1975. Approval for construction of the prototype line support platform was received. This phase of the project is scheduled for completion by June 1975.

8. ALTERNATE REPROCESSING TECHNIQUES

Current studies concerning alternate reprocessing techniques are aimed at a graphite/fuel separation method in which the majority of the graphite is mechanically removed. A cooperative experimental program is being conducted with HFH Systems, Inc., manufacturers of electrohydraulic equipment. These experiments are designed to (1) evaluate the capability of a high-frequency electric discharge to produce a controlled fracture of H-327 graphite, and (2) measure the effect of such a discharge or series of discharges on the integrity of both fertile and fissile particles.

8.1. INITIAL FEASIBILITY TEST - GRAPHITE/FUEL SEPARATION

The discharge probe necessary to start preliminary tests to separate the fuel from the graphite carrier by an electrohydraulic process has been manufactured per the G. B. Hayward Company drawing (see Fig. 32 of Ref. 8-1). A power supply with the capability of supplying 3000 joules of stored energy is being used to supply the discharge probe. The first test revealed the graphite block to be a better conductor than expected, and the discharge probe had to be modified. The modification consisted of machining the high voltage connector (see Fig. 8-1) to accept a sleeve of a polyurethane derivative called Texin. Figures 8-2 and 8-3 show the graphite test cylinder and the inverted pinch assembly.

The second test with the insulating modification consisted of inserting the probe into the center coolant hole of the H-327 graphite cylinder, which was approximately 15 in. long and 4 in. in diameter (Fig. 8-4). The coolant holes and fuel holes were empty for this test, and because the cylinder was not in a container, the results could be observed during the discharge cycle. The gap setting between the high voltage

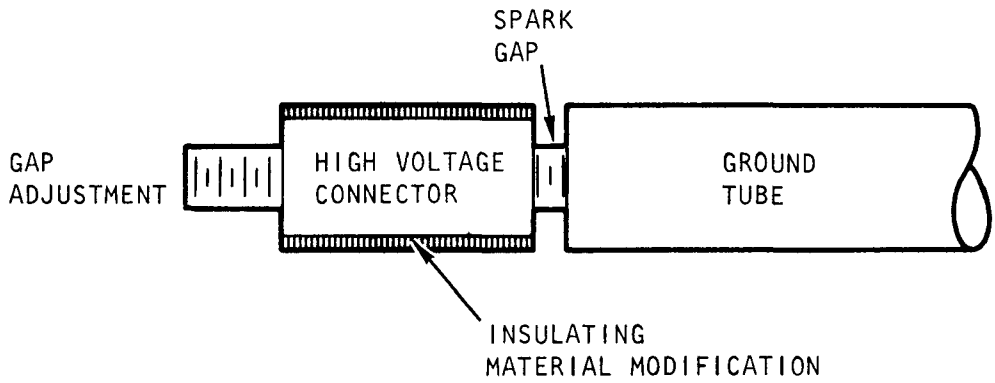

Fig. 8-1. Modified discharge probe

Fig. 8-2. Graphite test cylinder

Fig. 8-3. Inverted pinch assembly

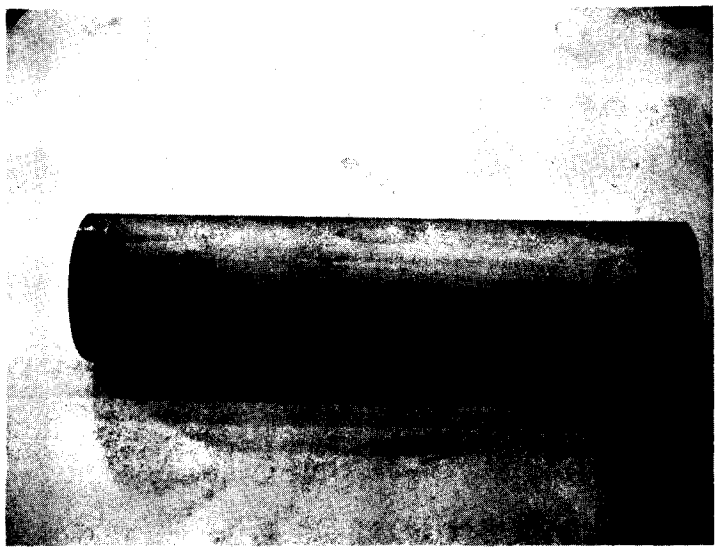

(a)

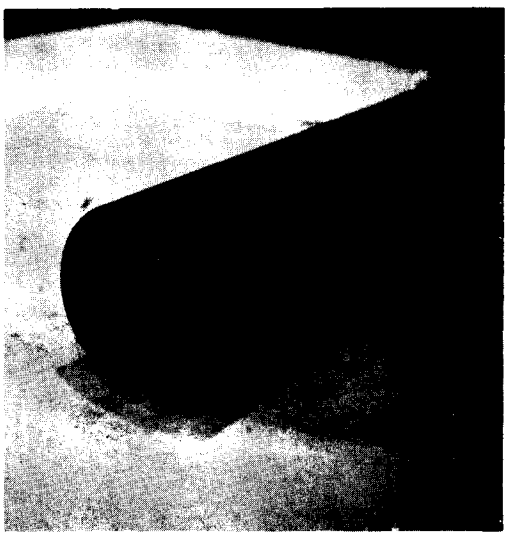

(b)

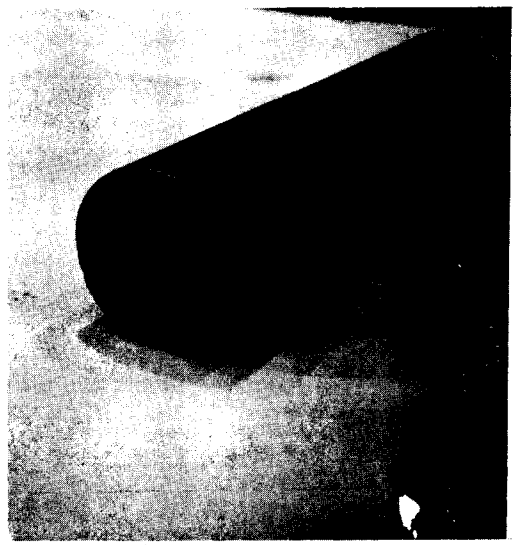

(c)

Fig. 8-4. Setup for second test with insulating modification

connector and the ground tube was set at 3/16 in. and the depth of the insertion of the probe was 2 in. Approximately 2500 joules of energy were released. No apparent change in the cylinder was observed on the outside (Fig. 8-5). The probe could not be removed without inserting a rod in the opposite end of the coolant hole and tapping it lightly to jar the probe loose. A visual inspection showed discharge indentations in the area of the discharge gap and one break-through approximately 1/8 in. in diameter into an adjoining fuel hole. Slightly pitted areas were also observed along the length of the grounding tube, which could result in loss of power.

The probe was then inserted in one of the outer coolant holes and discharged. The results are shown in Fig. 8-6. Photographs taken before and after the discharge are shown in Fig. 8-7. Following this discharge it was noted that the pitted areas on the ground tube had increased. This loss of power makes it necessary to insulate the ground tube before additional tests can be performed. The modifications will consist of applying insulating tubing over the full length of the ground tube.

The present goal is to complete the tests with the empty graphite cylinders by the end of March. Sample cylinders will then be loaded with reject fuel rods and the tests performed at the GA facility under controlled conditions. These tests should be completed by the end of April.

Fig. 8-5. Condition of cylinder after second test

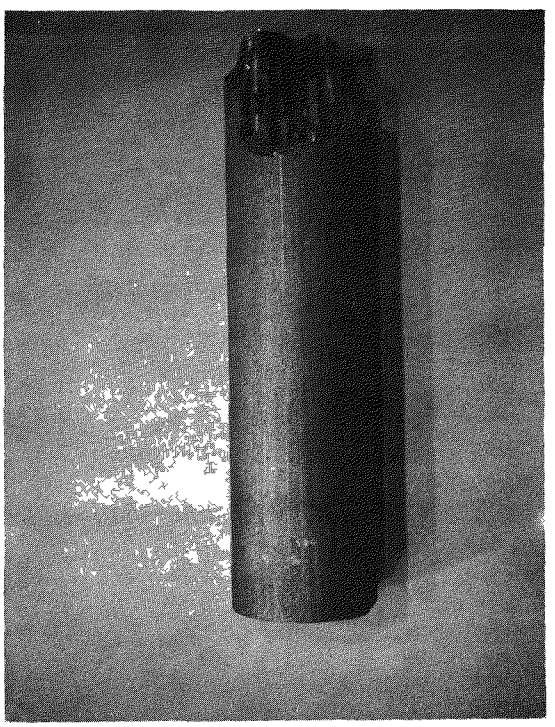

Fig. 8-6. Results of discharge with probe in an outer coolant hole

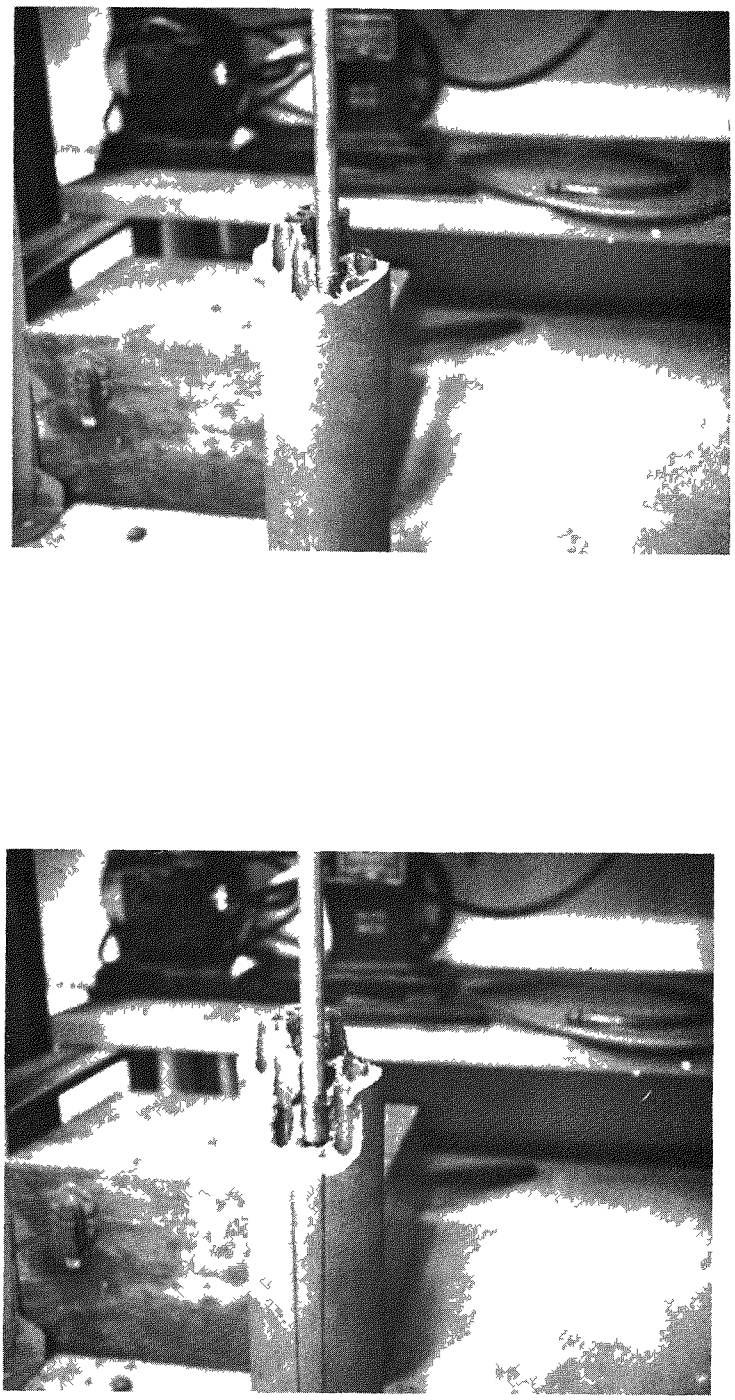

Fig. 8-7. Pitted area on ground tube before (top) and after (bottom) discharge

9. CONCEPTUAL DESIGN STUDY OF AN HTGR FUEL TARGET RECYCLE PLANT

The conceptual design study of a commercial-scale recycle plant for HTGR fuel performed in conjunction to the Ralph M. Parsons Company was completed. The design study is summarized in Ref. 9-1.

REFERENCE

9-1. Jackson, D., "HTGR Target Recycle Plant - Conceptual Design Summary and Design Qualification," ERDA Report GA-A13365, General Atomic Company, to be published.